DRAG MEASUREMENT ON A SUSPENDED SPHERE AND ITS APPLICATION TO CORROSIVE GAS VISCOSITY MEASUREMENT

By

RATAN KUMAR

A DISSERTATION PRESENTED TO THE GRADUATE SCHOOL
OF THE UNIVERSITY OF FLORIDA IN PARTIAL FULFILLMENT
OF THE REQUIREMENTS FOR THE DEGREE OF
DOCTOR OF PHILOSOPHY

UNIVERSITY OF FLORIDA

1992

ACKNOWLEDGEMENTS

I would like to acknowledge the contribution to this work to Prof. Samim Anghaie for his many invaluable ideas and criticisms, for his scrutinization and appraisal of the draft, and for his continual encouragement and support.

I would like to express my thanks to Dr. E. T. Dugan, Dr. R. Mei, Siddhartha Thakur and Gary Chen for many useful suggestions and discussions they provided. Thanks are also due to Dr. D. E. Hintenlang, Dr. J. F. Klausner and Dr. M. L. Muga.

Finally, I would like to express my thanks and gratitude to my wife, Kiran Sreewastav, and to my family who have provided me with unlimited amounts of patience, support and encouragement.

TABLE OF CONTENTS

CHAPTERS page

LIST OF TABLES

LIST OF FIGURES

Abstract of Thesis Presented to the Graduate School
of the University of Florida in Partial Fulfillment of the
Requirements for the Degree of Doctor of Philosophy

DRAG MEASUREMENT ON A SUSPENDED SPHERE AND ITS APPLICATION TO CORROSIVE GAS VISCOSITY MEASUREMENT

By

Ratan Kumar

December 1992

Chairman: Dr. Samim Anghaie
Major Department: Nuclear Engineering Sciences

The estimation of drag force exerted by fluid flow over a sphere is a fundamental problem and has received attention both for bounded and unbounded flow. An offshoot of this study on a sedimenting sphere in a cylindrical tube has provided an effective means to ascertain viscosity of fluids. However, low-drag measurement difficulties and other practical impediments had restricted the sedimentation study to the determination of liquid viscosity only. The current work incorporates an accurate microbalance to obtain the drag force exerted by gas flow over a suspended sphere. The drag measurements are carried out by an ultra precise thermal microbalance having a sensitivity of 0.1 microgram. The results obtained have been extended for viscosity measurements. The experimental findings provide enough impetus to propose a methodology that can assist in the

development of a drag based viscometer with good potential to handle corrosive gases.

In conjunction with the experimentation, a theoretical investigation afforded through dimensional analysis and numerical studies has been carried out. The examined phenomenon is the flow of a fully-developed gas in a cylinder over a centrally suspended sphere. Previous studies in this area had come up with correlations that established association between the coefficient of drag on a sphere in unbounded flow and cylindrically confined flow. These relationships, however, do not corroborate the experimental data well. This prompts the developement of a new correlation that can be explained physically.

Finally an attempt has been made to explain the observed experimental results by computational methods. Although the flow geometry is fundamental, it is difficult to numerically test it for drag measurements. Two different approaches have been taken in the computational fluid dynamics study. A body-fitted coordinate system using the streamfunction-vorticity method and a primitive variable technique in cylindrical coordinates were utilized. The results show that the streamfunction-vorticity method runs into some difficulty with the body-fitted coordinate system. The primitive variable approach appears more robust and can be recommended for future work with the body-fitted coordinate.

CHAPTER 1
INTRODUCTION

1.1 Motivation

Fluid flow in nuclear systems provides complex situations which are difficult to handle experimentally and theoretically. Several studies on advanced nuclear reactors for space application have been done but their implementation on a practical scale is still a serious challenge. One such proposed nuclear system for space power generation is shown in Figure 1-1. Uranium fuel in droplet form is sprayed into the reactor which generates about 750 megawatts of thermal energy. In order to simulate and test this idea from a thermalhydraulic point of view, thermophysical properties, like viscosity, of the working fluid and correlations for fluid flow around spherical bodies need to be ascertained. Highly reacting gases can have certain unresearched effects on the measuring devices. As a result, viscometers that are exposed to corrosive gases may provide unrealistic data. This motivates the current study to propose a viscometer that is not exposed to the unknown environment and has the attractiveness of a precise and sensitive measuring device. Another interesting feature of fluid flow around spherical bodies enclosed by

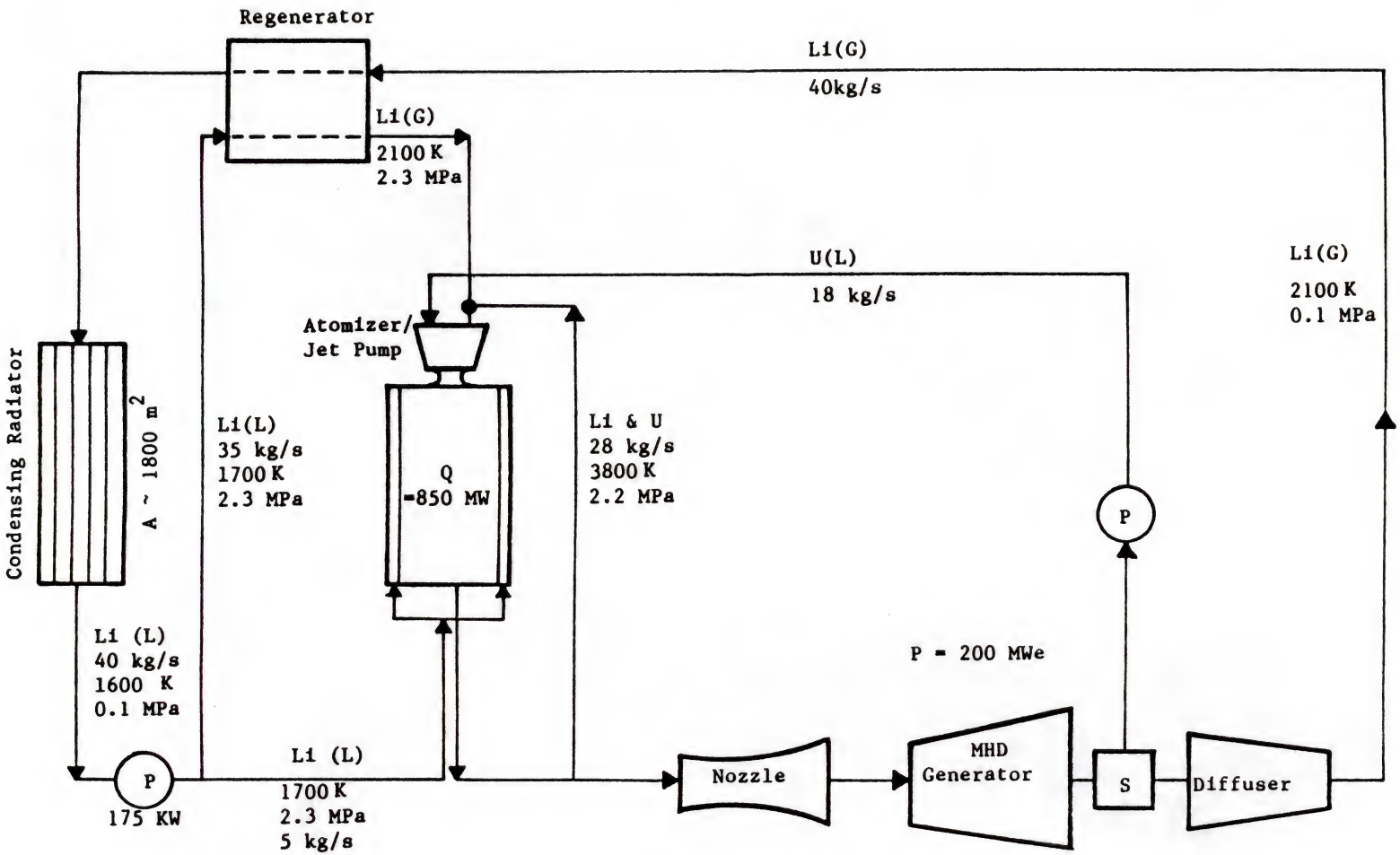

Figure 1.1 Schematic of 200 MWe uranium droplet fuel, superheated lithium reactor with mhd generator

walls is also discussed in this work. Past studies on pebble bed nuclear reactors stimulated interest in turbulent flow over cylindrically surrounded spheres. Theoretical work, in this area, has been performed for very low flow rates. In the intermediate laminar region, reliable data have been generated by interpolating between the turbulent and low flow rate regimes. The present study endeavors to highlight some aspects of laminar fluid flow over a rigid sphere in a tube by experimentation and analysis.

1.2 Discussion on Fluid Drag Force and Viscosity

When an object is placed within a flowing fluid stream, the latter experiences a change in its momentum and a force is exerted on the object. This force owes its existence to the viscosity of the fluid and to the pressure distribution over the body surface. The component of the force parallel to the direction of flow is called the drag and the normal component is called the lift. An ideal fluid maintains a slip condition at the solid wall and does not give rise to a drag force. However, this is in glaring contradiction to experimental observation where a drag force is always exerted on a body having a relative motion with respect to fluid. Treatment of real fluids takes into account a no-slip boundary condition and the viscosity of the fluid. Although the existence of viscosity had been considered in earlier

works, Prandtl (1904) incorporated it in the momentum equation by pioneering the boundary layer analysis.

The discussion on viscosity can be best understood by drawing an analogy with other resistive properties of material. All real substances offer certain resistance to deformation. In the case of a solid, if a shear stress is applied, then it is proportional to the strain and the constant of proportionality (the resistive factor) is called the modulus of torsion. In fluid, the shear stress is found to be proportional to the rate of strain and the proportionality constant is called viscosity. There are various concepts to define and describe viscosity of fluids, but the fundamental one as described by Newton is discussed.

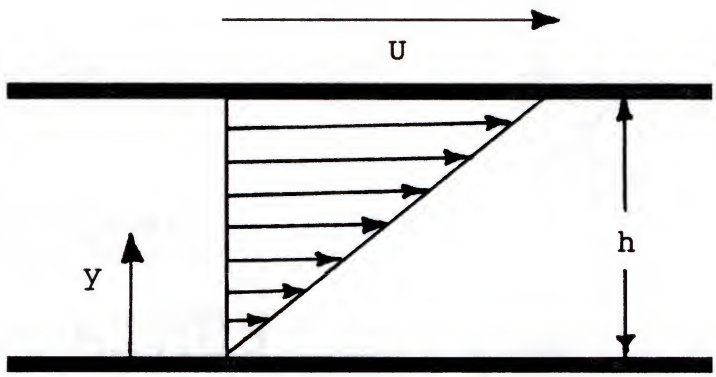

Figure 1-2 Velocity distribution between parallel plates

To define viscosity as obtained from Newton's law, we can visualize the motion of a fluid between two very long parallel plates one of which is at rest while the other moves with a constant velocity parallel to itself as shown

in Figure 1-2. From experiment it is observed that the fluid adheres to the walls i.e. u (@ y=0) = 0 and u (@ y=h) = U. If the velocity distribution is linear, then u(y) = (y/h)U. In order to support the motion, a tangential force needs to be applied to the upper plate and this will be in equilibrium with the frictional forces in the fluid. From experiment this force, taken per unit area, is proportional to velocity U and varies inversely with the distance h. Hence the frictional force per unit area, denoted by τ, is also proportional to U/h or generally du/dy. The proportionality factor between τ and du/dy is denoted by μ and is a property of the fluid.

$$\tau = \mu \frac{\partial u}{\partial y} \qquad (1\text{-}1)$$

The quantity 'μ' is called the viscosity of the fluid and Equation 1-1 is known as Newton's Law of Friction.
The physical concept behind this definition is that the transfer of momentum across any plane in the fluid is due to an exchange of molecules between fluid layers on either side of the plane. As a molecule crosses from one side with a certain velocity to the other side of the plane, it changes its velocity if collision occurs. A change of momentum on either side of the plane gives rise to a force parallel to the plane. The force is proportional to the difference in the flow velocity, given by the velocity with which the molecule started and the velocity which it attained after

collision. The fluid offers resistance to this shearing force by virtue of its transport property called viscosity. It should be noted that the above description is a simple case in one direction. The generalized case is offered by the Stoke's law of friction. The derivation of the stress system and the rate of strain for an infinitesimal fluid element has been dealt with in detail by Schlichting (1979). The relationship as obtained from Newton's law of friction can be easily deduced from the general case as derived in the Stokes' law of friction. One should, however, note that the fluids obeying Stokes' law are isotropic and Newtonian. A fluid is said to be isotropic when the relation between the components of the stress and those of the rate of strain is the same in all directions and Newtonian if the relation is linear. Fortunately, all gases and many liquids of interest belong to this class.

It can be concluded that viscosity is a measure of the fluid's tendency to dissipate energy when disturbed from equilibrium by the imposition of a flow field, which distorts the fluid. It appears as a proportionality constant when the shear stress is related to the velocity gradient in a linear way. While defining viscosity on the basis of molecular exchange, the existence of transport of any mass in a direction normal to the velocity on a scale larger than a molecular one is excluded. Thus, the definition is strictly restricted to laminar flow of fluids.

1.3 Viscosity as an Important Transport Property

In the above discussion it is observed that in order to have the shear stress, there must be a velocity gradient in the fluid. The momentum exchange across this gradient gives rise to the definition of viscosity. This correlation can be associated with other phenomenological relationships such as those pertaining to heat and mass transfer. In the latter cases there are coefficients that relate the flux of a quantity to its gradient. In the case of heat, the coefficient is called thermal conductivity while it is termed mass diffusivity in the situation of mass transfer. These properties of fluids (viscosity, thermal conductivity and mass diffusion coefficient) are imbedded in the rate equation describing the transport of a quantity relative to the medium through which it is passing.

The existence of viscosity and its incorporation into the solution of the fluid momentum equation allowes us to treat a real fluid different from an ideal one. Although ideal fluid theory, which neglects two important properties namely compressibility and viscosity, provides excellent results for air and water, it is unable to resolve the so called d'Alembert's paradox. The paradox arises since ideal fluid can exert only normal forces and this cannot explain the drag force on a body. Prandtl solved this disturbingly mysterious subject of aerodynamics with his work on boundary layer theory from 1904 onward. Omission of viscosity from

the momentum equation near the wall is no longer permissible (boundary layer equation) since the fluid viscosity now affords the calculation of drag force, which is essential in designing various aerodynamical bodies, fluid machineries, etc. The numerical value of viscosity, at various thermodynamic conditions, has become increasingly important in order to perform and simulate various aerodynamical studies and to calculate momentum in real fluids.

1.4 Gas Viscosity Measurement Techniques

The theory and practice of viscometry is based upon the hypothesis postulated by Sir Isaac Newton in his "Principia", concerning the magnitude of force required to overcome viscous resistance. Following Newton's fundamental work, the hydrodynamics of the next century were concerned only with the flow of ideal or nonviscous fluids. It was not until 1823 that Navier first stated the general equations for the motion in real fluids. Similar equations were deduced by Poisson (1831) and by Stokes (1845), who integrated them to give the velocity distribution in two cases of great importance in connection with the measurement of viscosity, namely, flow through a cylindrical tube and motion between co-axial cylinders.

Meanwhile on the experimental side both Hagen (1839) and Poiseuille (1846), working independently, obtained a relationship between the flow rate, pressure drop and

dimension of capillary tubes. This paved the path for Wiedemann (1856) and later Hagenbach (1860) to compute the viscosity of fluid flowing through the tube. In 1890 Couette devised a different method of measuring viscosity based on a system of two concentric cylinders; viscosities deduced in this way gave figures identical with those of Poiseuille's. Capillary tube and concentric cylinder viscometers are still the primary instruments employed these days for viscosity measurement. In fact, measurement by the oscillating disk viscometer (a version derived from the concentric cylinder viscometer) gives the standard values of viscosity for most of the common gases at room temperature. As a result, a short description of these viscometers is included below.

1.3.1. Capillary Viscometer

The capillary or transpiration viscometer (Figure 1-3) has been used as a primary instrument for viscosity measurements for well over a century. Although great care had been taken in the design of such an instrument, the evaluation of the viscosity has sometimes been carried out without the aid of adequate working equations, leading to inaccurate experimental results, despite the high precision of measurements. Experimental measurements are carried out by measuring the pressure drop and flow across a fully developed flow condition in a capillary tube.

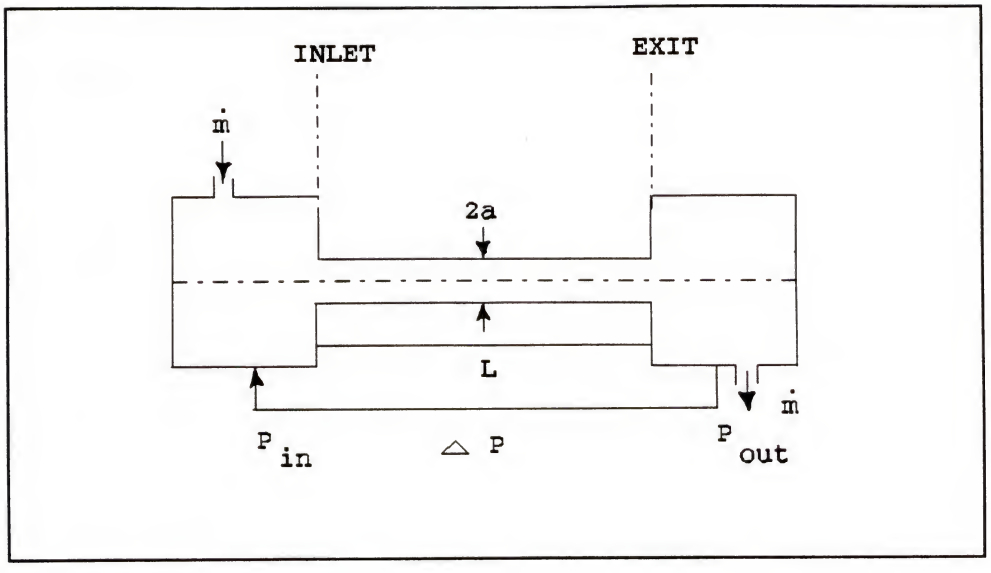

Figure 1-3 Capillary tube viscometer

For an incompressible fluid, the working equation for a capillary viscometer is given as

$$\frac{\Delta P}{m} = \frac{8(L+na)}{\pi a^4}\frac{\mu}{\rho} + \frac{m_o}{\pi^2 a^4 \rho} m \qquad (1\text{-}2)$$

where p = pressure drop across length L

m = mass flow rate of the fluid

a = radius of the capillary tube

m_o = kinetic energy correction term = 1.14

n = modified kinetic energy correction term including reservoir inlet shape = 0.69 ± 0.004.

ρ = density of the fluid.

The above equation holds good for $0.5 \leq Re \leq 100$, and the entrance to the capillary is sharp and square. Popular gas

viscometers employing capillary tube flow are Schultze's viscometer, Rapp's apparatus, Rankine's viscometer and Edward's constant volume viscometer.

1.3.2 Oscillating-Body Viscometer

These viscometers constitute a class where one body oscillates within a hollow body which is at rest (Figure 1-4). The concentric cylinder viscometer belongs to this family of viscosity measuring devices. It consists of an axially symmetric body which performs torsional oscillations in a fluid. The system is suspended from an elastic wire and the changes in the frequency, caused by the density and viscosity of the fluid, are measured and correlated to the viscosity of the fluid.

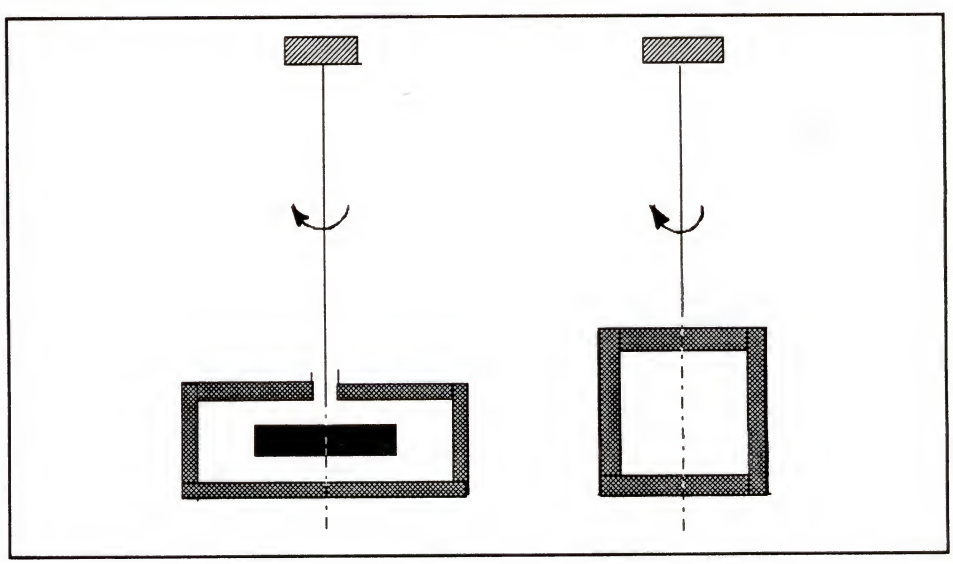

Figure 1-4 Oscillating body viscometer (fluid external and internal to the body)

The theory of all oscillating body viscometers can be formulated by a single mathematical schema (Kestin, 1988).

$$I\omega^2\left[\frac{d^2\alpha(\tau)}{d\tau^2}+2\Delta\frac{d\alpha(\tau)}{d\tau}+(1+\Delta_o^2)\alpha(\tau)\right]=M(\tau) \qquad (1\text{-}3)$$

Here $\alpha(\tau)$ is the angular displacement of the body from equilibrium, $\omega = (2.\pi/T_o)$ is the natural angular frequency of oscillation in a vacuum, T_o is the corresponding period of oscillation, $\tau = \omega t$ is the dimensionless time, I is the moment of inertia of the solid body, $I\omega^2$ is the spring constant, $M(\tau)$ is the frictional moment exerted by the fluid and Δ_o denotes the logarithmic decrement in a vacuum (for $M(\tau) = 0$).

Apart from the primary instruments, there are other devices that do not satisfy the accuracy of primary instruments but offer an opportunity to study a range of fluid states not available to the other techniques. The Torsional quartz-crystal viscometer and the falling body viscometer are two important members of the secondary class.

1.4 An Introduction to Drag Viscometer

Viscosity measurement for most viscometers is computed by ascertaining some parameter which can be precisely obtained experimentally. These parameters and the viscosity of the fluid are correlated through some accurate expressions which are derived analytically or numerically.

Viscosity of a fluid manifests its existence by providing drag on the body over which the fluid flows. However, the primary instruments do not measure the drag force but instead some secondary phenomenon associated with it. Viscosity measurement by utilizing the drag force has been limited to the falling sphere viscometer and liquids. The Reynolds number for such an exercise is in the creeping region, to exclude boundary layer separation and to derive an exact analytical expression. Even then some difficulty arises as the body may spin and not fall straight and deviate from the analytical conditions. Moreover, to obtain this small Reynolds number for gases, one has to employ micron-sized spheres. With this size constraint even the drag force is in the microgram range. Cosequently, many attempts to measure gas viscosity through direct drag measurement were unsuccessful. With the advent of the modern microbalance, this approach becomes feasible and has been employed in this work. The gas is allowed to flow over a sphere hung at the axis of a cylinder. Drag force is measured by an ultra- sensitive thermal microbalance. A relationship has been obtained to compute the viscosity from the drag force through dimensional analysis.

The set up of the drag viscometry system, has several advantages when it comes to measuring corrosive or extremely high temperature gases. The primary instruments have been very successful up to a temperature of 2000°K; beyond this

unascertained discrepancies take place. It is mainly because the measuring probes themselves are exposed to harsh conditions. Apart from this major shortcoming, in capillary tube viscometers there are other serious problems like the exact measurement of bore diameter due to thermal expansion, maintenance of an even temperature throughout the length of the capillary tube, ideal behavior of gases for the governing equations to hold good and in the case of coiled tubes, the maintenance of Dean number below the critical value of 10 for insignificant secondary flow. In all oscillating body viscometers some of the associated high temperature problems include selection of a suspension strand which has long-time elastic stability and low internal damping rate, oscillation time if measured through an optical telescope must take effects of refraction into account, and accounting for thermal expansion in the governing equation. As we shall see in the case of a drag based viscometer, we do not need to obtain an exact analytical solution. Results from dimensional analysis help in obtaining the value of viscosity quite accurately. The main measuring device, the thermal microbalance, is never exposed to the gas and is shielded from the unknown environment. The suspended sphere is subjected to the high temperature and a temperature gradient exists in the thermal boundary layer close it. As a result, the gas has a much lower temperature after it has flown over the sphere.

CHAPTER 2
SURVEY OF PREVIOUS EFFORTS FOR DRAG MEASUREMENT ON SPHERE

2.1 Drag on an Unbounded Sphere

The drag force on a body, exerted by the fluid flowing over it, is obtained by the solution of the Navier-Stokes' equation. However an exact result is not obtained in most of the cases. Analytical treatment of the Navier-Stokes equation for fluid flow is amenable at very low flow rates. At higher flow rates experimental results have been obtained for the drag force and analysis is done through numerical procedures. Since a host of physical phenomena occur for the flow over a sphere at different Reynolds numbers, empirical correlations differ for different flow regimes. Description of the flow field over a sphere has been provided in several text books. Broadly speaking the flow over a sphere remains unseparated until a Reynolds number of around 20. Beyond this there is onset of separation and the resulting wake remains steady until a Reynolds number of 130. After this discrete pockets of vortices begin to be shed and the wake looks unstable. For Reynolds numbers from about 20 to 400, the separation angle in degrees from the front stagnation point is given by $\theta_s = 180 - 42.5[\ln(Re/20]^{0.483}$. At Reynolds numbers beyond 400 the unsteady wake also becomes

asymmetric. Throughout the separation angle moves from behind the sphere in a forward direction; i.e., it moves against the flow direction. But at a Reynolds number beyond $2x10^5$ a drastic change in flow pattern takes place and the separation begins to move aft.

There is no single relation that is able to describe these different flow behaviours. For the case of a sphere G.G.Stoke (1845) was the first to give a solution for steady creeping flow past a rigid sphere. The analytical treatment was possible by neglecting the convective terms of the momentum equation. C.W.Oseen (1910) realized that the Stokes equation for creeping flow and finite Reynolds number is valid for distances less than a/Re, where a is the radius of the sphere and Re the Reynolds number. He incorporated the neglected inertial terms in a linearized form. Several series solutions were obtained for this Oseen equation by including from 1 to 24 terms. Following another line of thought I. Proudman and J. R. A. Pearson (1957)used perturbation techniques to solve the creeping flow over a sphere. But all these analytical exercises were limited to a Reynolds number of less than unity.

The boundary layer theory, which is an approximation of the Navier-Stokes equation obtained by neglecting the streamwise diffusion, has gained partial success in predicting fluid velocity. But it is applicable at higher Reynolds numbers (Re>3000) when the boundary layer thickness

is thin. There are severe limitations to this approach although it does provide a meaningful way to explain the fluid flow phenomenon. The major shortcomings are that: 1) the outer boundary, which is treated as potential flow, is true to the assumption until 30° from the front stagnation point; 2) once the flow separates, there is a convincing feedback by the downstream on to the oncoming flow; and 3) the boundary layer may not be negligible compared to body size at low flow rates. The latter effect has been accounted for by Gluckman (1971) through incorporation of a displacement thickness. Inspite of all this, not much headway has been made in this field for separated flows.

Numerical solution to the Navier-Stokes equation has been carried out to get drag measurement at higher flow rates when separation occurs. Due to computing difficulties encountered in the earlier days, the treatment was limited to a Reynolds number for which asymmetry had not set in. Several approaches to solve the Navier-Stokes' equation by the stream function-vorticity method were undertaken. Jenson (1959) and LeClair et al. (1970) used a steady state equation while Rimon and Cheng (1969) and Rafique (1971) used a time dependant momentum equation. Dennis and Walker (1971) expanded stream function and vorticity as a series of Legendres functions and their substitution into the governing equation resulted in a series of ordinary differential equations. However, this approach is not

attractive at higher Reynolds numbers since the number of terms to be included becomes prohibitively large.

Thus far the experimental study has unequivocally provided reliable values. The drag forces experimentally obtained have been presented in the form of a plot of coefficient of drag (C_D) vs. Reynolds number (Re) in several fluid mechanics books. In this study, the fluid situation is limited to laminar flows. Some of the important drag correlations in this regime are (Clift et al., 1978)

$$C_D=\frac{3}{16}+\frac{24}{Re} \quad ; \quad Re<0.01 \qquad (2\text{-}1)$$

$$C_D=\frac{24}{Re}[1+0.1315Re^{(0.82-0.05w)}] \quad ; \quad 0.01\leq Re\leq 20 \qquad (2\text{-}2)$$

$$C_D=\frac{24}{Re}[1+0.1935Re^{0.6305}] \quad ; \quad 20\leq Re\leq 260 \qquad (2\text{-}3)$$

$$\log_{10}C_D=1.6435-1.124w+0.1558w^2 \quad ; \quad 260\leq Re\leq 1500 \qquad (2\text{-}4)$$

where $w=\log_{10}^{Re}$. Other correlations for the drag forces have been judiciously compiled by R.Clift et al. (1978), and it was deemed unnecessary to duplicate the information here.

In conclusion, for free flow over a sphere, only experimental and numerical techniques can be used to provide accurate results at a high Reynolds number. In the experimental field the state-of-the-art instruments and measuring techniques will continue to provide accurate values. On the numerical side, both the finite difference

method and finite element method are being used as proficient techniques to gain success in this area.

2.2 Drag on a Bounded Sphere

The flow of fluid over a sphere confined by an external wall, is further complicated by the wall effects. As compared to an unbounded sphere, little work has been reported in this field. Theoretical work has been done for the creeping flow range. Coutanceau (1972) has provided some flow visualization results and Johansson (1974) worked out a numerical approach. These studies have been very limited in their function because of the various difficulties encountered.

In general, it has been found that the flow situation is governed by the size of the sphere, the cylinder size, the position and surface roughness of the sphere as well as the velocity profile of the oncoming flow (Figure 2-1). The effect of sphere and cylinder diameter size has been directly related in various correlations and this is noted later. The position of the sphere within the tube gives rise to an additional pressure drop within the latter. For standard, fully developed flow a smooth sphere, the drag forces on the sphere and the wall as a function of the sphere position has been looked into. Without going into

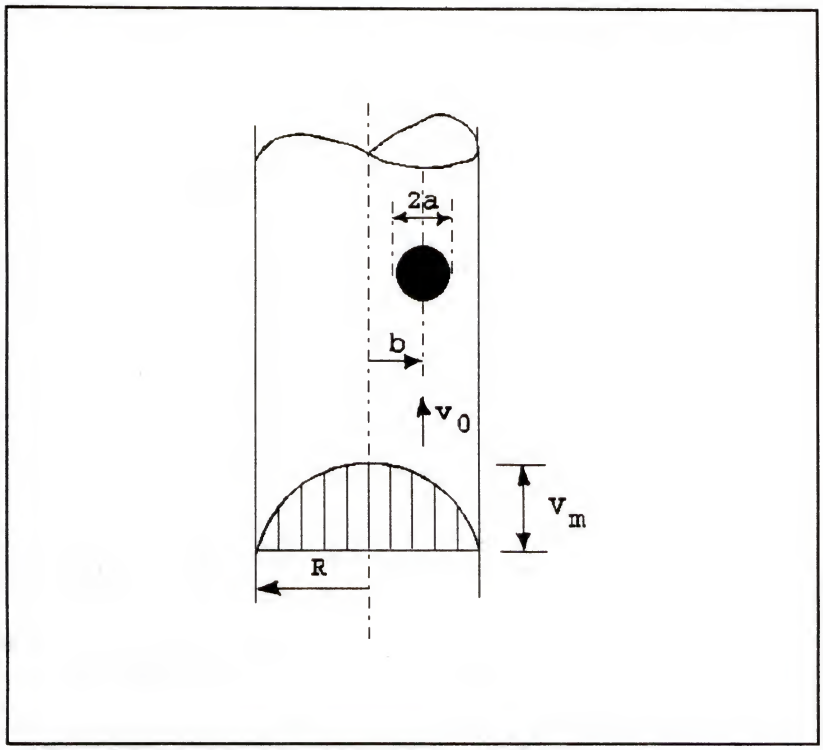

Figure 2-1 Sphere position and fluid motion in cylinder

mathematical details, it has been shown (Happel and Brenner, 1973) that to obtain a first approximation to the increased pressure drop arising from the presence of a particle in a bounded flow, the momentum theorem gives

$$F_w^+ = \left(\frac{V_0}{V_M} - 1\right) F \qquad (2\text{-}5)$$

where F_w^+ is the extra shearing force on the cylinder wall due to the presence of the sphere, V_m is the mean velocity with respect to the wall, v_0 is the approach velocity to the sphere and F is the drag force on the sphere. For a circular cylinder of radius R

$$\frac{V_0}{V_m} = [1 - (\frac{b}{R})^2] \qquad (2\text{-}6)$$

Thus from Equation 2-5 we find that if one moves from the cylinder axis (b/R =0) towards the wall (b/R =1), the direction of the extra force changes from being parallel to the drag to being oppositely directed. As a special case, when b/R = 0.707, the force no longer exists. For the case of determining the effects of surface roughness of the sphere, not much has been done at low to moderate flow rates. Achenbach (1974) has determined over the Reynolds number range (based on the minimum cross sectional area at the equator of the sphere) of $3x10^4<Re<2x10^6$ the effects of surface roughness. He showed that increasing the roughness parameter increased the critical drag coefficient to a maximum value of 0.4. However the Strouhal number for the vortex shedding remained unaffected and was equal its value for a smooth sphere.

Most of the work has been performed by experimentation. The results obtained can be divided on the basis that the sphere is falling in the fluid or it is held fixed against an oncoming fluid. In either case, studies have been performed to take into account the wall effect. A wall correction factor 'K' is normally used which gives the ratio of the drag force on the sphere in a bounded condition to that when the sphere is in infinite fluid flow.

2.2.1 Sphere Sedimenting in a Cylindrical Tube

Much work has been done for the case of a sphere sedimenting in a cylindrical tube. It was started as early as 1687 by Sir Isaac Newton and has received attention since then. As in the case of an unbounded sphere, there is difficulty in deriving a single expression for the fluid flow phenomenon. The interference effect of the cylindrical walls on the falling sphere is a function of Reynolds number and it decreases with increasing Reynolds number.

Table 2-1 Correlations for sphere sedimenting in a tube at low flow rates (Re<1)

Author	RELATIONSHIP FOR K ($C_D/C_{D\infty}$)
Ladenburg (1907)	$(1+2.1\beta)$; $\beta<0.1$
Faxen (1921)	$1/(1-2.104\beta+2.09\beta^3-0.95\beta^5)$; $\beta<0.2$
Francis (1933)	$(1-0.475\beta)^4/(1-\beta)^4$; $\beta<0.9$
Haberman (1958)	$(1-0.75857\beta^5)/(1-2.105\beta+2.0865\beta^3-1.7068\beta^5+0.72603\beta^6)$; $\beta<0.9$

Some of the important relationships for the wall correction factor "K" as a function of "ß" (diameter ratio of the sphere and the cylinder) for a sedimenting sphere on the axis of the cylinder,are shown in Table 2-1. The variation in the coefficient of drag with Reynolds number

has been plotted in Figure 2-2. For higher flow rates (Re>1000) some of the published values of "K" are provided in Table 2-2. The relationships in Table 2-1 were obtained by the analytical solution of the fluid flow equation at creeping range while results in Table 2-2 were through experimental procedure.

Table 2-2 Correlations for sphere sedimenting in a tube at high flow rates

AUTHOR	RELATIONSHIP FOR K ($C_D/C_{D\infty}$)
Newton (1687)	$(1-\beta^2)(1-\beta^2/2)^{0.5}$
Munroe (1888)	$1-\beta^{1.5}$
Lunnon (1928)	$1-0.23\beta$; $\beta<0.3$
Mott (1951)	$1/(1+16\beta^4)$; $0.5<\beta<0.7$ $1/(1+A\beta^2)$; $0.2<\beta<0.5$ and $1.8<A<3.2$

2.2.2 Sphere Fixed in a Cylindrical Tube

For the case of a sphere held fixed at the axis of the cylinder and against an oncoming flow, different correlations are available from the literature. In order to understand the phenomenon of fluidization, sedimentation and flow through fixed beds, researchers came up with relationships for the drag force on an unbounded and bounded

sphere. The important ones for creeping flows are give in Table 2-3.

Table 2-3 Correlations for sphere fixed in a tube at low flow rates (Re<1)

AUTHOR	RELATIONSHIP FOR K ($C_D/C_{D\infty}$)
Wakiya (1957)	$(1-0.1667\beta^2)/(1-2.105\beta+2.09\beta^3 1.11\beta^5)$
Brenner and Happel (1958)	$(1-0.1667\beta^2)/(1-2.105\beta)$
Haberman and Sayre (1958)	$(1-0.1667\beta^2-0.20217\beta^5)/(1-2.105\beta+2.0865\beta^3-1.7068\beta^5+0.72603\beta^6)$

For higher Reynolds numbers the notable relationships for "K" are

a) Fayon (1960) $K=[(1-0.1667\beta^2)/(1-2.105\beta+2.087\beta^3) + \{(C_A/C_S)-1\}\}$

where C_A and C_S are the actual coefficient of drag and the Stokes drag coefficient, respectively. The relationship is valid for Reynolds numbers less than 40 and $\beta<0.3$.

b) Clift et al. (1978) $K=1/(1-1.6\beta^{1.6})$; for $\beta<0.6$ and $100<Re<1000$

c) Achenbach (1972) $K=(1+1.4\beta^{4.5})/(1-\beta^2)^2$; for $Re > 10^5$.

A sphere may also exist in a cylinder without being sedimented or fixed by a support; it may be freely suspended. However, these freely suspended spheres generally do not remain fixed in space with respect to the containing tube. They may spin about their own axis and simultaneously rotate about the axis of the tube. Such dynamic effects are extremely difficult to handle analytically and cannot be predicted by dimensional analysis as a function of geometry although the phenomenon is itself related to the geometry. For these freely suspended spheres it has been found that for $\beta=0.2$, the spheres tend to stay to one side of the center of the tube and cling to the wall. Larger diameter spheres spin about their own axis and about the axis of the tube. Also, in spite of a fundamental difference in flow pattern past a fixed and freely suspended sphere, the drag coefficient is approximately the same for all practical purposes (Round et al. 1972). However, experiments conducted this way to correlate drag coefficient with Reynolds number for fixed spheres have not been considered in this study.

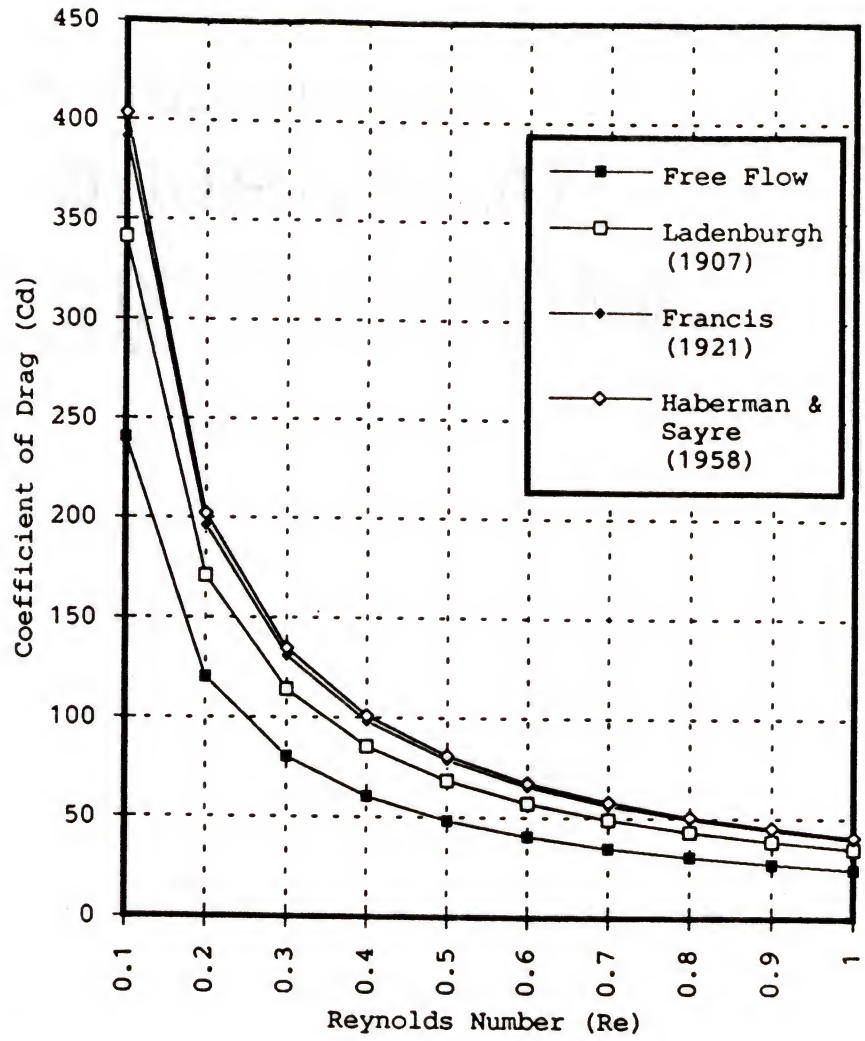

Figure 2-2 Plot of C_D vs. Re for sedimenting sphere in a tube

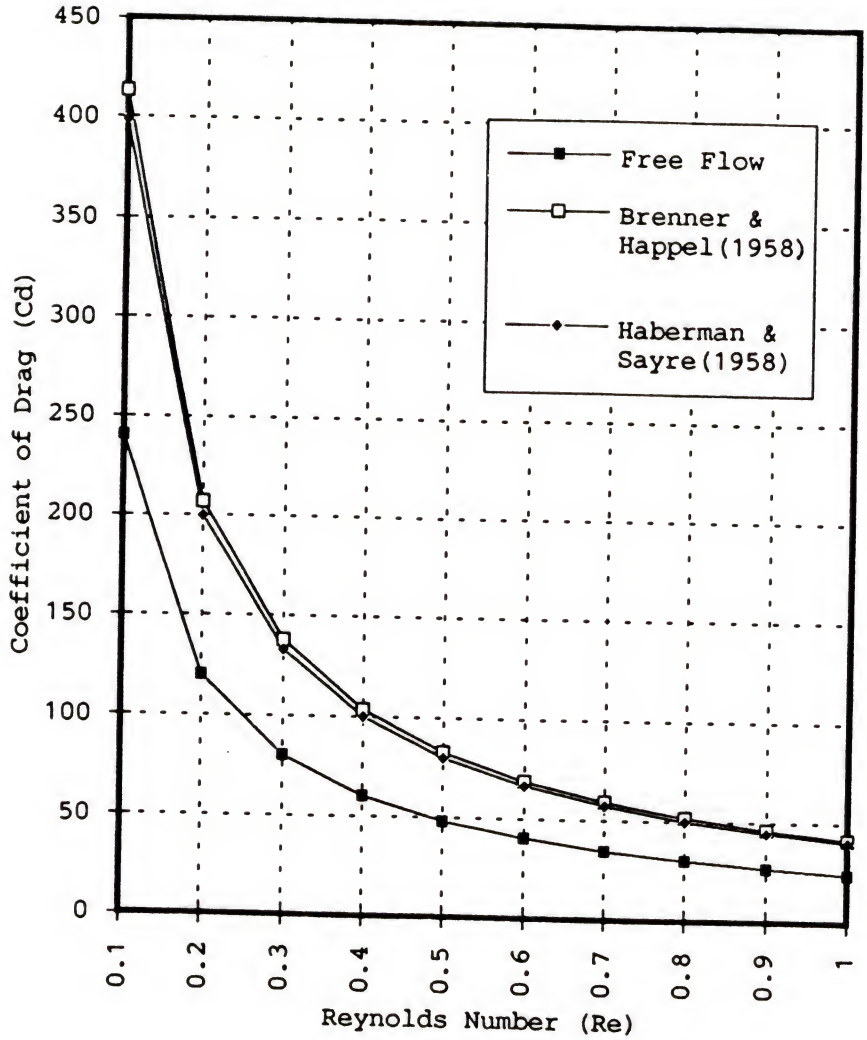

Figure 2-3 Plot of C_D vs Re for fixed sphere in a tube

CHAPTER 3
EXPERIMENTAL PROCEDURE

3.1 Considerations for Experimentation

For the results of any good experimentation to convey a meaningful information, some basic guidelines have to be adhered to. These guidelines vary with the nature of experiments. The current study has the objective of measuring the drag force over a bounded and suspended sphere. The measurements have then to be extended for the determination of viscosity. In general for primary viscometry, the experimental methods selected should satisfy the following conditions (Kestin and Wakeham, 1988):

a) Maintenance of a near-equilibrium state by use of small shear rates.

b) The preservation of hydrodynamic stability or, at least, the reduction of the effects of unavoidable instabilities to a negligible level.

c) The availability of a faithful mathematical model of the process and of an accurate solution in the form of an adequate working equation and a complete set of corrections.

d) High resolution in the detection of the major effect and operation at its lowest value consistent with the desired precision and the sensitivity of the working equation.

Compliance to these conditions usually helps in obtaining reliable values of viscosity for fluids.

3.2 Description and Working Principle of Apparatus

The experiment was performed by setting up the system as shown in Figure 3-1. Drag force measurement was done by using a Cahn Instrument manufactured C2000 model microbalance. The thermal microbalance is a very sensitive weight and force measurement instrument. It is designed for weights and forces up to 3.5 gram-force and is sensitive to changes as small as 0.1 microgram. The balance is divided into two sections; one section is the control unit where all controls and outputs are contained and the other section is the weighing unit which detects the actual weight or force. The weighing unit may be operated in vacuum, flowing gas or atmospheric conditions. The balance consists of (1) a balance beam mounted to, supported by and pivoting about the center of a taut ribbon; (2) a torque motor coil located in a permanent magnetic field and also mounted to the taut ribbon; (3) sample suspension fixtures; (4) a beam position sensor system; and (5) controls, circuitry and indicators (Figure 3-2). Weights or forces to be measured are applied to the sample (left) side of the beam which produces a force about the axis of rotation. An electric current flowing in the torque motor also produces a force about the same axis which is equal and opposite to the force from the beam if

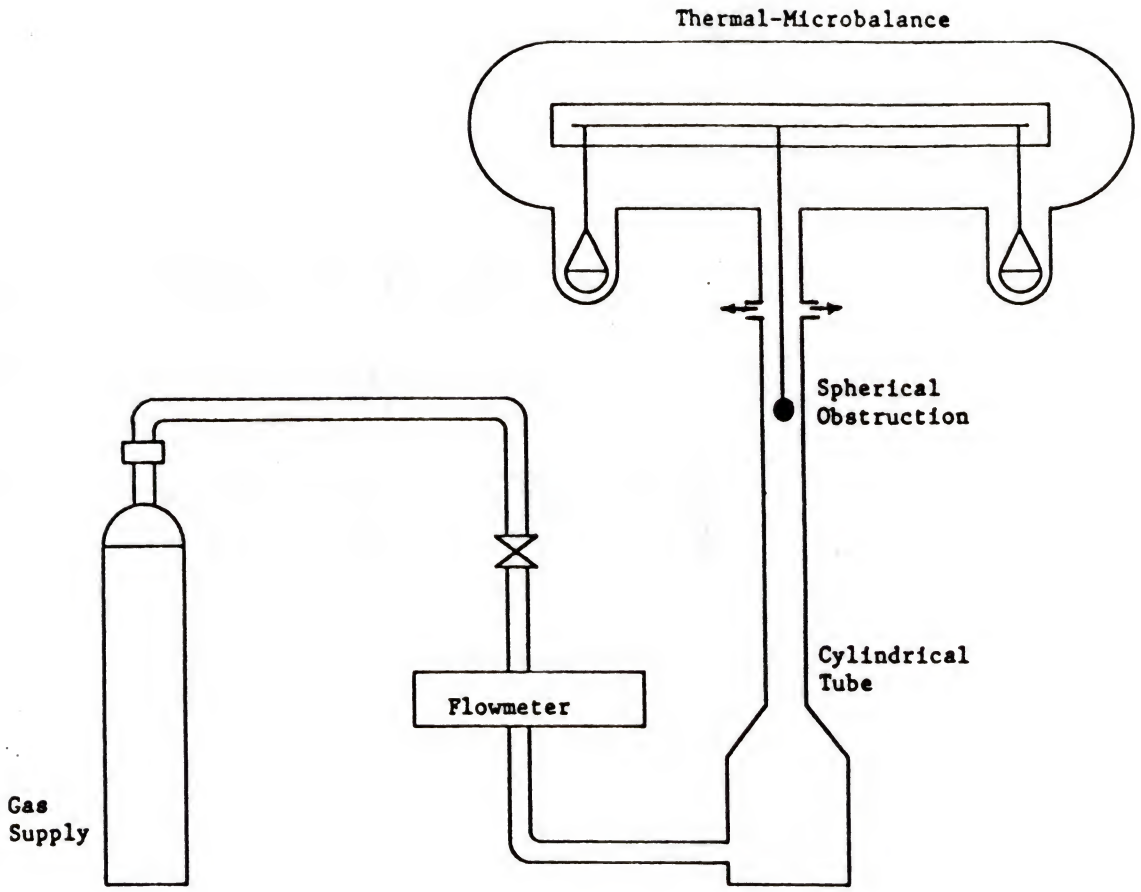

Figure 3-1 Experimental set-up for drag measurement

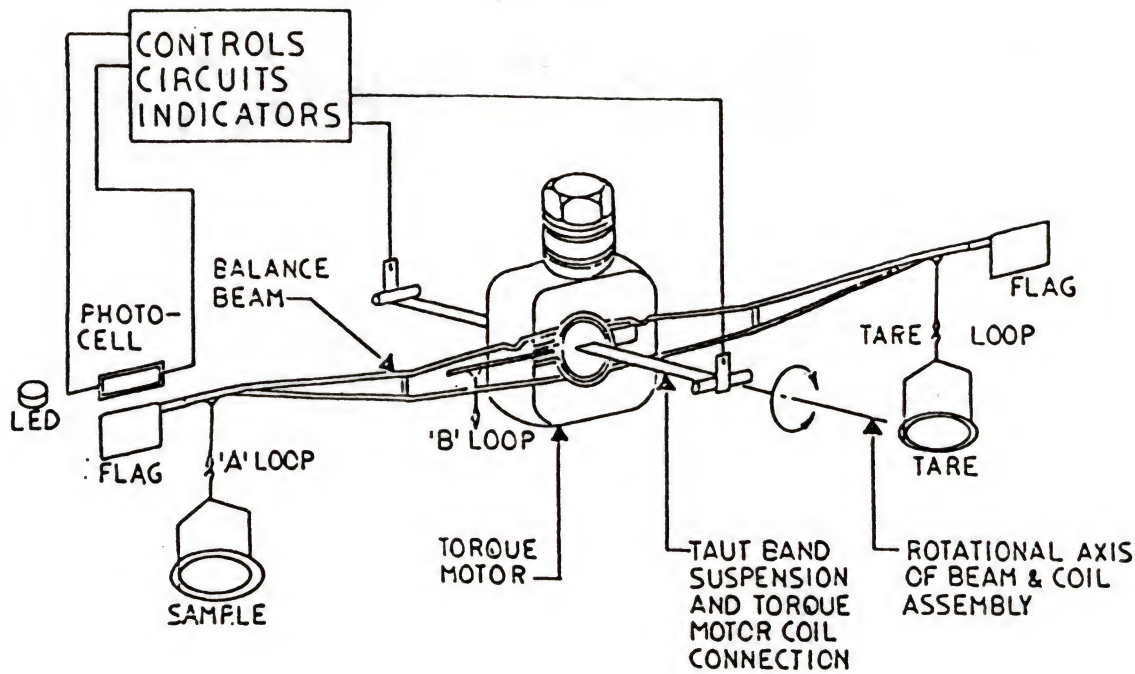

Figure 3-2 Microbalance beam assembly

the beam is at the reference beam position. This reference position is detected by the beam position sensing system. A greater force on the beam will require a greater opposite force from the torque motor to keep the beam at the reference position. Therefore, the current necessary to produce the required torque motor force is a direct measure of the force on the beam. The process of calibration allows this current to be measured in units of mass (grams) or force. The sensitivity and readability is 0.1 micrograms; repeatability is 10^{-5} of the total load (max. 0.2 microgram); accuracy is ±0.1% of the recorder range plus 1.5 X 10^{-4} of the suppression range for absolute weighing.

The gas flow meter used was an Omega Engineering Inc. FMA 800 series mass flow meter with a range of 0-50 Lt/min. Like most mass flow sensors, it measures mass flow directly without the need for temperature or pressure corrections, and the controllers can automatically control flowrate regardless of variation in line pressure (over a limited pressure range). The measuring unit features a corrosion resistant stainless steel and Viton construction and a 50 micron inlet screen to prevent contamination of the sensor. The flow body has a leak less than 10 atm-cc/sec of helium. The FMA 800 series mass flow sensor operates on the principle of heat transfer, by sensing the change in temperature (ΔT) along a heated section of a capillary tube. Part of the total flow is forced through the capillary by

means of a pressure differential of approximately 0.45 psi. The required maximum flow rate determines the number of discs; these are bolted together and constitute the laminar flow device. The design of the discs is such that flow conditions in both the capillary and laminar flow device are comparable, thereby resulting in proportional flow rates through them. The ΔT sensed by the upstream and downstream temperature sensors on the capillary depends on the amount of heat absorbed by the mass of the gas flow. The mass of the gas being virtually independent of the temperature and pressure makes the instrument independent of temperature and pressure variations i.e. a mass flow meter.

3.3 Experimentation

During experimental measurements, consideration was given to the tube size, flow rate and sphere diameter and its weight. Teflon balls of different diameter (β= 0.35, 0.42, 0.49, 0.56) were centrally hung into a long cylindrical tube of diameter 22.45 mm. The spheres were suspended by means of a fine nylon string (d=0.07 mm) from loop B of the microbalance (Figure 3-2). No special attempt to determine the sphericity of the teflon balls was made. Drag measurement using the C2000 microbalance was dictated by maximum mass restriction of 3.5 grams and this was a guide line for choosing the light weight and smooth teflon balls. Operating limits were calculated approximately to

insure that the tube Reynolds number was small enough to avoid either incipient transition to turbulence or unduly long entrance length. A rough estimate for the entrance length L_e in tubes can be obtained from the relationship $L_e/D = 0.06\ Re$; where D is the tube diameter and Re is the Reynolds number based on the mean flow velocity. In all the measurements reported here, this criterion was satisfied.

Drag on the sphere was obtained by flowing nitrogen gas with a Reynolds number (based on mean velocity and tube diameter) of 40 to 1000. The difference in reading, as given by the microbalance, with the gas flowing and with no gas flow gives us the total drag force exerted on the ball and the string. The drag on the string was calculated by using different string lengths for hanging the same ball under the same flow conditions. The difference of the two readings, at two different string lengths, was due to the drag on the string alone. This value was subtracted from the original reading to obtain the drag on the sphere alone. For example; let D_1 = Drag on sphere (D_{sp1}) + Drag on first string (D_{st1})

D_2 = Drag on sphere (D_{sp2}) + Drag on second string (D_{st2})

If the length of the second string (L_2) is greater than the first (L_1) then the drag on the string per unit length is

$(D_{unit}) = (D_2 - D_1)/(L_2 - L_1)$.

$\therefore$, $D_{sp1} = D_1 - (D_{unit})L_1$

or $D_{sp2} = D_2 - (D_{unit})L_2$

The two values of D_{sp} obtained in this way, maintaining the same flow conditions for the sphere and tube, should be equal if the approximation is good. Table 3-1 provides some of the values obtained to justify the point.

Table 3-1 Table of drag values obtained by two different string lengths

Re	ß (d/D)	D_{unit} (N/m)	D_{sp1} (N)	D_{sp2} (N)
187.46	0.35	1.28419E-8	2.71619E-8	2.71619E-8
429.32	0.35	1.39126E-7	6.71933E-8	6.71933E-8
680.08	0.35	2.16715E-7	1.45222E-7	1.45222E-7
187.40	0.42	5.45800E-8	2.96641E-8	2.96641E-8
434.38	0.42	1.11728E-7	1.01855E-7	1.01855E-7
678.37	0.42	1.63716E-7	2.14169E-7	2.14169E-7
185.69	0.49	1.01428E-7	3.76202E-8	3.76196E-8
430.96	0.49	1.50775E-7	1.31952E-7	1.31951E-7
677.95	0.49	2.78858E-7	2.73101E-7	2.73097E-7
194.84	0.56	1.11124E-7	5.58023E-8	5.58022E-8
431.15	0.56	2.15246E-7	1.91915E-7	1.91915E-7
675.27	0.56	3.54523E-7	4.05596E-7	4.05596E-7

In Table 3-1 the Reynolds number is based on tube diameter and mean velocity of flow.

Therefore it is safe to assume that the method to obtain value of drag force on the sphere by using two different string lengths is quite accurate. Figure 3-3 shows the coefficient of drag obtained during this experiment for sphere to cylinder diameter ratio (ß) of 0.5, and as given by other authors.

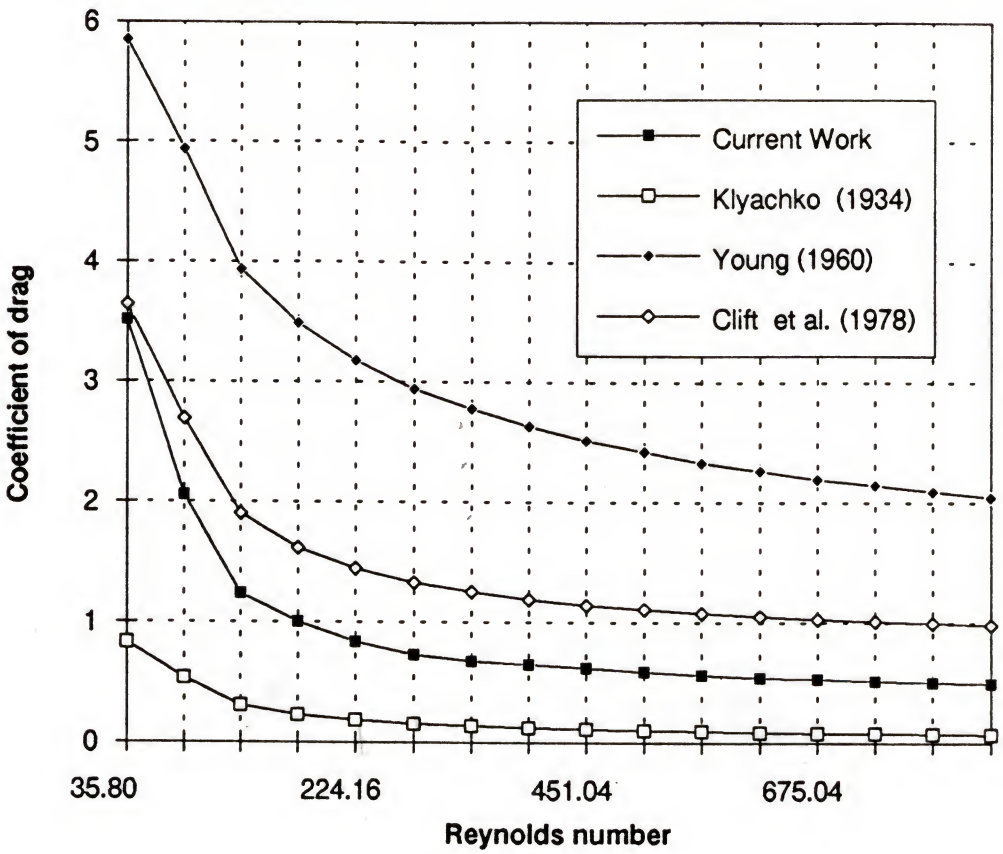

Figure 3-3 Coefficient of drag (C_D) vs. Reynolds number (ß=0.5)

3.4 Experimental Observations

In order to conduct a meaningful experiment it is necessary to obtain a steady operational point. Some of the salient features which were observed during the experimental runs and which in turn helped us to set up a good experimental platform are briefly discussed here. It was noticed that if the sphere was hung too low in the cylinder two problems arose: a) the undeveloped flow caused oscillation in the drag reading output and b) the drag on the string, which should be low for approximate elimination, becomes comparable to the sphere drag. This problem is overcome by utilizing a fully developed flow condition. In this situation the readings obtained are steady. It was also observed that the repeatability of the experiment was dependant on the ball diameter. When ß (=d/D) is equal to 0.5, experimental results repeatedly matched the same values. Although not much work was done to corroborate it, an eccentric position of the sphere seemed to affect the readings by making it unstable. Thus care should be taken to hang the sphere in the central position. Lastly, elimination of string drag by using two different string lengths, under the same set-up, provided excellent results for calculating the drag on the sphere alone. Drag measurements by this tactic gave matching results for sphere drag with two different string lengths for 4 decimal places (in mg scale).

This helps us to accurately plot the dependance of the coefficient of drag on flow Reynold's number.

For viscosity measurements the following points need to be addressed. Firstly, a low flow rate is needed. This assures that the fluid has deviated a negligible amount from its equlibrium condition. Since viscosity is a thermophysical property, it is dependant on the thermodynamic condition. In order to measure it, a velocity gradient needs to be created. This dissipation creates a temperature change, however small it may be. To keep the change to a minimum, creeping flows are normally employed. Thus, good measurements are performed in the presence of very small gradients and the average of pressure,temperature and density values suffice to indicate the local thermodynamic state. Our experiments have been performed at higher Reynolds number to basically understand the physics at several flow rates. However, the accuracy of the measuring instrument is capable of making very sensitive and precise measurements at low flow rates. Secondly, the preservation of hydrodynamic stability is attained through fully developed flow, using a sphere diameter which is half that of the cylinder ($\beta = 0.5$), and the central positioning of the sphere in the cylinder. Thirdly, an exact mathematical expression for the drag force exerted on a sphere centrally suspended in a tube and experiencing a Poiseuille flow is given by the Haberman and Sayre (1958) equation

$$DRAG = -6\pi\mu R U_{max} \frac{(1-\frac{2}{3}\beta^2-0.20217\beta^5)}{(1-2.105\beta+2.0865\beta^3-1.7068\beta^5+0.72603\beta^6)}$$

(3-1)

The negative sign indicates that the drag is opposite to the direction of the flow. And finally, the high resolution in the detection of the major effect, which happens to be the drag force, is deftly acquired through modern ultra precise instruments. All these properties contribute to making the measurement of viscosity through drag force measurement a successful approach.

3.5 Viscosity from Drag Measurement

The total drag on an object in a stream of fluid consists of skin friction and the form or pressure drag. The former is the integral of all the shearing stresses taken over the surface of the body while the latter is the integral of normal force. The sum of the two is called the total or profile drag. For free flow the skin friction can be calculated with some accuracy by employing boundary layer theory and it is here that the role of viscosity also comes into the picture. The form drag which does not exist in frictionless flow, is due to the fact that the presence of a boundary layer modifies the pressure distribution on the body as compared to an ideal fluid. However, the computation of form drag is very difficult. Consequently, reliable data

on total drag is in general obtained by measurement. Once the total drag (profile drag) is obtained, the coefficient of drag (C_D) for the body can be calculated from:

$$D=\frac{1}{2}\rho U^2 A C_D \qquad (3\text{-}2)$$

where D is the profile drag, ρ is the density of the fluid, U is the velocity of the fluid and A the cross sectional area of the body. From dimensional analysis, we find that for a particular configuration and flow condition there is a unique curve for C_D and the flow Reynolds number (Re). The main aim is to accurately plot this curve. After this curve has been obtained, viscosity can be calculated as follows:
a) The sample gas is flown over the bounded sphere and the mean flow velocity is accurately determined by a flowmeter. Care should be taken so that the sphere is centrally positioned in the tube and the velocity is fully developed.
b) From equation 3-2 the coefficient of drag (C_D) is calculated. It is assumed that the density of the gas is known and so is A, the cross sectional area of the sphere.
c) From the plot of C_D vs. Re, the Reynolds number is obtained which gives the value of the viscosity.

Values of viscosity were obtained for oxygen and helium gas at room temperature by this method. Table 3-2 shows the some of the errors that were obtained during this study.

Table 3-2 Errors obtained at room temperature during viscosity measurements

Reynolds Number	O_2 Error (%)	He Error (%)
150.0	0.77	0.92
200.0	0.71	0.88
250.0	0.70	0.90
300.0	0.68	0.85
400.0	0.65	0.83
500.0	0.82	0.93

CHAPTER 4
PROBLEM ANALYSIS

4.2 Drag Force on a Cylindrically Bounded Sphere

A short description of this problem has already been provided in Section 2.2.2. Since this happens to be the backbone for comparison of our results with different work, some more information is provided here.

Due to the complexity of the general Navier-Stoke's equation, analytical derivation of the drag force has been limited to the creeping flow regime. In this region the Navier-Stokes equation reduces to a linear, fourth order, partial differential equation. Initial treatment concerned uniform flow (Lamb 1932) and later boundary conditions were imposed by considering an infinitely long cylindrical tube (Lee 1947; Haberman & Sayre 1958). Finally solution for creep flow about a sphere bounded by cylindrical walls and suspended in a Poiseuille flow was undertaken. Johanssen (1974) reported numerical calculations of flow around a sphere fixed on the axis of a Poiseuille flow. Only solutions for ß (d/D) = 0.1 were reported. The term ß is the diameter ratio of the sphere (d) and the cylinder (D). Some experiments were carried out at slightly higher Reynolds number. Fayon and Happel (1960) performed experiments upto

Reynolds numbers of 40 while Eichhorn and Small (1964) extended the study upto Reynolds numbers of 250. However, these works were handicapped, as concluded by their authors themselves, in not measuring the drag accurately and in their inability to change some important variables which were related to the operating characteristics of the apparatus and intrinsic to the experimental set-up.

At the other end of the flow spectrum, experiments have been performed for flow past spheres at very high Reynolds number ($Re > 10^5$) (McNown & Newlin 1951; Achenbach 1974). The basic attempt was to relate the coefficient of drag to the flow Reynolds number based on the mean approach velocity and ß (=d/D). The cylindrical wall increases the supercritical drag coefficient well above the value of 0.3, as arbitrarily chosen to define critical number for a sphere in an unbounded flow. The critical Reynolds number based on the mean approach velocity decreases from 3.65×10^5 in an unbounded fluid to 1.05×10^5 for d/D=0.916.

Taking these results into account, Clift et al (1978) have tried to bridge the region between the high and low flow regimes by interpolation. However, this curve fitting method does not model any actual experimental data and the results are open to doubts. The existing experimental findings in the laminar region (Klyachko 1934; Young 1960) offer results which are not in agreement. This is primarily due to the varied experimental approach, the manner in which

inlet flow conditions were obtained, and other diverse operational parameters involved.

To the authors knowledge, no experiment has been performed to measure drag on a sphere in a Poiseuille flow with a device having a sensitivity of 0.1 micrograms. Together with this precise thermal-microbalance an accurate gas flow meter with an accuracy of ±1% is employed. Very smooth teflon balls of different diameters (d= 7.88 mm, 9.49 mm, 11.06 mm and 12.67 mm) were centrally hung by means of a nylon string. The whole experiment was performed with the gas flowing through a 22.45 mm diameter cylindrical tube.

4.3 Coefficient of Drag for a Bounded Sphere

The drag force exerted on a sphere bounded in a Poiseuille flow is a function (Figure 4-1) of approach velocity u_0, fluid density ρ, fluid viscosity μ, sphere diameter d, the tube diameter D, the eccentricity n and the surface roughness of the ball ϵ; viz.

$$F_D = f(u_o, \rho, \mu, d, D, n, \epsilon) \qquad (4\text{-}2)$$

The teflon balls had a very smooth surface and were accurately hung at the center of the cylinder. This eliminated n and ϵ and in terms of dimensionless parameters the above relationship can be expressed as:

$$\frac{2F_D}{\rho u_o^2 A} = f\left(\frac{\rho u_o D}{\mu}, \frac{d}{D}\right) \qquad (4\text{-}3)$$

where A is the cross sectional area of the sphere at its equatorial plane.

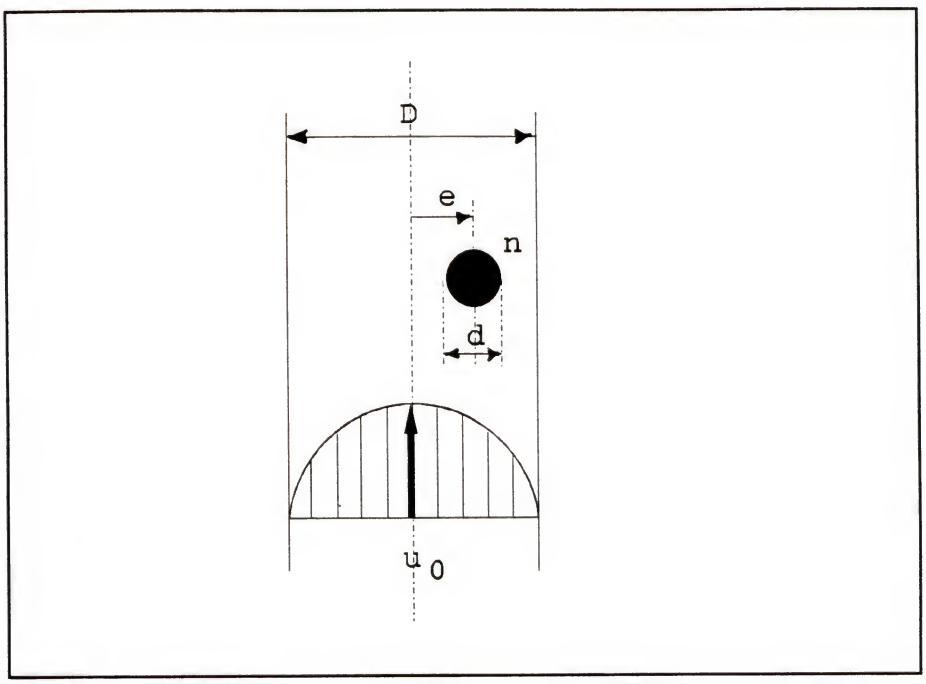

Figure 4-1 Parameters effecting drag on a sphere within a circular tube

The drag forces exerted on the sphere can also be written as :

$$2F_D=C_D\rho u_o^2 A \qquad (4\text{-}4)$$

From Equations (4-3) and (4-4) the drag coefficient is given by:

$$C_D=f(Re,\beta) \qquad (4\text{-}5)$$

where Re is the Reynolds number based on the mean approach velocity and the tube diameter D.

Klyachko (1934), worked on sedimentation of solid

particles in fluids and gave the following relationship for C_D and Re, Re being based on centerline velocity and sphere diameter.

$$C_D=\frac{24}{Re}+\frac{4}{3\sqrt{Re}} \qquad (4\text{-}6)$$

where Re < 1000 and $0.224 \leq d/D \leq 0.548$.

Fayon and Happel (1960) performed experiments within Re of 40, and Re had the same definition as Klyachko's:

$$\frac{W}{6\pi\mu ua}=\frac{1}{1-2.105(\frac{a}{R})+2.087(\frac{a}{R})^3}+(\frac{C_A}{C_S}-1) \qquad (4\text{-}7)$$

where W is the weight of the solid body, u is the mean approach velocity, μ is the fluid viscosity, a is the radius of the spherical body, R the radius of the enclosing cylindrical pipe, C_A the drag coefficient for the sphere in an unbounded system as obtained from experiment and C_S the drag coefficient according to the Stoke's law.

In the range 10^4 < Re < 10^5, McNown and Newlin (1951) studied the cylindrical wall effect on the drag of a sphere by measuring the pressure distribution of the flow of air around a sphere. McNown, Lee and McPherson (1948) had earlier related C_D with d/D as

$$C_D=(\frac{40}{Re})(1-\frac{d}{D})^{-\frac{5}{2}} \qquad (4\text{-}8)$$

in the range Re < 200. They then interpolated the results to plot the variation of C_D with Re in the range 200 < Re <10^4.

Here too the Reynolds number (Re) is based on the centerline velocity and the diameter of the sphere.

Young (1960) obtained an expression for C_D by suspending the spheres eccentrically in a tube. For a Reynolds number between 35 and 1115 he proposed a relationship

$$C_D = Re^{-\frac{1}{3}}\left[94.5\left(\frac{d}{D}\right)^{2.57}+10\right] . \qquad (4-9)$$

In the above correlation, Young defined Reynolds number on the basis of the mean velocity of flow in the pipe and the pipe diameter.

Eichhorn and Small (1964) investigated the fluid dynamic forces on spheres suspended in Poiseuille flow. Small spheres were suspended in a cylindrical tube containing a laminar upward flow of water. Experiment was performed in the Reynolds number range of 80 to 250. They could not come up with an accurate and definitive statement about the form of Re_D and C_D, because of insufficient and inaccurate data.

Clift et al. (1978) combined the relationship for many observed data that fell in the laminar range but were mostly influenced by the work of McNown and Newlin (1951). As a result, they observed that for Re (based on the approach or centerline velocity and sphere diameter) lying between 100 to 10^4

$$C_D = \frac{C_{D\infty}}{[1-1.6(\frac{d}{D})^{1.6}]} \quad ; \qquad \frac{d}{D} \leq 0.6 \qquad (4\text{-}10)$$

where $C_{D\infty}$ is the drag coefficient on a sphere in an unbounded flow.

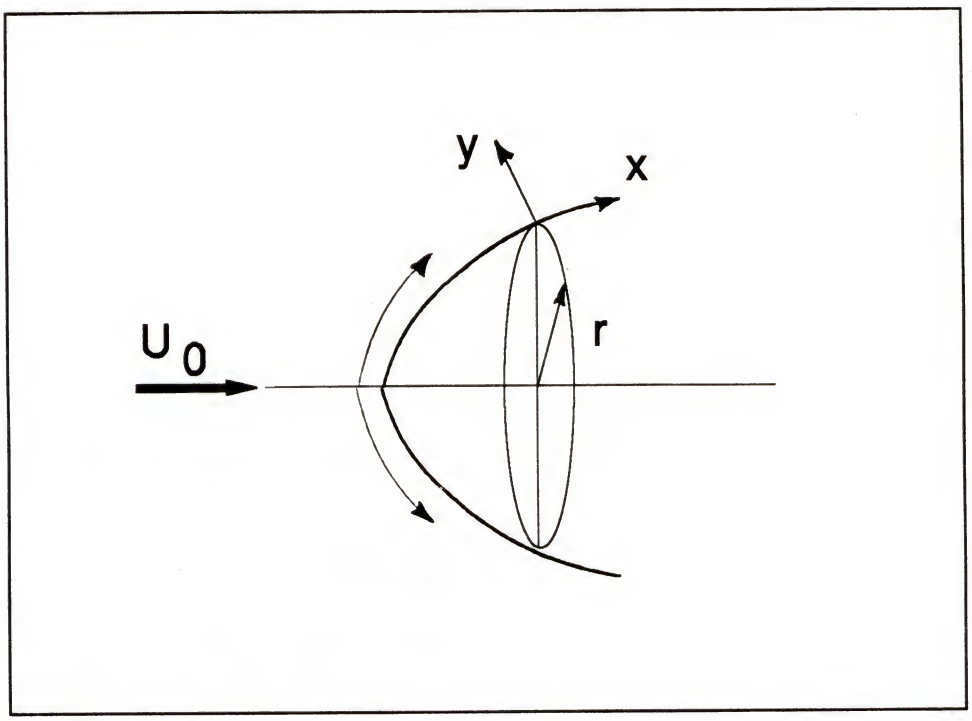

Figure 4-2 Curvilinear coordinate system

4.4 Fluid Flow Analysis

An exact solution of the Navier-Stokes equation allows the evaluation of fluid flow parameters throughout the flow domain. In our case, as in most of the practical instances, unfortunately no exact analytical treatment of the momentum equation is possible and recourse has to be taken to either numerical or experimental techniques to estimate the flow

conditions. In the case of an unbounded sphere it is found that for a Reynolds number of 3000, the boundary layer approximation to the Navier-Stokes equation gives a correct estimate of the separation angle. On the same lines it is assumed that for a very small diameter of the sphere compared to the diameter of the cylinder and for high flow rates, the boundary layer analysis may be able to predict the separation angle.

The steady state boundary layer equations, according to Boltze (1908), are

$$u\frac{\partial u}{\partial x}+v\frac{\partial u}{\partial y}=-\frac{1}{\rho}\frac{\partial p}{\partial x}+\nu\frac{\partial^2 u}{\partial y^2} \qquad (4\text{-}11)$$

$$\frac{\partial (ur)}{\partial x}+\frac{\partial (vr)}{\partial y}=0 \qquad (4\text{-}12)$$

Here a curvilinear system of co-ordinate is adapted, (Figure 4-2) where x is measured along the body surface and y perpendicular to it. Variables u and v are the velocities in the x and y direction, respectively, p is the pressure, ν the kinematic viscosity of the fluid, and r the radius of curvature of the body. Equations 4-11 and 4-12 have been solved for an unbounded fluid by Schlichting (1968). We find that the boundary conditions governing the boundary layer equation over the sphere are the same, both for bounded and unbounded fluid. At y = 0 , i.e. at the body surface, a no-

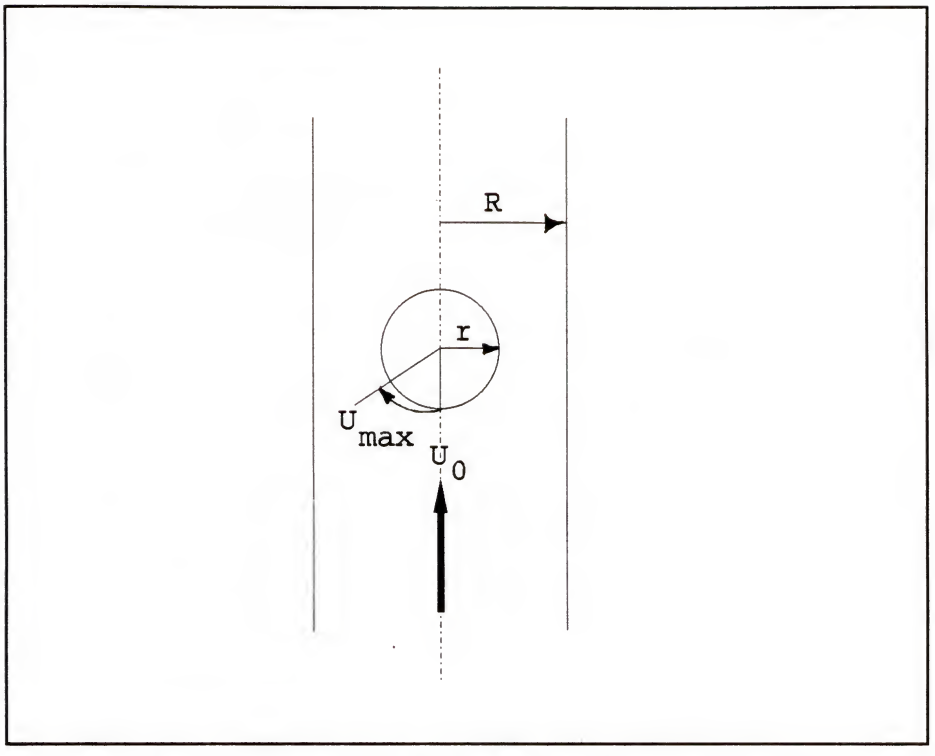

Figure 4-3 Accelerated flow along a sphere in a tube

slip condition exists viz. u = v = 0. At y = δ (boundary layer thickness) for an unbounded flow $\partial u/\partial y = 0$ since there is potential flow beyond the boundary layer thickness. In our case, however, at y = δ, u = $U_{max}(x)$ and hence $\partial u/\partial y = 0$ (Figure 4-3). Thus, both the upper and lower limits for the boundary layer are satisfied by the same conditions and we can carry out the analysis as done for a sphere in infinite flow. The change that needs to be incorporated is the variation of $U_{max}(x)$ over the body surface. It is not accelerated as given by the potential flow, but accelerated due to the change in the flow cross sectional area viz. $[\pi.R^2(1 - \beta^2\sin^2\phi)]$ as well as due to the body curvature.

Here R is the radius of the cylinder, ß is the diameter ratio of the sphere and the cylinder and ϕ is the angle from the front stagnation point at which the cross sectional area is being measured. As a result $U_{max}(x)$ will vary as $U_0 \sin\phi/(1-ß^2\sin^2\phi)$.

The computations are carried out by choosing

$$U_{max}(x) = u_1 x + u_3 x^3 + u_5 x^5 + \ldots \qquad (4\text{-}13)$$

$$\text{and } \Psi(x,y) = \sqrt{\frac{\nu}{2u_1}}\,[u_1 x f_1(\eta) + 2u_3 x^3 f_3(\eta) + 3u_5 x^5 f_5(\eta) + \ldots \qquad (4\text{-}14)$$

where u_1, u_3, u_5 etc. are the unknown coefficients for U_{max}'s dependance on x; $f_1(\eta)$, $f_3(\eta)$, $f_5(\eta)$ etc. are the functional coefficients as obtained from the Blasius series; $\eta = y\sqrt{(2u_1/\nu)}$ is the dimensionless distance from the wall with ν being the kinematic viscosity of the fluid and $\Psi(x,y)$ is the stream function. For an axially symmetric case we have for the x-direction velocity

$$u(x) = \frac{1}{r}\frac{\partial(\psi r)}{\partial y} = \frac{\partial \psi}{\partial y} \qquad (4\text{-}15)$$

which from Equation 4-14 gives

$$u(x) = u_1 x f_1' + 2u_3 x^3 f_3' + 3u_5 x^5 f_5' + 4u_7 x^7 f_7' \ldots \qquad (4\text{-}16)$$

If the outer velocity is accelerated according to our assumption:

$$U_{max}(x) = KU_0 \frac{\sin\phi}{(1-\beta^2\sin^2\phi)} \qquad (4\text{-}17)$$

where K is an arbitrary constant, then

$$U_{max}(x) = KU_0\left(\frac{T_1\phi}{1!} + \frac{T_3\phi^3}{3!} + \frac{T_5\phi^5}{5!} + \frac{T_7\phi^7}{7!} + \ldots\right) \qquad (4\text{-}18)$$

where the terms in the parantheses are obtained by expanding $(\sin\phi)/(1-\beta^2\sin^2\phi)$ as a power series and the terms T_1, T_3, T_5, T_7, etc are computed and found to be

$$T_1 = 1$$

$$T_3 = 6\beta^2 - 1$$

$$T_5 = 120\beta^4 - 60\beta^2 + 1$$

$$T_7 = 5040\beta^6 - 4200\beta^4 + 546\beta^2 - 1$$

For a sphere in infinite flow it is observed that $\beta=0$ and $K=1.5$.

Since $\phi=(x/r)$, where r is the radius of curvature at a distance x from the front stagnation point, we can compare the coefficients of x in Equations 4-13 and 4-18 to get: $u_1 = K\,U_0T_1/r$, $u_3 = K\,U_0\,T_3/r^3$, $u_5 = K\,U_0T_5/r^5$ ... and so on. Substituting the values of these coefficients into Equation 4-16 we obtain:

$$u(x) = KU_0\left[\left(\frac{x}{r}\right)f_1'\frac{T_1}{1!} + 2\left(\frac{x}{r}\right)^3 f_3'\frac{T_3}{3!} + 3\left(\frac{x}{r}\right)^5 f_5'\frac{T_5}{5!} + 4\left(\frac{x}{r}\right)^7 f_7'\frac{T_7}{7!} + \ldots\right] \qquad (4\text{-}19)$$

The shear stress is obtained at the surface (y=0) by Newton's equation:

$$\tau_0=\mu\left(\frac{\partial u}{\partial y}\right)_0 \tag{4-20}$$

Since $\eta=y\sqrt{(2u_1/\nu)}$, we get

$$\left(\frac{\partial u}{\partial y}\right)_0=\left(\frac{\partial u}{\partial \eta}\frac{d\eta}{dy}\right)_0=\left(\frac{\partial u}{\partial \eta}\right)_0\sqrt{\frac{2KU_0}{r\nu}} \tag{4-21}$$

As a result of this, the shear stress is now given by

$$\tau_0=\mu\sqrt{\frac{2KU_0}{r\nu}}\left[KU_0\left\{\left(\frac{x}{r}\right)f_1''+2\left(\frac{x}{r}\right)^3 f_3''\frac{T_3}{3!}+3\left(\frac{x}{r}\right)^5 f_5''\frac{T_5}{5!}+\ldots\right\}\right] \tag{4-22}$$

In order to make a comparison with the unbounded flow case, we set K=1.5 and obtain

$$\frac{\tau_o}{0.5\rho U_{max}^2}=\frac{7.3485}{\sqrt{Re}}F(\beta,\phi) \tag{4-23}$$

where τ_o = the shear stress

ρ = density of the fluid

U_{max} = maximum velocity in the conduit

Re = flow Reynolds number based on sphere diameter

$$\text{and, } F(\beta,\phi)=\frac{\phi T_1 f_1''}{1!}+\frac{2\phi^3 T_3 f_3''}{3!}+\frac{3\phi^5 T^5 f_5''}{5!}+\frac{4\phi^7 T^7 f_7''}{7!}+\ldots \tag{4-24}$$

values of f_1", f_3", f_5" and f_7" can be obtained from the literature and are provided in Appendix A.

For flow separation τ_o = 0 i.e. $F(\beta,\phi)$= 0. Substituting the relevant values of T_i and f_i'' (i=1,3,5 ...) we get:

$$\phi(0.9277)+\phi^3(2.095\beta^2-0.3641)+\phi^5(3.2466\beta^4-1.5495\beta^2)+$$
$$\phi^7(4.396\beta^6-3.4907\beta^4+0.4687\beta^2-0.0015)=0 \qquad (4-25)$$

where Φ is the separation angle. We find that the angle of separation is dependant on the sphere diameter, if the cylindrical wall's dimension is unchanged, unlike in the case of unbounded fluid where the angle of separation is constant. Table 4-1 provides values of flow separation angle as a function of sphere-to-cylinder diameter ratio (ß=d/D).

Table 4-1 (ß=d/D) vs. separation angle (ϕ_{sep})

Diameter ratio (ß)	Separation Angle (ϕ_{sep}) in degrees
0.0	109.60
0.1	123.86
0.2	109.36
0.3	108.46
0.4	92.61
0.5	88.35
0.6	90.53
0.7	106.16

Figure 4-4 shows the variation of shearing stress over the surface of the bounded sphere for a laminar boundary

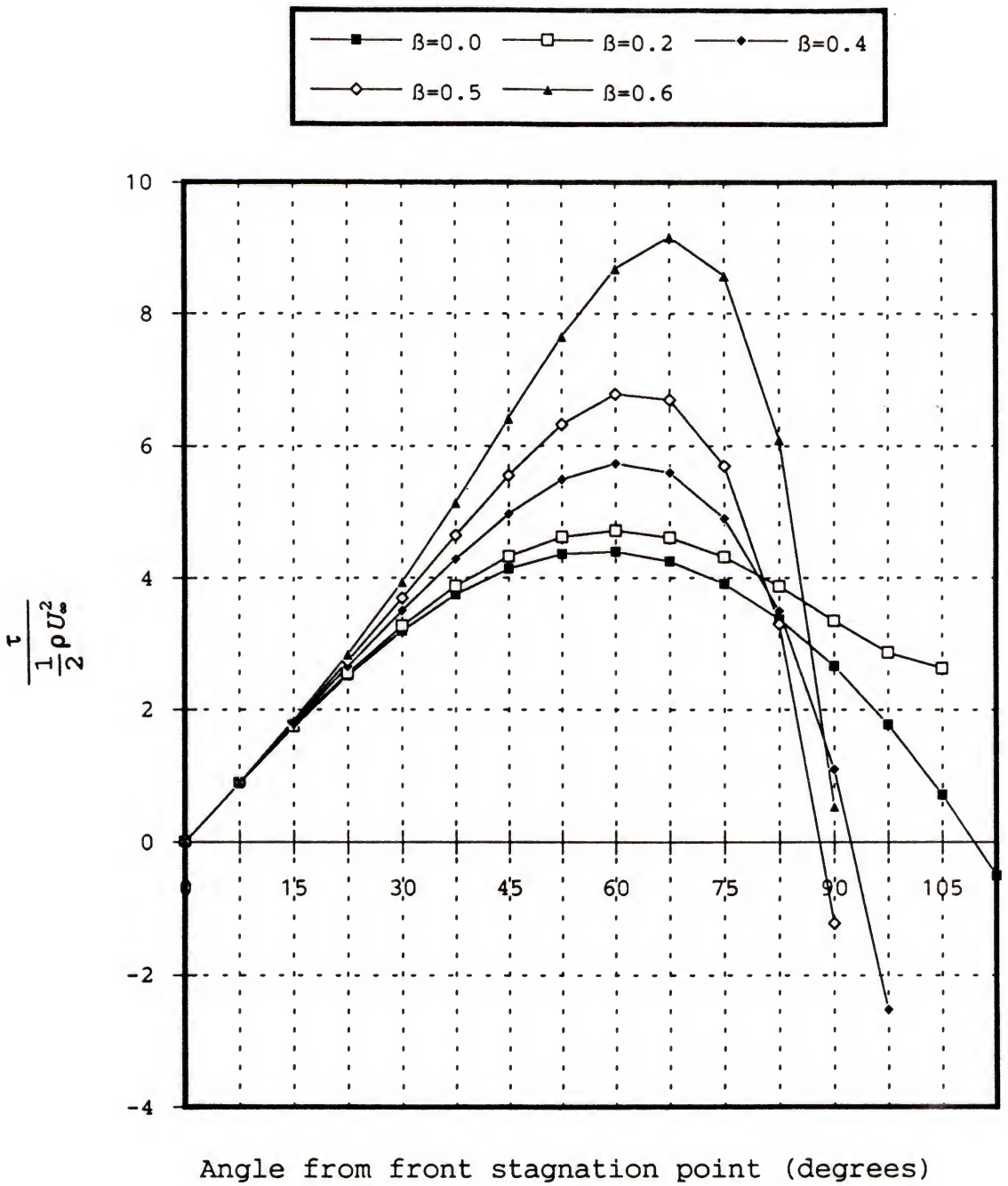

Figure 4-4 Shear stress distribution on a bounded sphere for laminar boundary layer

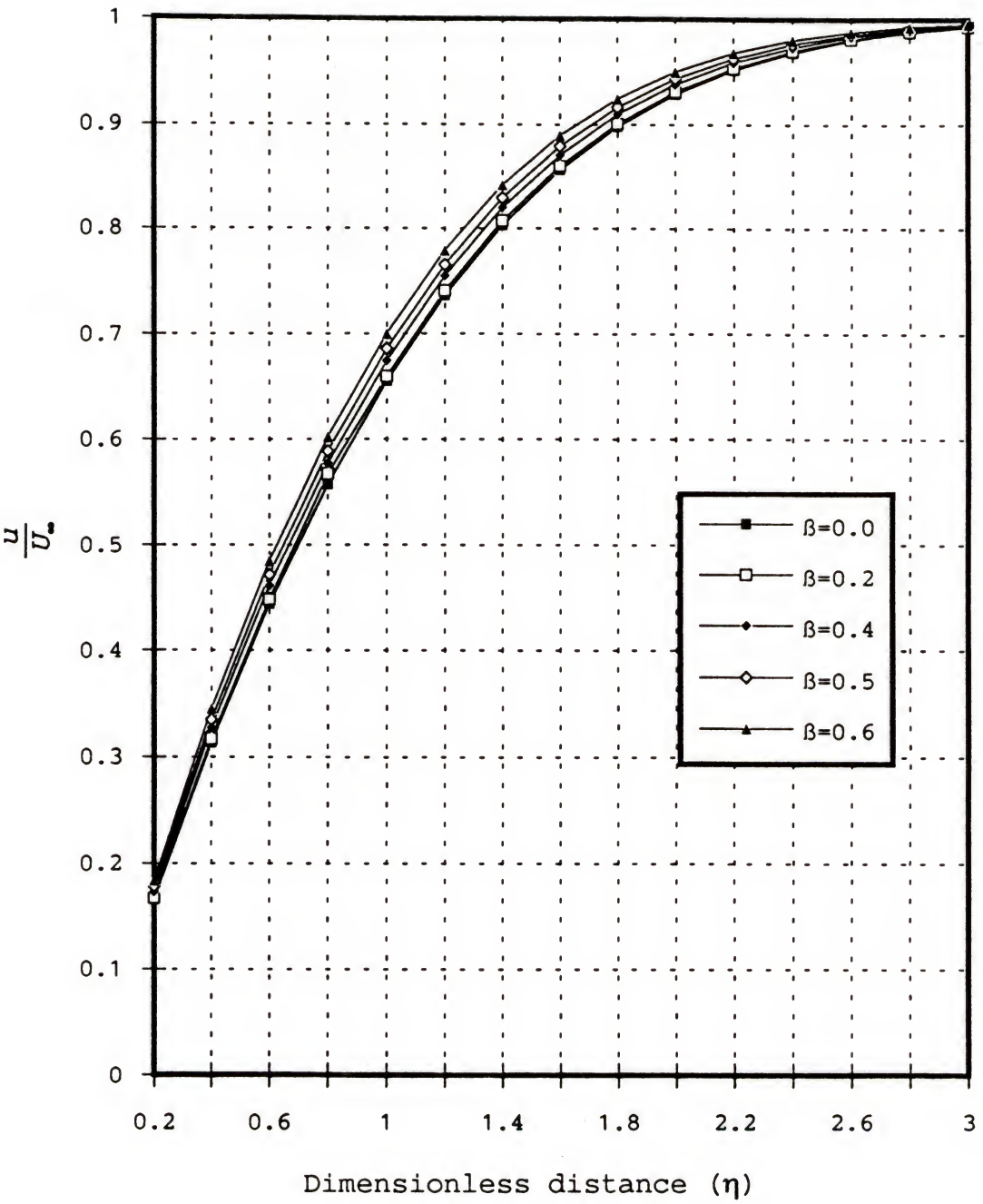

Figure 4-5 Velocity distribution as a function of η

layer. The points at which the shear stress takes null values are the front stagnation point (ϕ=0) and the separation point ($\phi=\phi_{sep}$). Comparison of the sphere in free flow with different spheres in bounded flow is afforded by choosing K=1.5. For ß=0, the separation angle gives the exact value as has been provided by Schlichting (1968). Figure 4-5 gives a plot of the velocity distribution for various spheres as a function of the dimensionless abscissa η. The results have been plotted at a point where the flow angle from the front stagnation point is 30 degrees. This value of angle is based on the following reason. It has been found that the boundary layer approximation on an unbounded sphere takes the potential flow as the outer condition and from experiments it is found that this assumption is true until an angle of 30 degrees. It is reiterated that boundary layer analysis gives a realistic result for the case of an unbounded sphere only when the Reynolds number is around 3000. It is assumed here that at higher flow rates and for a small diameter of the sphere with respect to the cylinder, the above analysis may shed some light on the separation angle. However in order to get some accurate results in this area, numerical analysis, should be employed. Chapter 6 is devoted to the solution of the Navier-Stokes equation, for the geometry of interest to this research, by finite difference methods.

CHAPTER 5
MODELLING OF EXPERIMENTAL DATA

5.1 Error Analysis

During any experiment a collection of data is usually obtained for different items. The data acquired for each individual parameter then combine to provide the actual result. Thus in order to determine the coefficient of drag, we must have the values for the drag force, flowrate, diameters of the sphere and the cylinder and the value for the density of the gas. Each of these parameters has some estimated or characteristic error associated with it and they combine to give the uncertainty in the final result. In general a quantity x which is a function of u,v,w ... has an error associated with it which can be briefly stated as follows (Bevington, 1969):

$$x = f(u,v,w \ldots) \tag{5-1}$$

The variance σ_x^2 for x in terms of variances σ_u^2, σ_v^2 ... which are actually known is

$$\sigma_x^2 \simeq \sigma_u^2 \left(\frac{\partial x}{\partial u}\right)^2 + \sigma_v^2 \left(\frac{\partial x}{\partial v}\right)^2 + 2\sigma_{uv}^2 \left(\frac{\partial x}{\partial u}\right)\left(\frac{\partial x}{\partial v}\right) + \ldots \tag{5-2}$$

The covariance σ_{uv}^2 can be neglected on the following grounds. If the fluctuations in u,v are uncorrelated, then

one hopes to obtain almost equal number of positive and negative values for this term and expect its contribution to vanish. On the basis of the above mathematical background one can now proceed to perform error analysis for the experimental values obtained in the current study.

If 'F' is the drag force on the sphere, 'ρ' the density of the gas, 'U' the mean velocity of flow, 'A' the characteristic area and C_D the coefficient of the drag then

$$F=\frac{\rho U^2 A C_D}{2}=KU^2 A C_D \qquad (5\text{-}3)$$

where K = $\rho/2$

In the experiment the value of the flow rate was measured and velocity was deduced from it. On substituting the values of mean velocity 'U' and area 'A' in terms of flow rate and diameters, i.e. $U = (4Q)/(\pi D^2)$ and $A = (\pi d^2)/4$, where 'Q' is the flow rate and 'D' and 'd' are the diameters of the cylinder and sphere respectively we get

$$F=KQ\left(\frac{d}{D}\right)^2 C_D \qquad (5\text{-}4)$$

$$\therefore,\ C_D=\frac{1}{K}\left(\frac{D}{d}\right)^2\frac{F}{Q} \qquad (5\text{-}5)$$

To get the final variance σ_{cD}^2 through Equation (5-2) one needs to get the partial derivatives from Equation (5-5) and they are

$$\frac{\partial C_D}{\partial D}=\frac{1}{K}\frac{2D}{d^2}\frac{F}{Q} \qquad (5\text{-}6)$$

$$\frac{\partial C_D}{\partial d} = -\frac{2}{K}\frac{D^2}{d^3}\frac{F}{Q} \qquad (5\text{-}7)$$

$$\frac{\partial C_D}{\partial F} = \frac{1}{K}\left(\frac{D}{d}\right)^2\frac{1}{Q} \qquad (5\text{-}8)$$

$$\frac{\partial C_D}{\partial Q} = -\frac{1}{K}\left(\frac{D}{d}\right)^2\frac{F}{Q^2} \qquad (5\text{-}9)$$

Therefore, following Equation (5-2) and neglecting the covariance, we get

$$\sigma_{C_D^2} \simeq \sigma_D^2\left(\frac{\partial C_D}{\partial D}\right)^2 + \sigma_d^2\left(\frac{\partial C_D}{\partial d}\right)^2 + \sigma_F^2\left(\frac{\partial C_D}{\partial F}\right)^2 + \sigma_Q^2\left(\frac{\partial C_D}{\partial Q}\right)^2 \qquad (5\text{-}10)$$

$$\sigma_{C_D^2} \simeq \frac{\sigma_D^2}{K^2}\left(\frac{2D}{d^2}\frac{F}{Q}\right)^2 + \frac{4\sigma_d^2}{K^2}\left(\frac{D^2}{d^3}\frac{F}{Q}\right)^2 + \frac{\sigma_F^2}{K^2}\left(\frac{D^2}{d^2}\frac{1}{Q}\right)^2 + \frac{\sigma_Q^2}{K^2}\left(\frac{D^2}{d^2}\frac{F}{Q^2}\right)^2 \qquad (5\text{-}11)$$

Dividing Equation (5-11) throughout by C_D^2, we get

$$\frac{\sigma_{C_D^2}}{C_D^2} = 4\left(\frac{\sigma_D}{D}\right)^2 + 4\left(\frac{\sigma_d}{d}\right)^2 + \left(\frac{\sigma_F}{F}\right)^2 + \left(\frac{\sigma_Q}{Q}\right)^2 \qquad (5\text{-}12)$$

In the current experiment the drag force 'F' can be measured with an uncertainty of ±0.001%, the flowrate 'Q' has an uncertainty of ±1% while the uncertainties in the sphere diameter and cylinder diameter are ±0.1% and ±2.0% respectively. These are the maximum errors prescribed by the manufacturers. As a result, the maximum variance we get is $(\sigma_{CD}/C_D) = \pm 0.041279$.

If eccentricity of the sphere is also considered as one of the governing factor, f(ß), then it appears as $f(ß)^2$ in

the error propagation equation. If the error due to eccentricity is 1% then $(\sigma_{CD}/C_D) = \pm 0.0439137$. On inspection it is evident that the major error in this experiment is due to the measurement of cylinder diameter. It is very easy to obtain precisely bored tubes. Moreover as far as error in the flow is concerned, it should be noted that the range of the instrument was 0-50 Lt/min. The maximum error occurs at the higher ranges of flow. While conducting viscosity experiments, one has to employ the lower flow rates as has been discussed ahead. As such while designing a sophisticated drag based viscometer, some of the typical error values that can be safely assumed for now are: ±0.0001%(for drag force), ±0.1% (for flow rate), ±0.001% (for sphere diameter), ±0.01% (for cylinder diameter) and ±0.01% (for eccentricity). These combine to provide a total uncertainty in drag coefficient measurement as $(\sigma_{CD}/C_D)=\pm 0.003$.

5.2 Data Modelling

An efficient way to model the drag force data, is to plot the variation of coefficient of drag (C_D) with the flow Reynolds number (Re). Since the flow characteristics vary with the Reynolds number, a convenient way is to model the data for each flow phenomenon. Before one starts on this venture, one should be careful in ascertaining the Reynolds number which by definition is the ratio of the fluid's inertial force to the viscous force it exerts. The inertial

force is a function of the flow velocity. For an infinite flow over a sphere this velocity is the constant approach velocity. But for a flow in a pipe when the fully developed condition has been reached, the velocity distribution is parabolic and is given by the Hagen-Poiseuille formulation:

$$u=2U_{mean}[1-\frac{r^2}{R^2}] \qquad (5\text{-}13)$$

Therefore when comparing the bounded flow with an infinite flow to discern the wall effects, the disparity in the velocity must be appropriately taken into account.

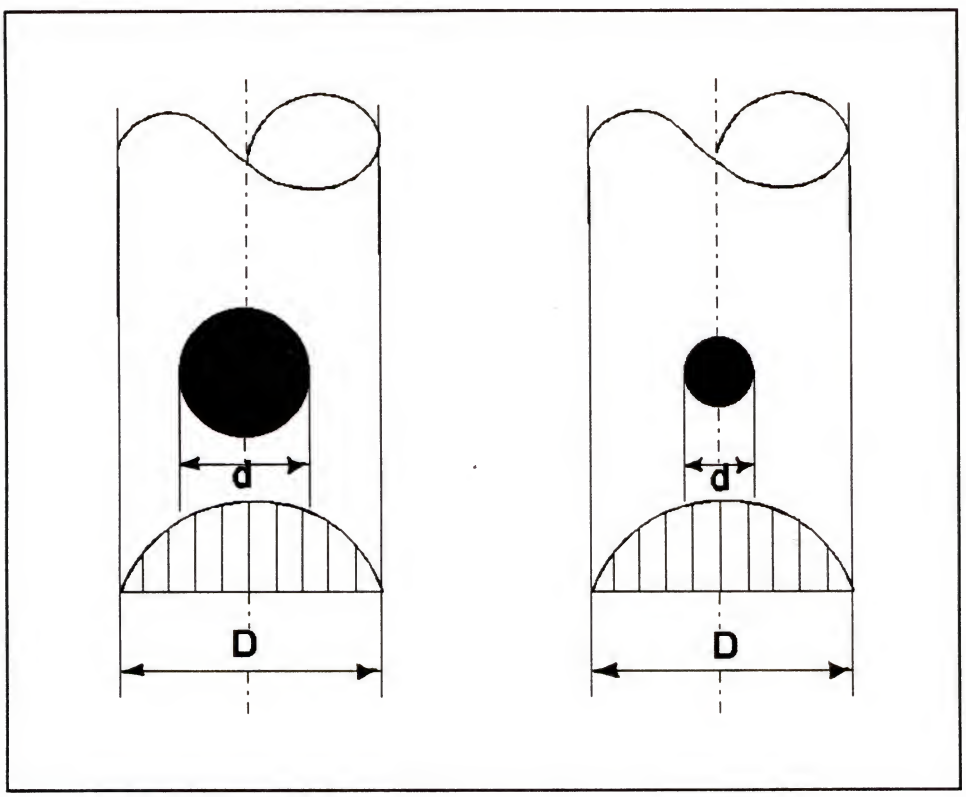

Figure 5-1 Velocity profile seen by different spheres

Also, as can be seen from Figure 5-1,the two different sized spheres encounter different velocity distributions for the same cylinder. While performing dimensional analysis authors have generally chosen two different characteristic velocities to calculate the Reynolds number. One is the mean velocity U_{mean} in the tube [$U_{mean}=Q/(\pi R^2)$ where Q is the flowrate and 'R' is the tube radius] while the other is the centerline velocity U_{max} ($U_{max}=2U_{mean}$). The choice of U_{mean} is based on the grounds that the velocity distribution preceding the particle, which is a function of pipe Reynolds number, will have considerably more influence on the drag coefficient. But the use of U_{mean} looks erroneous on the grounds that not all spheres face the mean velocity. The smaller sphere in Figure 5-1, encounters more of the velocity near the centerline which is much more than the mean velocity. Figures 5-2 and 5-3 show the variation of C_D with Re and sphere to cylinder size (d/D) respectively, as has been obtained in the current experiment. By choosing U_{mean} to define the Reynolds number, a plot in the form of Figure 5-2 is obtained. Figure 5-3 shows that for ß(sphere to cylinder diameter ratio)=0.5 the coefficient of drag (C_D) is minimum. This can be explained on the basis of the velocity distribution encountered by the spheres. The smaller sphere does not lie in the path of the mean velocity and faces more of the velocity grouping around the centerline. This velocity distribution is larger than the

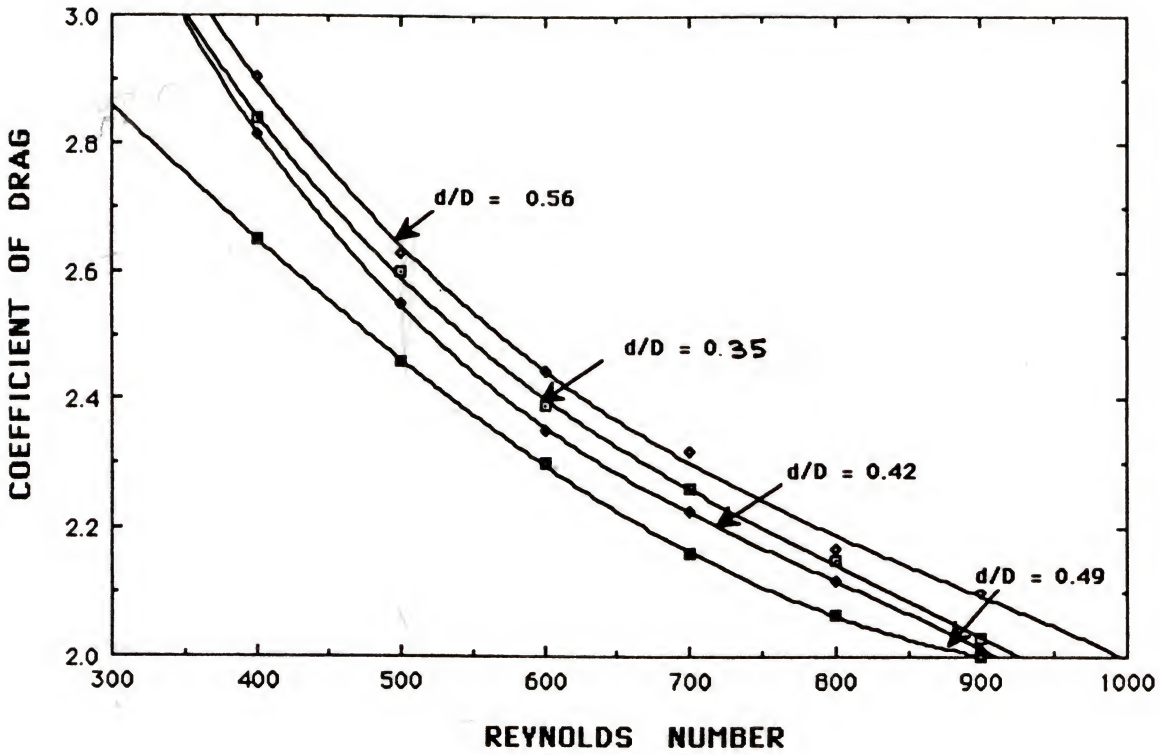

Figure 5-2 Coefficient of drag (C_D) vs. Reynolds number (Re) for different spheres in a tube

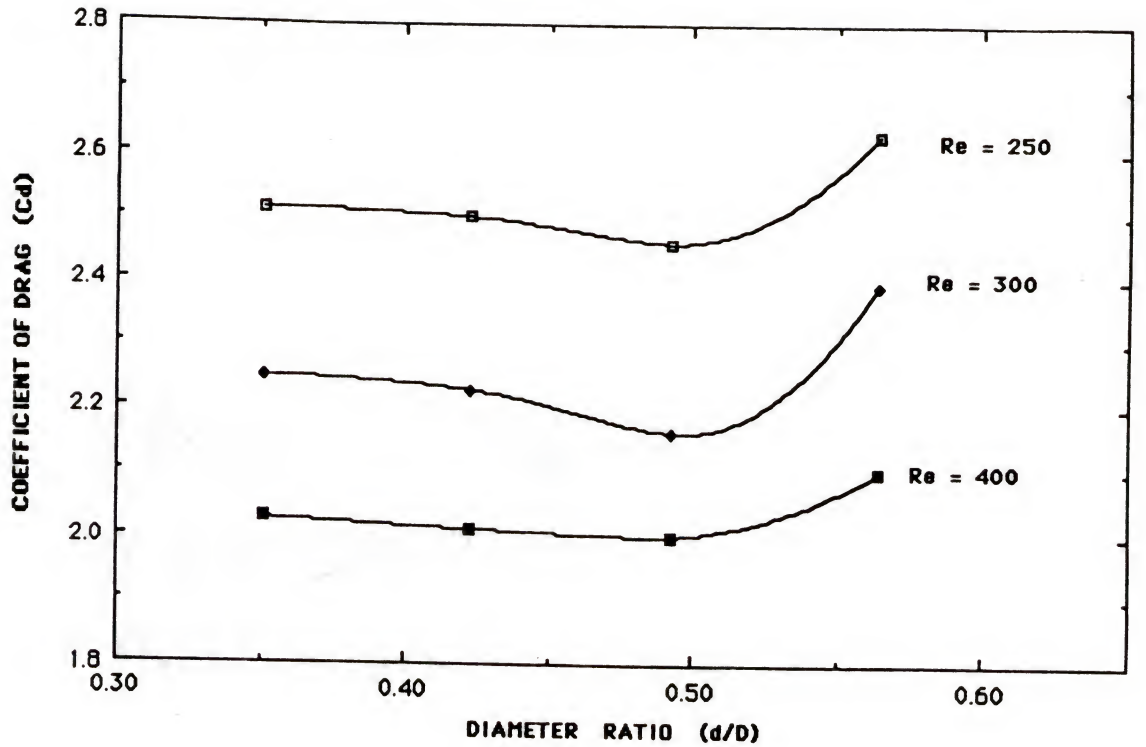

Figure 5-3 Coefficient of drag (C_D) vs. diameter ratio (d/D) for different Reynolds number

mean velocity. Thus choosing U_{mean} as the characteristic velocity for the expression

$$C_D = \frac{DRAG}{\frac{1}{2}\rho U_C^2 A} \qquad (5\text{-}14)$$

overestimates the coefficient of drag, since the actual drag force exerted is due to a larger velocity than the mean velocity. The reverse is true in the case of larger spheres. The use of U_{max} is more justified since all the spheres which are centrally suspended, at least meet it. Figure 3-3 had made a comparison of the coefficient of drag as obtained by various authors on the basis of centerline velocity. However, a more appropriate choice of velocity can be had. This is based on the ground that there is a velocity distribution flowing over the sphere and a characteristic velocity must be derived from it.

When obtaining the coefficient of drag (C_D) from Equation 4-1, one observes that it is the ratio of the drag force (D) experienced by the body to the dynamic force carried by the fluid ($0.5\rho U^2$). So a more judicious choice of the characteristic velocity would be one that exerts the same dynamic force as enthrusted by the velocity distribution seen by the sphere. The velocity distribution in the pipe is given by the Hagen-Poiseuille Equation 5-13. The total dynamic force exerted by this velocity distribution on the sphere is $(1/2)\rho\int U_{max}^2[1-(r/R)^2]dr$ where

the integral is bounded between 0 and 'a' with 'a' and R being the radius of the sphere and cylinder, respectively. The characteristic velocity (U_C) is given by

$$U_C^2 = \frac{\int_0^a u^2 dr}{\int_0^a dr} \qquad (5\text{-}15)$$

U_C^2 gives the same dynamic force as exerted by the velocity distribution seen by the sphere. Since the velocity distribution is the parabolic profile given by Equation 5-13 we get from Equation 5-15

$$U_C = 2U_{mean}\sqrt{(1-\frac{2}{3}\beta^2+\frac{\beta^4}{5})} \qquad (5\text{-}16)$$

Hence, the characteristic velocity (U_C) is equal to $U_{max}.\sqrt{(1-2ß^2/3+ß^4/5)}$, where ß=r/R and U_{max} is the centerline velocity and twice U_{mean}. With this characteristic velocity it is fruitful to perform an analysis between a bounded and an unbounded flow. In the derivation of the characteristic velocity, the average value obtained was for a linear distribution. It is obvious that a better averaging for this type of flow would be by taking the cross-sectional average. If we denote the characteristic velocity obtained in this way by U_{C1} then

$$U_{C1}^2 = \frac{\int_0^a u^2 2\pi r dr}{\int_0^a 2\pi r dr} \qquad (5\text{-}17)$$

and it provides

$$U_{C1} = 2U_{mean}\sqrt{(1-\beta^2+\frac{\beta^4}{3})} \quad . \qquad (5\text{-}18)$$

For the same flow rate, the velocity has a constant value U_∞ for infinite flow and U_C or U_{C1} for a bounded flow. The result is that the Reynolds number in an infinite flow and bounded flow is now defined by choosing the characteristic velocity and is given by $Re=(\rho U_C d)/\mu$ where d is the sphere diameter, and U_C is given by the term $U_{max}.\sqrt{(1-2ß^2/3+ß^4/5)}$ where U_{max} is the centerline velocity and ß is the diameter ratio between the sphere and cylinder. Equipped with these definitions for the Reynolds number and the characteristic velocity, a comparison between bounded and unbounded flow brings out remarkable closeness in the values of the coefficient of drag for different cases. The equation which relates the value of the coefficiemnt of drag for bounded spheres ($C_{D\beta}$) as is observed in this work, to the published values of coefficient of drag for unbounded spheres ($C_{D\infty}$) is given by

$$C_{D\beta} = \frac{C_{D\infty}}{(1.0-\lambda^2)} \qquad (5\text{-}19)$$

where $\lambda=\beta$ when we choose U_C and $\lambda^2=0.9\beta^2$ when U_{C1} is chosen.

The error is given by : ERROR = $|(C_{D\infty} - C_{D\beta})/C_{D\infty}| \times 100$ where $C_{D\infty}$ can be obtained from standard relationships as given by Equations 2-3 and 2-4. Table 5-1 provides the absolute values for error in drag coefficient evaluation. The error is obtained when comparing our experimental data to the values obtained for $C_{D\beta}$ from Equation 5-19. In Table 5-1 E1 and E2 are respectively the absolute error (%) obtained by choosing U_C and U_{C1}. It should be noted that although the maximum error is around 6.5% the relationship for $C_{D\infty}$ has itself an error of more than 6.5% associated with it. This has been noted by Clift et al. (1978) who obtained the relationship ($C_{D\infty}$) for the unbounded sphere by fitting experimental data through linear regression. The experimental data, as collected during this study, was first curve fitted through least square method by assuming a polynomial form of the form:

$$y = a + bx + cx^2 + dx^3 + ex^4 + \ldots \qquad (5\text{-}20)$$

Table 5-2 shows the coefficients obtained for fitting experimental values of this work for different spheres and Reynolds number between 200 and 800.

Table 5-1 Table showing absolute errors in coefficient of drag measurement using relationship (5-19)

Reynold No.(Re)	ERROR (%)	ß=0.35	ß=0.42	ß=0.49	ß=0.56
250.0	E1	1.44	6.52	0.75	7.00
	E2	1.02	4.32	0.71	4.16
300.0	E1	2.12	3.58	0.47	6.16
	E2	1.52	2.26	0.35	3.95
350.0	E1	2.86	0.08	2.07	4.51
	E2	1.98	1.15	1.95	3.01
400.0	E1	3.46	2.60	3.64	3.65
	E2	2.46	1.63	2.85	2.12
450.0	E1	3.98	3.97	4.91	1.10
	E2	2.52	2.58	3.55	0.41
500.0	E1	4.68	4.42	5.83	0.56
	E2	3.10	3.15	3.95	1.22
550.0	E1	5.90	4.32	5.91	1.16
	E2	2.65	2.98	3.98	0.39
600.0	E1	5.61	4.19	4.62	0.92
	E2	4.12	2.71	3.28	0.52
650.0	E1	6.22	4.64	5.23	0.06
	E2	4.02	3.05	3.55	0.35

Table 5-2 Coefficients used for fitting experimental data

ß	a	b	c	d	r	r^2
0.35	1.3651	-3.662 E-3	6.4061 E-6	-4.265 E-9	0.99	0.98
0.42	1.8944	-6.052 E-3	9.9561 E-6	-5.710 E-9	0.99	0.99
0.49	1.5271	-3.418 E-3	4.5935 E-6	-2.232 E-9	0.99	0.99
0.56	2.2202	-5.979 E-3	8.1808 E-6	-3.773 E-9	0.99	0.98

The coefficients thus obtained allowed us to perform comparison at different Reynolds number. Although this form of comparison can be extended beyond Reynolds number 650 but it has not been reported here due to lack of data at higher Reynolds number for ß=0.35 and 0.42. Also, below Reynolds number of 250, the data were tested and the results were consistant until Reynolds number of 200. Below the Reynolds number of 200, the fluid flow phenomenon is different, and data from this work was not sufficient enough to provide a new correlationship.

CHAPTER 6
NUMERICAL STUDY of FLUID FLOW

6.1 Introduction

There are several tools, in the form of numerical algorithms, available at present to perform computational studies of the fluid momentum equation. According to the complexity of the physical phenomenon the Navier-Stokes equation can either be simplified to a boundary-layer type equation, parabolized Navier-Stokes equation, or can be retained in its full form. A comprehensive discussion on the solution of these fluid mechanics equations by finite difference method has been provided by Anderson et al. (1984). The full blown Navier-Stokes equation itself can be differently treated for compressible or incompressible fluid flow. Numerical techniques that handle compressible situations run into convergence difficulties for incompressible case. As a result, the treatment of these two flow situations require separate methodologies. For the circumstances that govern our problem, viz. laminar flow of gas over a cylindrically surrounded rigid sphere, the incompressible Navier-Stokes equation has been solved. There are two popular approaches to handle the incompressible fluid momentum equation: a) Stream Function-Vorticity method

and b) Primitive- Variable approach. The application of the former method has been successful for two dimensional cases but runs into severe difficulties in three dimensional problems and during pressure calculations. In spite of this the Streamfunction-Vorticity method has some distict features to offer. On the other hand Primitive- Variable approach is widely used these days and is not limited to two dimensional situations. In the current study, both the methods have been employed.

6.2 Governing Equations and Discretization

The Navier-Stokes equation in a cylindrical coordinate (r,θ,z) system has been used for the computational fluid dynamics study (Figure 6-1).

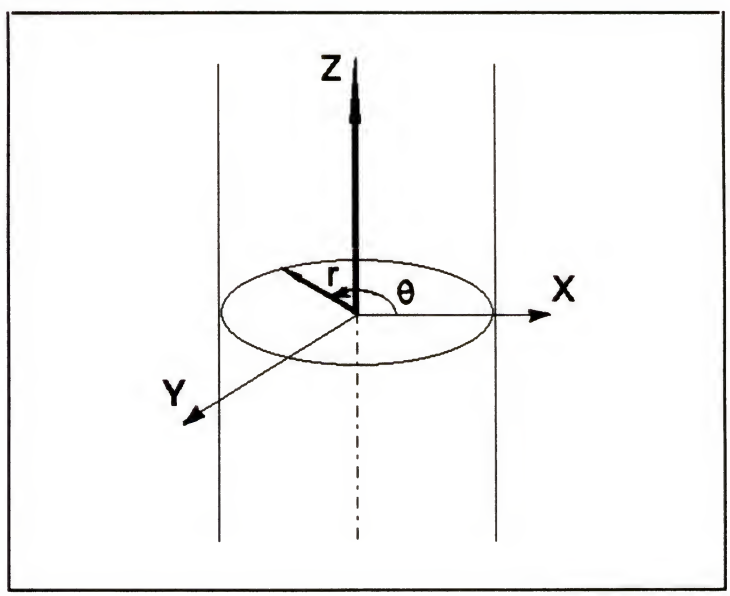

Figure 6-1 Cylindrical coordinate system

The flow is assumed to have symmetry about the 'θ' direction and as a result we are interested in only axisymmetric flow. Strictly speaking this narrows the study to Reynolds numbers where asymmetry has not set in. For a sphere in infinite flow, this symmetric flow restriction limits the Reynolds number to values within 240.

6.2.1 Primitive Variable Equations

If we assume a Newtonian fluid with constant viscosity and the absence of body forces, then for two-dimensional axisymmetric flow (i.e. symmetry and no velocity component in the 'θ' direction) the expressions for the momentum and continuity equations are:

$$\frac{\partial u}{\partial t}+u\frac{\partial u}{\partial z}+v\frac{\partial u}{\partial r}=-\frac{1}{\rho}\frac{\partial p}{\partial z}+\nu\left(\frac{\partial^2 u}{\partial z^2}+\frac{\partial^2 u}{\partial r^2}+\frac{1}{r}\frac{\partial u}{\partial r}\right) \qquad (6\text{-}1)$$

$$\frac{\partial v}{\partial t}+u\frac{\partial v}{\partial z}+v\frac{\partial v}{\partial r}=-\frac{1}{\rho}\frac{\partial p}{\partial r}+\nu\left(\frac{\partial^2 v}{\partial z^2}+\frac{\partial^2 v}{\partial r^2}+\frac{1}{r}\frac{\partial v}{\partial r}-\frac{v}{r^2}\right) \qquad (6\text{-}2)$$

$$\frac{\partial u}{\partial z}+\frac{1}{r}\frac{\partial (rv)}{\partial r}=0 \qquad (6\text{-}3)$$

Here 't' is the time, 'u' is the velocity component in the 'z' direction, 'v' is the velocity component in the 'r' direction, 'ν' is the kinematic viscosity of the fluid, 'ρ' is the density of the fluid and 'p' is the pressure. Equations (6-1) and (6-2) are the momentum equations in the 'z' and 'r' directions respectively while Equation (6-3) is the fluid continuity equation. The above set of equations

are referred as the "Primitive" equations since they are written in terms of the primitive variable 'u','v' and 'p'.

6.2.2 Stream Function-Vorticity Equations

The pressure term in Equations 6-1 and 6-2 can be eliminated by cross differentiation and applying Equation 6-3 and the vorticity (ζ) relation for axisymmetric flow

$$\zeta = \frac{\partial v}{\partial z} - \frac{\partial u}{\partial r} \tag{6-4}$$

the following equation with vorticity as the dependent variable is obtained.

$$\frac{\partial \zeta}{\partial t} + u\frac{\partial \zeta}{\partial z} + v\frac{\partial \zeta}{\partial r} - \frac{v\zeta}{r} = \nu\left(\frac{\partial^2 \zeta}{\partial z^2} + \frac{\partial^2 \zeta}{\partial r^2} + \frac{1}{r}\frac{\partial \zeta}{\partial r} - \frac{\zeta}{r^2}\right) \tag{6-5}$$

If a slightly modified version of the continuity equation (Equation 6-3),

$$\xi\left[\frac{1}{r}\frac{\partial (rv)}{\partial r} + \frac{\partial u}{\partial z}\right] = \frac{\xi}{r}\frac{\partial (rv)}{\partial r} + \xi\frac{\partial u}{\partial z} = 0 \tag{6-6}$$

is added to the left side of Equation (6-5), we get the "vorticity transport" equation:

$$\frac{\partial \xi}{\partial t} + \frac{\partial u\xi}{\partial z} + \frac{\partial v\xi}{\partial r} = \nu\left(\frac{\partial^2 \xi}{\partial z^2} + \frac{\partial^2 \xi}{\partial r^2} + \frac{1}{r}\frac{\partial \xi}{\partial r} - \frac{\xi}{r^2}\right) \tag{6-7}$$

Introducing the incompressible stream-function (ψ) defined by

$$\frac{1}{r}\frac{\partial \psi}{\partial r} = u \quad , \quad \frac{1}{r}\frac{\partial \psi}{\partial z} = -v \qquad (6\text{-}8)$$

into the continuity equation (Equation 6-3) gives the following equation for the vorticity in terms of the stream-function

$$-\zeta = \frac{1}{r}\left(\frac{\partial^2 \psi}{\partial z^2} + \frac{\partial^2 \psi}{\partial r^2} - \frac{1}{r}\frac{\partial \psi}{\partial r}\right) \qquad (6\text{-}9)$$

Equations 6-7, 6-8, and 6-9 constitute the 'Streamfunction - Vorticity' equations.

6.2.3 Discretization

In order to solve the partial differential equations numerically, first the physical space is divided into a discrete number of points which conform to some cartesian system and form a grid. Then the governing equations - Equations 6-1, 6-2 and 6-3 for the primitive method and Equations 6-7, 6-8 and 6-9 for the stream function-vorticity formulation are discretized to break them down into algebraic equations that can be solved numerically. Several techniques like the use of Taylor series, polynomial fitting, integral method, and the control volume approach can be utilized for discretization. The efficacy of one method over the other is problem dependant and cannot be ascertained beforehand. However the control volume approach offers some interesting features. It provides a balance of some physical quantity on a region in the vicinity of the grid point. This means that the governing physical law is

satisfied over a finite region rather than a single point. Moreover, the different equations formed by the control volume approach tend to have the conservative property which is essential to many problems.

An inspection of the transport equations shows that the dependent variables (u,v,ζ) obey a certain conservative principle. In general if 'Φ' is a dependent variable, then the differential equation in a conservative form can be written as

$$\frac{\partial(\rho\phi)}{\partial t}+\frac{\partial(\rho u\phi)}{\partial z}+\frac{\partial(\rho v\phi)}{\partial r}=\frac{\partial}{\partial z}(\Gamma\frac{\partial\phi}{\partial z})+\frac{\partial}{\partial r}(\Gamma\frac{\partial\phi}{\partial r})+S \qquad (6\text{-}10)$$

where 'Γ' is a diffusion coefficient and 'S' is the source term. In Cartesian tensor notation we have

$$\frac{\partial(\rho\phi)}{\partial t}+\frac{\partial(\rho U_i\phi)}{\partial X_i}=\frac{\partial}{\partial X_i}(\Gamma\frac{\partial\phi}{\partial X_i})+S \qquad (6\text{-}11)$$

where U_i is the fluid velocity in the direction X_i. The four terms appearing in the equation are the unsteady term, the convective term, the diffusive term, and the source term. The equation as a whole represents the conservation of flux. The total flux J_i consists of a)the convective flux ($\rho U_i\Phi$) due to the motion of the fluid and b)the diffusive flux $[\Gamma(\partial\Phi/\partial x_i)]$ generated by the gradients of Φ. The physical meaning of expressing the terms in such an order has been given by Patankar (1980). One can easily see that Equations 6-1,6-2 and 6-7 can easily be cast into the generalized form as given by Equation 6-10. Therefore it is meaningful to

discretize the generalized equation and then substitute and solve for the variables of interest like u,v or ξ.

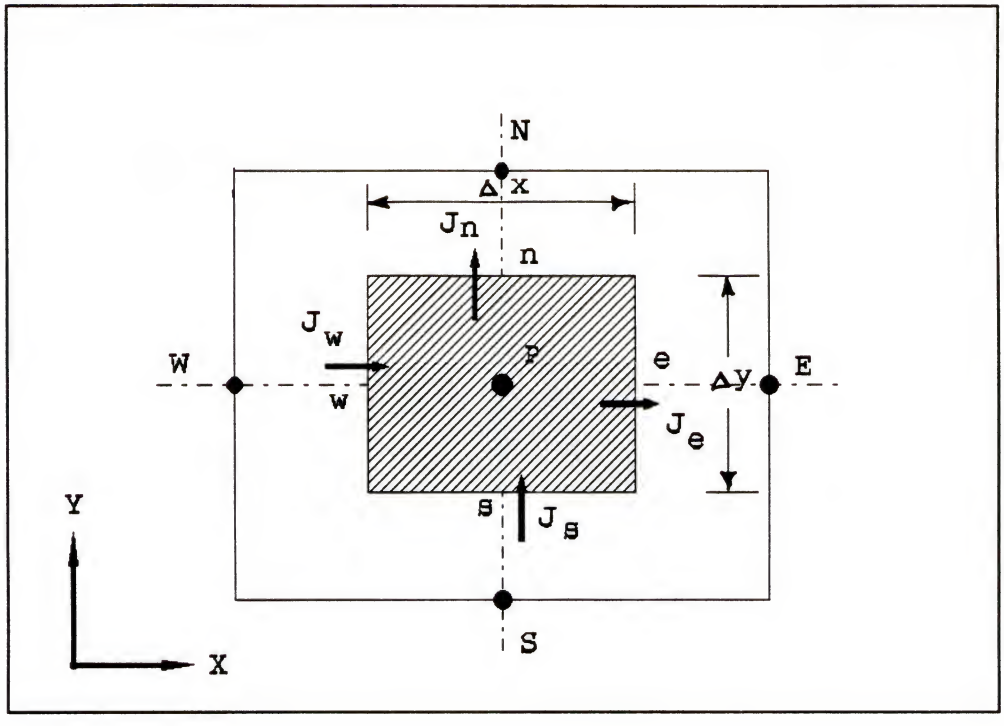

Figure 6-2 Control Volume around a grid point 'P'

In the control volume approach the discretization is done by integrating the governing equation over a region. In Figure 6-2, a control volume is chosen around the grid point 'P' and Equation 6-10 is integrated over it. Discretization in this manner results in the following algebraic equation (see Appendix A and Patankar (1980)):

$$a_P\Phi_P=a_E\Phi_E+a_W\Phi_{W+}a_N\Phi_N+a_S\Phi_S+b \qquad (6\text{-}12)$$

The definition of the terms a_P, a_E, a_W, a_N, a_S and b is given in Appendix A. This resulting algebraic equation is solved

numerically by observing boundary conditions, the nature of the equation, and applying a proper differencing scheme on a proper set of grid lines. The next task, therefore, is to generate an appropriate grid.

6.3 Grid Generation

The generation of grid points within the physical space is an important consideration. More often than not, results are needed on surfaces of the problem and we must have grid points on it. From Figure 6-3 we observe that if grid lines are aligned along the z and r direction of the cylinder then it is difficult to ascertain values on the sphere surface. For example, points A,C do not lie at the intersection of grid lines like points B and D. Therefore, some interpolation needs to be done to calculate values at points like A and C. On the other hand, if we choose a spherical coordinate system then the cylinder surface has too few grid points on it and the cylinder is not accounted for properly. This poses a classic problem where one orthogonal coordinate system (spherical) is embedded in another (cylindrical). If the size of the sphere is very small compared to the tube diameter, then a) a cylindrical system would have given some fruitful results provided no values were needed on the sphere surface and b) a spherical system would have provided results for the sphere but very little and debatable results

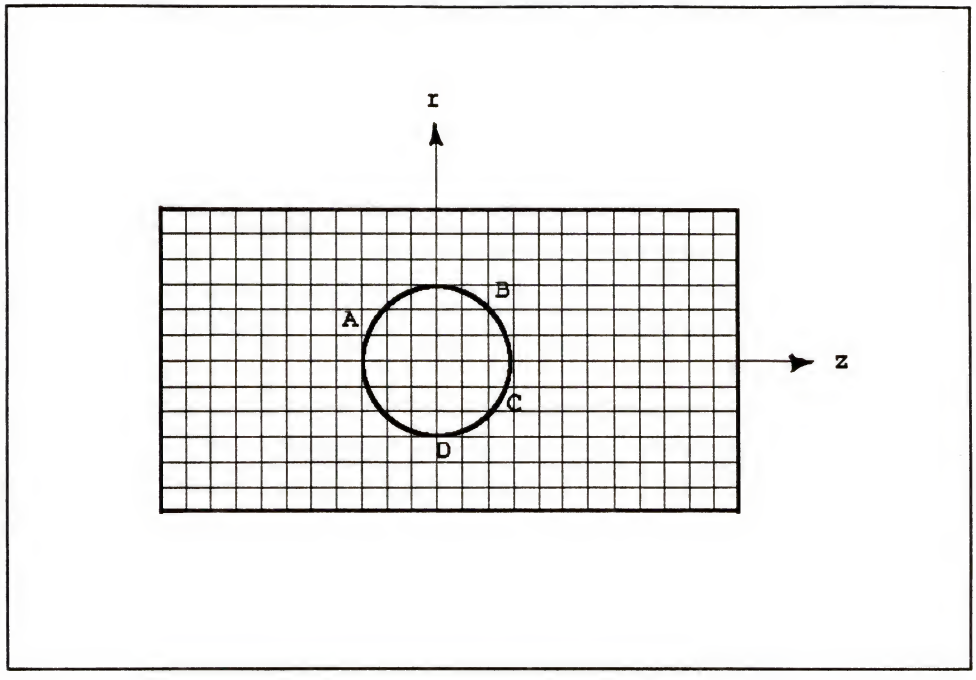

Figure 6-3. A r-z coordinate for a sphere in a cylinder

for the whole flow situation. But in the current problem, the size of the sphere is not necessarily small. Also, the imposition of one orthogonal cartesian coordinate on the physical domain will require some sort of interpolation for the implementation of the boundary conditions. Since boundary conditions play a dominant role, the interpolation creates inaccuracies at sensitive places. In addition, uneven grid spacing near the boundaries are created which make the programming cumbersome.

The dilemma may be overcome by choosing a body fitted coordinate system. As the name indicates, the coordinate system is aligned along the body surfaces and need not be

orthogonal. This is implemented by transformation of the physical problem (from an unevenly spaced and non-orthogonal gridded region) to a computational space (evenly spaced and orthogonal grids). A typical evolution of the computational space from a physical domain is shown in Figure 6-4. It is to be noted that the computational region is obtained by twisting and deforming the physical domain. The result of this systematic deformation leaves a space where we have orthogonal grids at equal spacing. The fluid dynamics equation are now solved on the computational domain. The central issue in this process is identifying the location of the grid points in the physical domain. This means obtaining the x and y values of the grid points in the physical space that correspond to P(i,j) in the computational domain. During this identifying process for grid points several desirable features must be aimed at (Hoffman 1989)

a) the mapping should generate one-to-one correspondence, i.e. grid lines of the same family should not cross
b) the grid distribution should be smooth
c) the grid lines should be orthogonal and
d) there should be an option for grid clustering.

Some of the promising techniques that help to obtain some and sometimes all of the above desirable features are: the algebraic method, the partial differential method and conformal mapping. A detailed discussion of these can be

elicited from Thompson et al. (1985). For our problem we have used two options for generating the grid points:

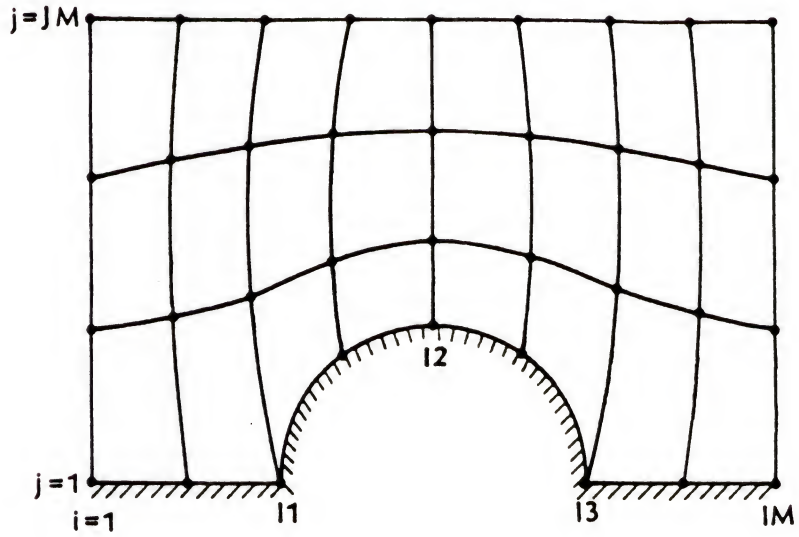

a. Physical domain

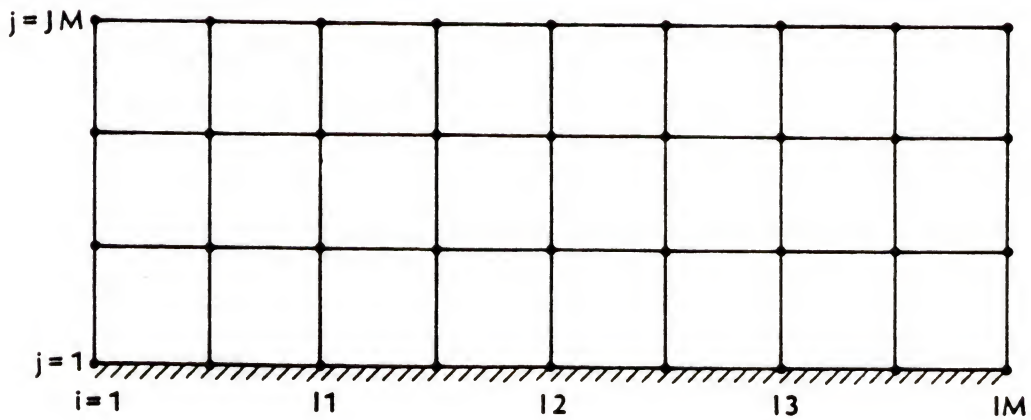

b. Computational domain

Figure 6-4. Transformation from physical to computational domain

an axisymmetric (r-z) coordinate and a body fitted coordinate with the grid generated by the partial differential method. Amongst the various options in this class (elliptic, parabolic and hyperbolic), an elliptic grid generator was chosen since it is widely used in cases having a well defined geometry. If (x,y) are the variables of grid points in the physical space and (ξ,η) in the computational space, then the values of (x,y) within the physical space are determined by solving the set of Equations 6-13 and 6-14.

$$ax_{\xi\xi}-2bx_{\xi\eta}+cx_{\eta\eta}=0 \qquad (6\text{-}13)$$

$$ay_{\xi\xi}-2by_{\xi\eta}+cy_{\eta\eta}=0 \qquad (6\text{-}14)$$

where

$$a = x_{\eta}^2 + y_{\eta}^2$$

$$b = x_{\xi}x_{\eta} + y_{\xi}y_{\eta}$$

$$c = x_{\xi}^2 + y_{\xi}^2$$

To solve Equations 6-13 and 6-14 by iterative methods like the Gauss-Seidel technique, they are arranged as:

$$x_{i,j}=\left[\frac{a}{(\Delta\xi)^2}(x_{i+1,j}+x_{i-1,j})+\frac{c}{(\Delta\eta)^2}(x_{i,j+1}+x_{i,j-1})-\frac{b}{(2\Delta\xi\Delta\eta)}\right.$$
$$\left.(x_{i+1,j+1}-x_{i+1,j-1}+x_{i-1,j-1}-x_{i-1,j+1})\right]/\left\{2\left(\frac{a}{(\Delta\xi)^2}+\frac{c}{(\Delta\eta)^2}\right)\right\}$$

(6-15)

$$Y_{i,j}=[\frac{a}{(\Delta\xi)^2}(Y_{i+1,j}+Y_{i-1,j})+\frac{c}{(\Delta\eta)^2}(Y_{i,j+1}+Y_{i,j-1})-\frac{b}{(2\Delta\xi\Delta\eta)}$$
$$(Y_{i+1,j+1}-Y_{i+1,j-1}+Y_{i-1,j-1}-Y_{i-1,j+1})]/\{2(\frac{a}{(\Delta\xi)^2}+\frac{c}{(\Delta\eta)^2})\}$$

(6-16)

To begin the solution by the elliptic method, first an initial distribution of x and y coordinates of grid points within the physical space is specified. The coefficients a,b and c are determined by finite difference approximation. A second order accurate differencing scheme is employed. For example, the value of x_η at interior points is given by

$$x_\eta=\frac{x_{i,j+1}-x_{i,j-1}}{2\Delta\eta}$$

and at the boundary (e.g., at j=1) it is given by

$$x_\eta=\frac{-3x_{i,1}+4x_{i,2}-x_{i,3}}{2\Delta\eta}$$

For the first iteration the value of x and y are provided by the initial distribution and subsequently from the previous iteration, i.e., the computation of the coefficients lags behind by one iteration level. This iterative process is continued until a specified value of convergence is reached. For the current problem the following strategy is adopted

$$ErrorX=\sum_{i=2,j=2}^{i=IM1,j=JM1} ABS(x_{i,j}^{k+1}-x_{i,j}^{k})$$

$$ErrorY = \sum_{i=2,j=2}^{i=IM1,j=JM1} ABS(y_{i,j}^{k+1} - y_{i,j}^{k})$$

$$ErrorT = ErrorX + ErrorY$$

where k represents the iteration level. The convergence is reached once ErrorT $\leq \epsilon$, where ϵ is a small value and is equal to 10^{-3} in this case. On using the r-z coordinate the sphere is approximated by a step like structure while the numerical grid generation exactly traces all the boundary. Figure 6-5 shows the grid lines in the two situations. For the current problem each yields a solution which is partially correct.

6.4 Solution Technique

Once the differential Equation 6-11 is discretized and reduced to the algebraic form, Equation 6-12 needs to be solved to yield the desired results. Several methods that are employed to solve algebraic equations can be utilized. One should note that the resulting equation is two-dimensional and the dependence of the coefficients (a_E, a_W etc.) on the variable Φ delineates it as a nonlinear equation. Several iterative techniques are available to solve this type of nonlinear equation- Gauss-Seidel method, Point Successive relaxation, Line Successive relaxation, etc. For our problem, Point Successive relaxation

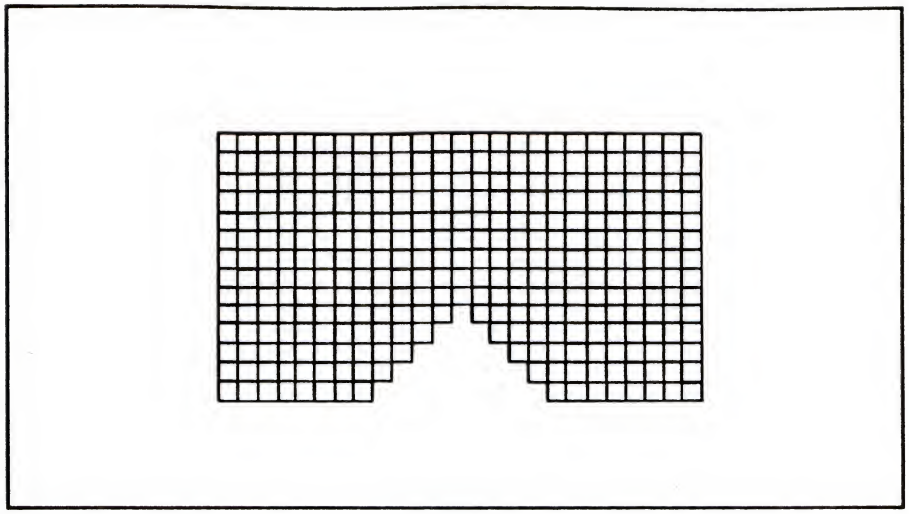

a. Physical region using r-z coordinate

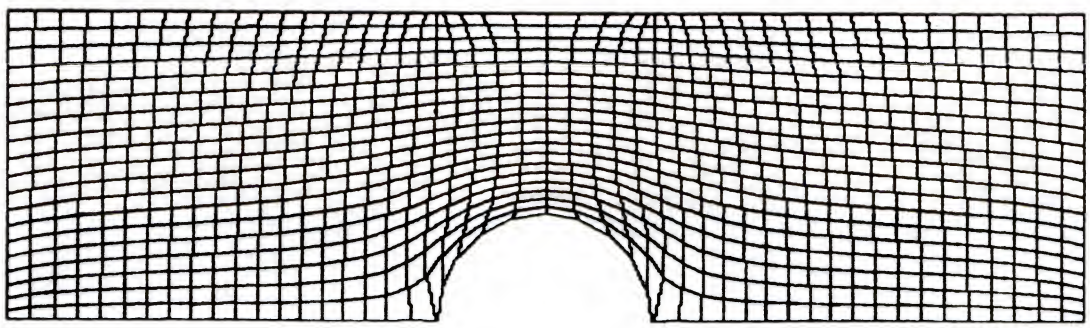

b. Physical region using boundary fitted coordinate

Figure 6-5. Grid lines using different coordinates

was used for the Stream function-Vorticity method and Line Successive relaxation method for the Primitive-Variable method. The relaxation parameter is introduced as follows:

$$a_P\phi_P=\sum a_i\phi_i+b \tag{6-17}$$

where i=E,W,N and S.

$$\phi_P=\frac{1}{a_p}\sum a_i\phi_i+b \tag{6-18}$$

If Φ_P^* is the known value at 'P' from previous iteration then adding $(\Phi_P^*-\Phi_P^*)$ to right hand side of Equation 6-18 and rearranging terms one gets

$$\phi_P=\phi_P^*+\frac{1}{a_p}(\sum a_i\phi_i+b-a_P\phi_P^*) \tag{6-19}$$

As the solution proceeds, Φ_P^* must approach Φ_P. A relaxation parameter (ω) is introduced to accelerate this process. The value of ω determines its nomenclature; if it is less than unity then it is called underrelaxation, else it is overrelaxation.

The above iterative technique as applied to Point and Line Successive relaxation can be found in several standard books of Computational Fluid Dynamics.

Before one applies the iterative strategy for the solution of the algebraic equation, a generalized form is formed so that different differencing schemes can be handled. It has been found that for a convective-diffusive equation such as Equation 6-11, it is the handling of the non-linear convective term which assures the accuracy of the

solution. This handling depends on the problem and flow conditions and good differencing schemes try to model them accurately. The differencing schemes can be divided into two groups. One is based on one-dimensional flux balance (lower order scheme) and cannot work well in regions were flow is not aligned with the grid lines. Some of the well known differencing methods falling under this bracket are the upwind scheme, hybrid scheme, central differencing, exponential, power-law, etc. The other schemes use a better differencing technique to handle grid to flow skewness and some of them are the Locally Analytical Differencing Scheme,

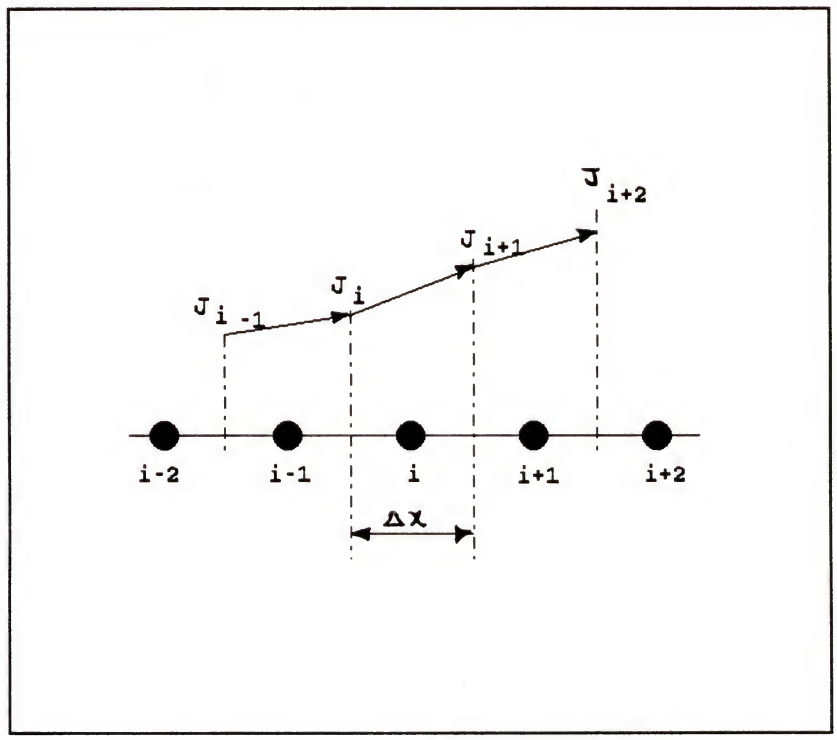

Figure 6-6 Flux variation across a cell in Linear flux spline scheme

the Linear Flux-Spline Scheme, the Cubic Flux-Spline Scheme, Controlled Numerical Diffusion with Internal Feedback, etc. An overview of these methods can be found in Karki et al. (1988). The problem with lower order schemes is that they do not respond well to the presence of sources or sinks in the control volume nor to multidimensional effects. The skewness between the grid and the flow gives rise to significant numerical diffusion (numerical error) and lower order schemes fall short in their performance. The higher order scheme tries to remove these shortcomings. The linear flux-spline scheme assumes a linear variation of the total flux, as shown in Figure (6-6), as opposed to the preservation of flux that is assumed by lower order techniques. In order to combine all the differencing schemes under one umbrella, Equation (6-12) is rewritten here and the coefficients are defined as follows:

$$a_P\phi_P = a_E\phi_E + a_W\phi_W + a_N\phi_N + a_S\phi_S + b$$

where $a_E = D_eA(|P_e|) + \max(-F_e, 0)$

$a_W = D_wA(|P_w|) + \max(F_w, 0)$

$a_N = D_nA(|P_n|) + \max(-F_n, 0)$

$a_S = D_sA(|P_s|) + \max(F_s, 0)$

The values of D_i and F_i (i=e,w,n & s) are given in Appendix B.

Table 6-1 Value of A(|P|) for various schemes

SCHEME	FORMULA FOR A(|P|)
CENTRAL DIFFERENCE	$1 - 0.5\|P\|$
UPWIND	1
HYBRID	$MAX(0,1 - 0.5\|P\|)$
POWER LAW	$MAX[0,\{1 - 0.5\|P\|)\}^5]$
EXPONENTIAL	$\|P\|/[EXP(\|P\|)-1]$

Physically D_i is the conductance through face i, F_i is the flow rate through face i and P_i is the Peclet number given by the ratio of the flow rate to conductance through face i i.e. $P_i=F_i/D_i$. The function A(|P|) for lower order schemes is given in Table 6-1 and can be selected according to the method used. Unfortunately for the linear flux-spline the coefficients cannot be tabulated in the table but the values of the coefficients are provided in the works of Karki et al. (1988).

6.5 Implementation

The solution strategy for the Stream Function - Vorticity method and Primitive variable method are different. Before one starts working out the details for them it is necessary to lay down the boundary conditions (Figure 6-7) that regulate the solution.

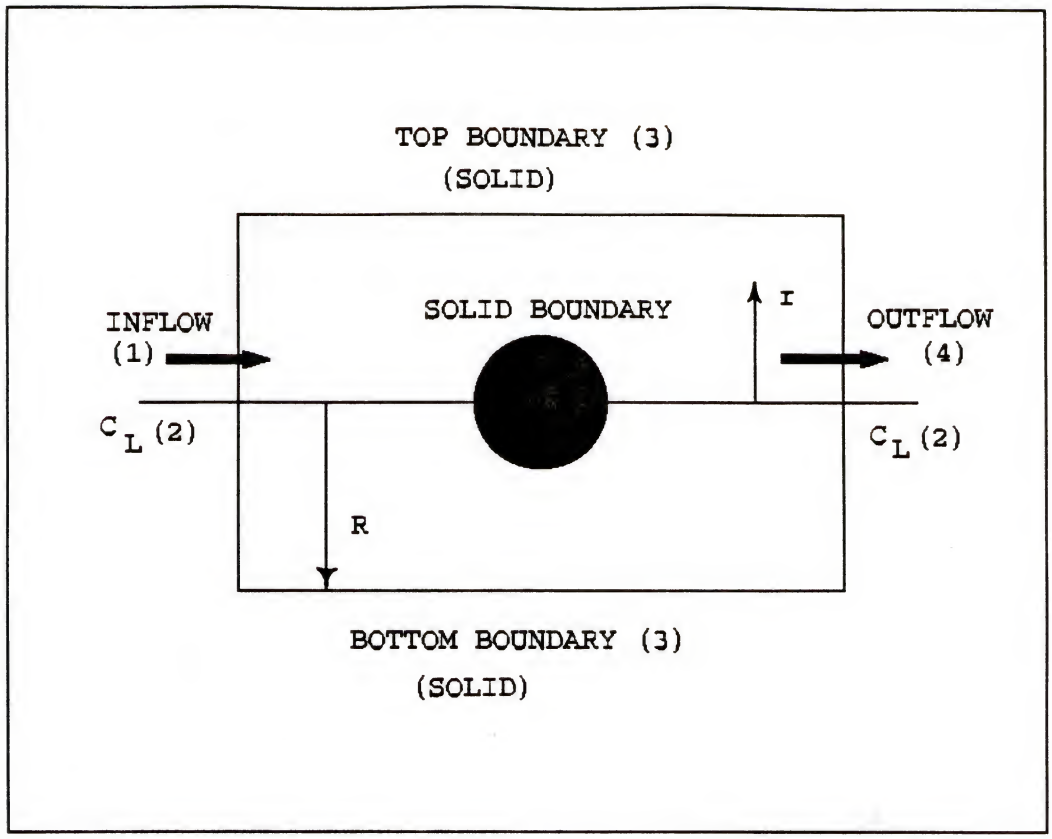

Figure 6-7 Boundary Conditions existing for the problem

Inflow. For the streamfunction - vorticity method, two different types of velocity inflow conditions were used (surface 1):

a) a constant velocity at the inlet

i.e. $u=U_{mean}$, $v=o$;

which yields the stream function $\Psi_{1,j} = (U_{mean}r^2)/2$ and

b) a fully developed velocity profile

i.e. $u=2U_{mean}(1-r^2/R^2)$, which is the Hagen-Poiseuille equation. The stream function becomes

$$\Psi_{1,j} = 2U_{mean}[(r^2/2) - (r^4)/(4R^4)]$$

Both conditions a) and b) can be put in a single form like:

$$\Psi_{1,j} = (Ar^4/4) + (Br^2/2) \qquad (6\text{-}22)$$

For condition a) A=0 and $B=U_{mean}$ and for b) $A=-U_{mean}$ and $B=U_{mean}$. The vorticity in either case is obtained from Equation (6-4).

For the primitive variable method, a constant inflow velocity (u=constant and v=0) was used.

Centerline. The centerline is shown as surface 2. For the streamfunction - vorticity method, the streamline can be assigned an arbitrary constant value, and is taken as zero. Since the streamline was given a constant value at this surface, the radial velocity v becomes zero ($\partial\Psi/\partial z = 0$). The assumption of axial symmetry results in $\partial u/\partial r = 0$. With $\partial v/\partial z = 0$ (since v=0 along centerline) and $\partial u/\partial r = 0$ the vorticity is zero along the centerline.

In the primitive variable approach, a symmetric boundary resulted in using v=0 and $\partial u/\partial r = 0$.

Solid boundary. The solid surfaces are the cylinder and sphere walls and have been labelled as (3). The value of the stream function on the walls of the cylinder is constant as warranted by Equation 6-22.

$$\psi_{wall} = \text{constant; on cylinder wall}$$

On the surface of the sphere the stream function has the same value as the centerline.

$$\psi_{sphere} = 0$$

Also at the solid surface a no slip condition exists which makes $u = v = 0$

The vorticity is calculated by using its definition. A detailed discussion of utilizing different differencing schemes is provided by Roache (1982). Regardless of the wall orientation or the boundary value of ψ, we find

$$\zeta_w = \frac{2(\psi_{w+1} - \psi_w)}{r\Delta n^2} + O(\Delta n) \qquad (6\text{-}23)$$

where Δn is the distance from the wall point (w) to the next closest vertical point (w+1). With this definition (Equation 6-23) there is no problem in calculating the vorticity for walls aligned with the cylindrical grid. However, for an inclined surface, such as that presented by the sphere surface, some interpolation needs to be done.

For the primitive variable approach a no-slip condition results in u=v=0 for the solid walls.

Outflow. The outflow is labelled as surface (4). It is a challenging problem in computational fluid dynamics to choose this condition beforehand. It is highly problem dependant. For this problem the boundary condition for stream function and vorticity as used by Fanning and Mueller (1973) was utilized. This means that a linear extrapolation of values in the axial direction was made.

$$\psi_{IM,j} = 2\,\psi_{IM-1,j} - \psi_{IM-2,j} \qquad (6\text{-}24)$$

$$\zeta_{IM,j} = 2\,\zeta_{IM-1,j} - \zeta_{IM-2,j} \qquad (6\text{-}25)$$

In the above equation IM is the x value of the outflow boundary.This condition allows the flow to continue in the general direction as dictated by the two interior points adjacent to the boundary. The velocities at the outflow were computed using centered and one-sided differencing

$$u_{IM,j}=\frac{\psi_{IM,j+1}-\psi_{IM,j-1}}{2r\Delta r} \qquad (6\text{-}26)$$

$$v_{IM,j}=\frac{\psi_{IM,j}-\psi_{IM-1,j}}{r\Delta z} \qquad (6\text{-}27)$$

By using the above method stable results were obtained. It must be noted that 'wiggles' are produced if proper outflow conditions are not used. This has been discussed by Roache (1982) pg. 161. Also upwind differencing scheme and the use of gradient condition $\partial\xi/\partial z = 0$ do not produce wiggles or oscillations in the solutions.

For the primitive variable approach, linear extrapolation of velocity was used.

Initial condition. Two types of initial conditions were used. The first was the extension of the inflow condition throughout the interior region. However, for the stream function vorticity method only the flat velocity distribution as the inflow condition converged easily. The second method utilized a converged solution at some different Reynolds number.

6.6 Calculation of Flow Variables

The two different methods used to calculate the flow variables warrant different implementation strategy.

Streamfunction-Vorticity. The following steps are undertaken to calculate the flow variables by this method.

a) The grid points are first generated. This involves the numerical grid generation using elliptic equations like Equations 6-13 and 6-14.

b) Once the grid points within the physical space are determined an initial value for all the flow variables is assigned to them. The process starts by providing values of the streamfunction and correspondingly computing the values of velocity and vorticity through proper relational equations.

c) The vorticity transport equation (Equation 6-7) is then solved to get the value of vorticity at the next time step. This now gives us the new values of vorticity at each grid point.

d) From the Poisson's equation (Equation 6-9), the value of the streamfunction is updated. A point successive relaxation technique was used to solve the Poisson's equation.

e) The new values of the streamfunction now help in deriving the velocity components in the 'z' and 'r' directions respectively, through Equation 6-8.

f) The new boundary values of the streamfunction (Ψ) and vorticity (ξ) are calculated by using new ψ and ξ values at the interior points.

g) The solution proceeds by going back to c) in calculating ξ and follows steps d) through f). This procedure goes on until a convergence level or the desired time level is reached and this provides the final solution.

Primitive Variable Approach. The values of the flow variables for this method are obtained by using the SIMPLE algorithm. This algorithm is discussed in detail by Patankar (1980) and is briefly outlined here.

a) As in the case of the streamfunction-vorticity method, initially the grid points within the physical space are first laid out. In this case boundary fitted co-ordinate are not used and an (r-z) axisymmetric cylindrical system is used.

b) The initial condition is given by providing a value of pressure (p^*) at each grid point.

c) The momentum Equations 6-1 and 6-2 are discretized using the control volume approach and following Appendix B

$$a_e u_e = \sum a_{nb} u_{nb} + b + A_e (p_p - p_e) \qquad (6\text{-}28)$$

$$a_n v_n = \sum a_{nb} v_{nb} + b + A_n (p_p - p_n) \qquad (6\text{-}29)$$

The summation sign is used to add the contribution of the four (E,W,N,S) neighboring points. 'A' is the cross sectional area and 'b' is the source term. The velocity

components are used in a staggered form. From the guessed value of the pressure field (p^*) and the neighboring velocities u_{nb} and v_{nb}, a tentative set of velocities u_e^* and v_n^* can be estimated from Equations 6-28 and 6-29

$$u_e^* = \sum a_{nb} u_{nb}^* + b + A_e (p_p^* - p_e^*)/a_e \qquad (6\text{-}30)$$

$$v_n^* = \sum a_{nb} v_{nb}^* + b + A_n (p_p^* - p_n^*)/a_n \qquad (6\text{-}31)$$

d) The velocities u_e^* and v_n^* will in general not satisfy the continuity equation (Equation6-3). If a correction p′ is applied to the guessed value of p^* such that

$$p = p^* + p' \qquad (6\text{-}32)$$

then one gets the corresponding corrected value of the velocity u′ which is defined by

$$u = u^* + u' \qquad (6\text{-}33)$$

e) By subtracting Equation 6-30 from Equation 6-28 one gets

$$a_e u_e' = \sum a_{nb} u_{nb}' + A_e (p_p' - p_e') \qquad (6\text{-}34)$$

The term $\sum a_{nb} u'_{nb}$ can be considered as negligible and is dropped. Equations 6-28, 6-30,6-32 and 6-33 combine to give a velocity correction formula

$$u_e = u_e^* + d_e (p_P' - p_E') \qquad (6\text{-}35)$$

where $d_e = A_e/a_e$. In a similar manner we get for v_n,

$$v_n = v_n^* + d_n (p_P' - p_N') \qquad (6\text{-}36)$$

where $d_n = A_n/a_n$.

f) The pressure correction term (p′) is derived from the continuity equation and is given by the algebraic form:

$$a_P p'_P = a_E p'_E + a_W p'_W + a_N p'_N + a_S p'_S + b \qquad (6\text{-}37)$$

where $a_E = (\rho Ad)_e$

$a_W = (\rho Ad)w$

$a_N = (\rho Ad)_n$

$a_S = (\rho Ad)_s$

$a_P = a_E + a_W + a_N + a_S$

$b = (\rho Au^*)_w - (\rho Au^*)_e + (\rho Au^*)_s - (\rho Au^*)_n - (\rho_P - \rho_P^o)(\Delta V/\Delta t)$

Here 'ρ' is the density of the fluid , 'ΔV' is the volume of the control volume used for discretization and Δt is the increment in time.

g) The new pressure term p′ is used as the new guessed pressure p^*. Calculation is returned to step 'c' and the procedure is continued until the desired convergence is reached.

6.7 Test Cases

Before starting the solution to our problem, some test cases were run to determine the efficacy of the coded programs. The deviation of the computed results from known results, serves to analyze the effectiveness of the computer code. Different cases were run for the streamfunction-vorticity method and for the primitive variable method.

In the streamfunction-vorticity case a boundary fitted coordinate system was used. As a preliminary test, fluid

flow through a cylindrical pipe was considered. It is well known that for laminar flow a parabolic profile is attained after the flow has fully developed. To test this, a cylinder with sufficient length was considered and a flat velocity profile at the tube inlet was taken. The flow Reynolds number based on this mean velocity was 50. The grid was generated to get its concentration towards the centerline. The transformation of the physical coordinate (r-z) to the computational coordinate (ξ-η) is given by

$$z=\xi \tag{6-38}$$

$$r=H\frac{(\Omega+1)-(\Omega-1)\{[(\Omega+1)/(\Omega-1)]^{1-\eta}\}}{[(\Omega+1)/(\Omega-1)]^{1-\eta}+1} \tag{6-39}$$

where Ω is a clustering parameter within the range of 1 to ∞. As the value of Ω approaches 1, more grid points are clustered near the bottom surface and which happens to be the centerline of the cylinder in our case. Figure 6-8 shows the grid lines as they appear on the physical and computational space. It was observed that the value of the parameter Ω determined the accuracy of results obtained. When Ω had a value of 2 the error in determining the centerline velocity was 0.35%. With the decrease in the value of Ω, the error increases. Figure 6-9 shows the flow parameters as obtained by using β equal to 1.6. Figure 6-10 is a plot of the absolute error obtained in calculating the centerline velocity by changing the numerical value of Ω.

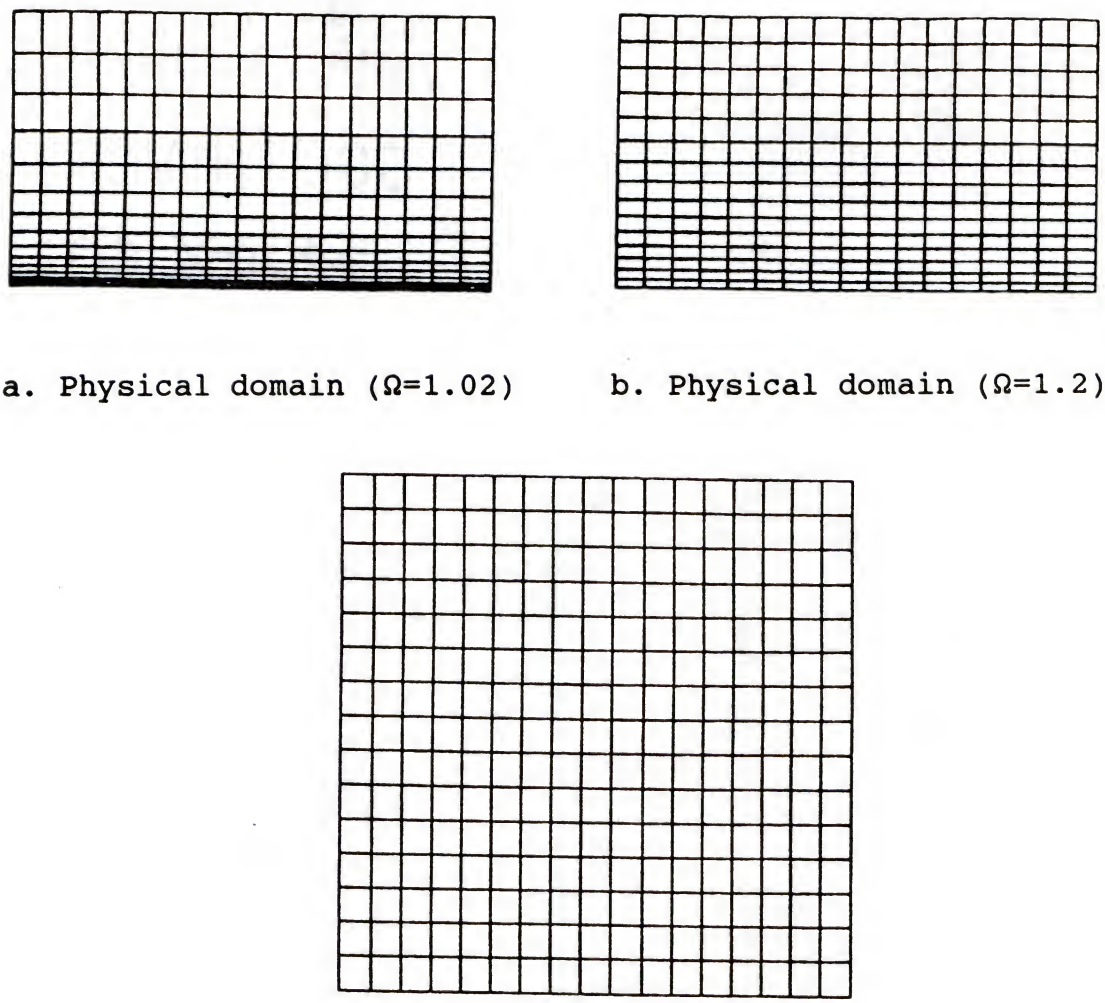

a. Physical domain (Ω=1.02)

b. Physical domain (Ω=1.2)

c. Computational domain

Figure 6-8 Physical and computational domain generated by transformation Equations 6-38 and 6-39.

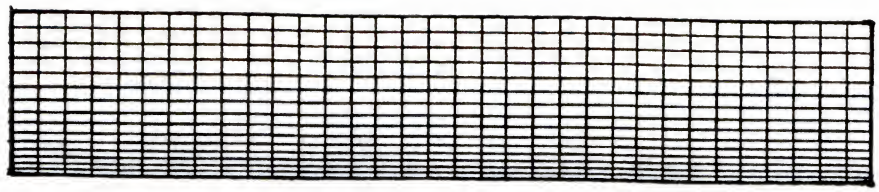

a. Grid lines

b. Stream function contour lines

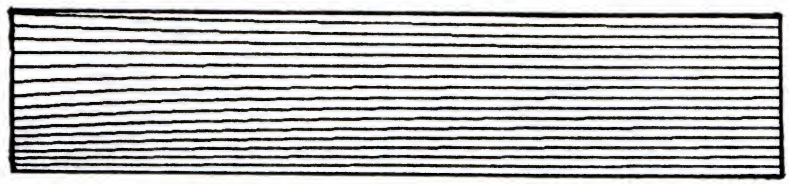

c. Vorticity contour lines

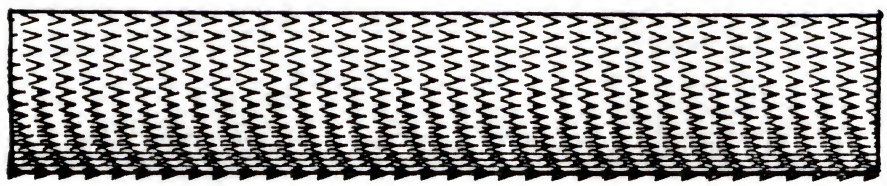

d. Velocity vectors

Figure 6-9. Grid lines and flow parameters for β=1.2

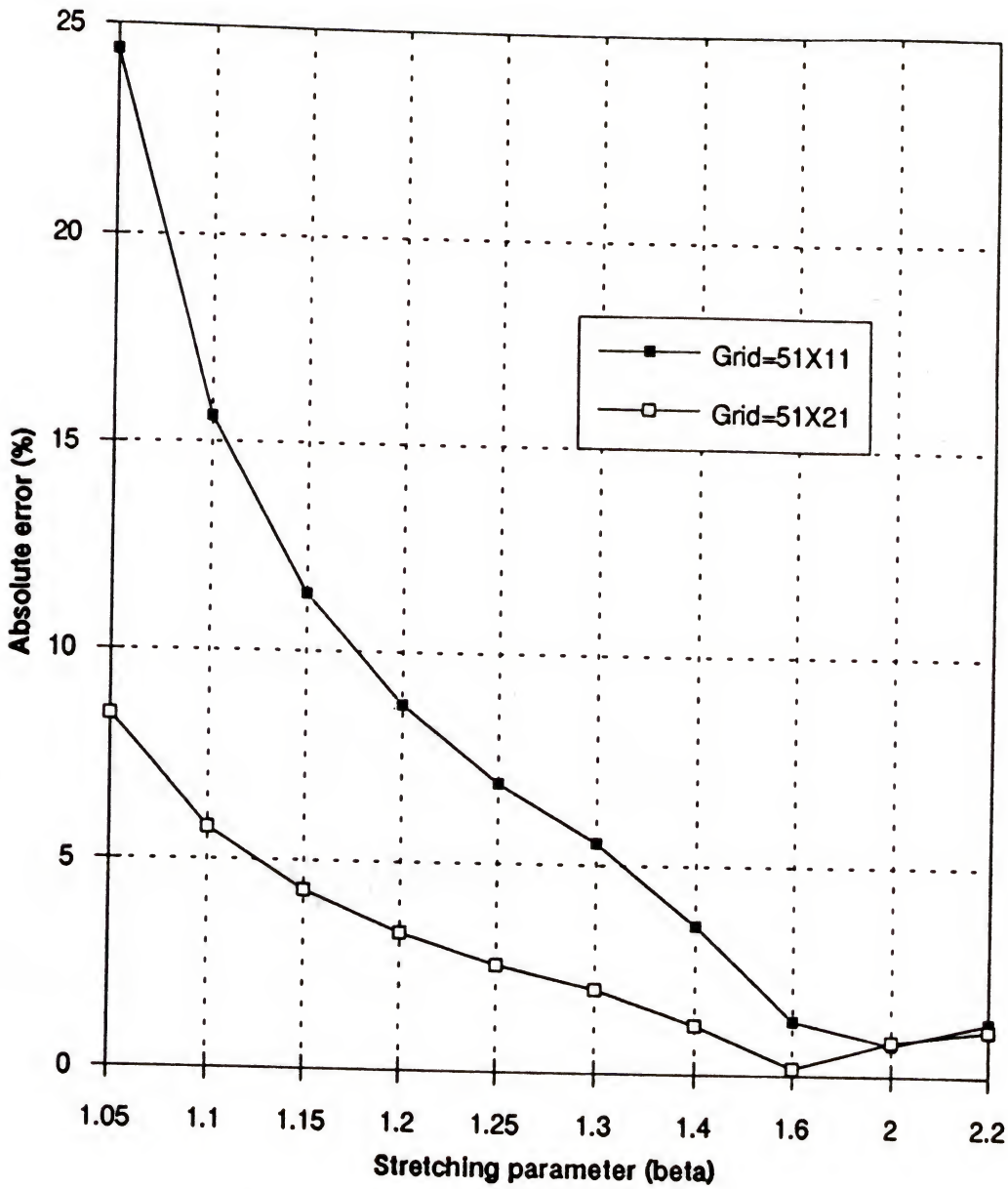

Figure 6-10. Absolute error in determining the centerline velocity for Reynolds number of 50

As a second case, a cylindrical pipe was again considered, but it had a bell shaped constriction. Figure 6-11 a. shows the shape of the physical space. Lee and Fung (1970) had performed some numerical study on such a system and Bentz and Evans (1975) conducted an experimental study by using a laser Doppler anemometer. The axisymmetric constriction was specified by the equation

$$r=\frac{D_0}{2}\left[1-\frac{1}{2}\exp\left(-16\frac{z^2}{D_o^2}\right)\right] \qquad (6\text{-}40)$$

were 'r' is the value of the local radius of curvature of the wall, D_o is the diameter of the tube, and 'z' is the distance in the axial direction. Reynolds numbers of 2 and 25 were used to compare results with the published values. The results are plotted and shown in Figure 6-11 b and 6-11 c. It can be noticed that the error from the present work is larger than the previous numerical work. Lee and Fung (1970) had however used conformal mapping to generate the grid lines and this eliminated any error arising during the mapping from physical to computational regime. Also, it was observed in the present work that the error propagated during the iterative computation of the streamfunction values and not during the calculation of the vorticity transport equation. This was tested by using analytical values of metrices during the iterative calculation of the streamfunction. The vorticity values obtained from the transport equation did not vary much if numerically

a. Axisymmetric bell shaped constriction

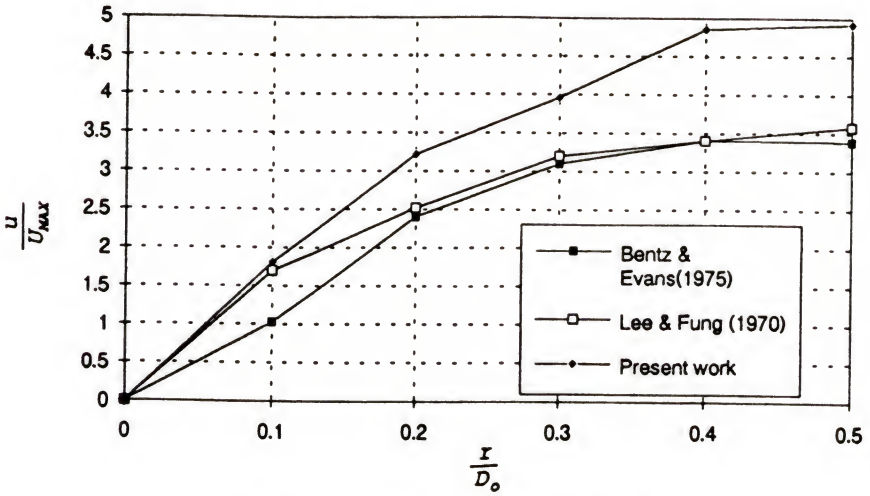

b. Reynolds number = 2

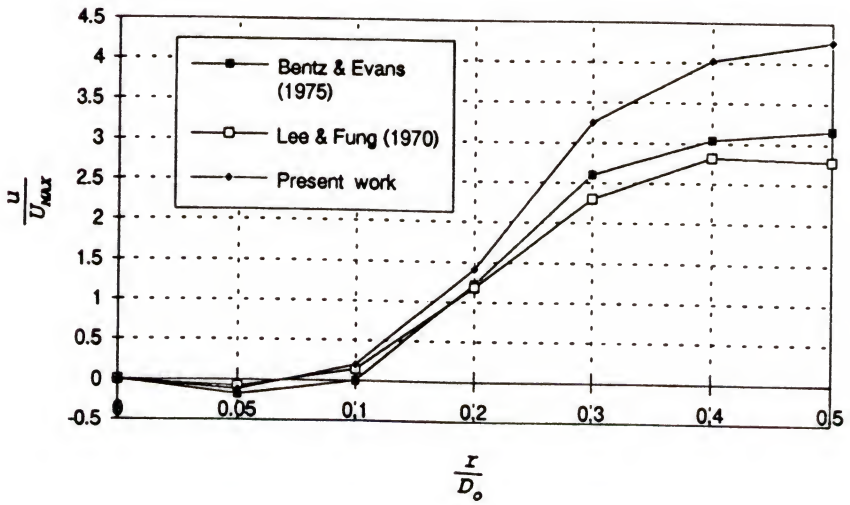

c. Reynolds number = 25

Figure 6-11 Grid points and nondimensional velocity values at the center plane

generated values of the metrices were used instead of the analytically known values. However this point can be stated emphatically only after rigorous testing of several cases and which was not done here.

When the streamfunction-vorticity method was applied to problem of sphere within a cylinder, convergence became a major problem. This can be explained in the light of the test cases run. In order to get good values near the surface of the sphere, the value of the stretching factor β is chosen close to 1. But as can be seen from Figure 6-10, even in simple cases this resulted in significant error. Also as had been explained earlier, when the flow is not aligned to the grid, error arising from numerical diffusion becomes dominant. In the present geometry both these factors play a contributory role. In the case of bell shaped constriction, the value of the Reynolds number was less and convergence did not create a problem although the results were not quite accurate. Similarly,in the case of a sphere within a cylinder, the convergence was not difficult when flow Reynolds number (based on the tube diameter and mean flow velocity) was equal to 30 and 55 respectively. If the Reynolds number is based on the sphere diameter then in both the cases it did not exceed 20. Figure 6-12 shows some of

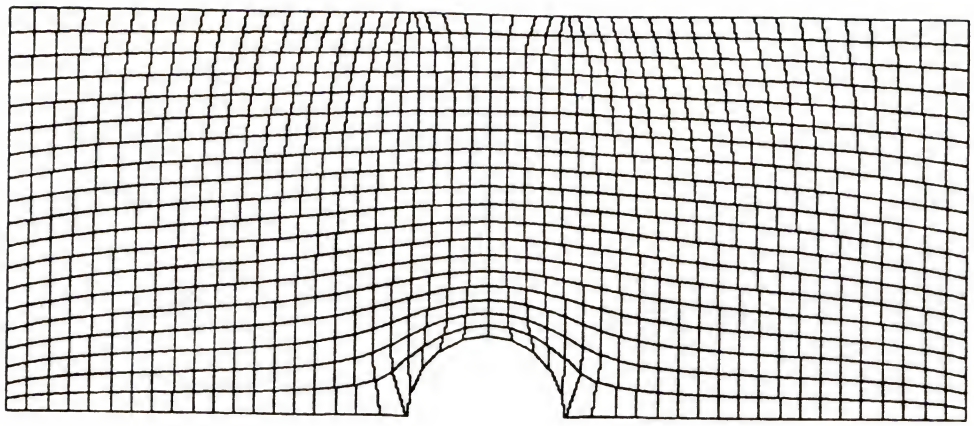

a. β= 0.2

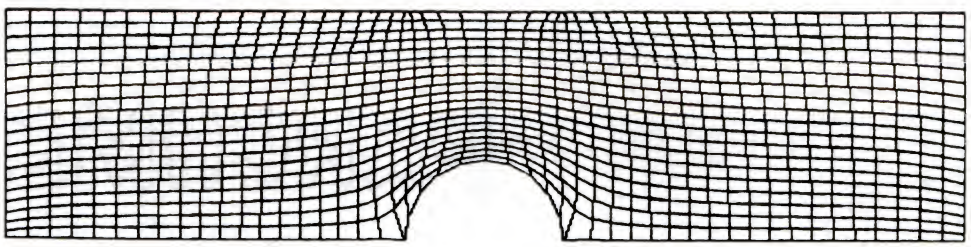

b. β=0.35

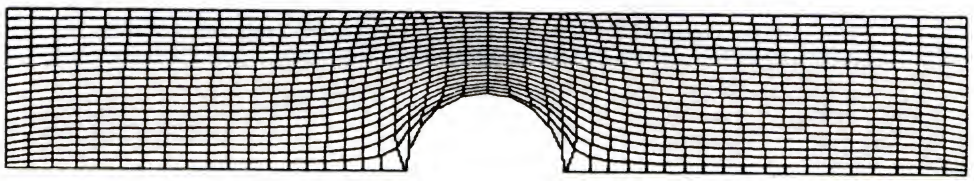

c. β=0.5

Figure 6-12 Different diameter ratio (d/D) considered

the different sphere to cylinder diameter ratios (β) that were considered. Figures 6-13 and 6-14 give an estimate of how the streamfunction, vorticity and the velocity vectors look like for different Reynolds numbers. Also from Figure 6-15, one finds that the value of vorticity on the surface of the sphere did not fall below zero. This indicates that the flow did not separate for the Reynolds number considered. This is fine since it has been found that the flow separation takes place when the Reynolds number (based on sphere diameter) reaches 20. Beyond Reynolds number of 100 convergence was not obtained. Some of the possible reasons for this have been discussed earlier.

As a result numerical testing was carried out by primitive variable approach. This program incorporated a linear flux spline scheme to reduce error when the flow is not aligned with the grid lines. Although the surface of the sphere was not traced out correctly through a 'r-z' coordinate, but results obtained were meaningful. The robustness and exactness of the program had already been tested by Karki et al. (1988), and no further test cases are shown here. Figure 6-16 shows the separation angle as a function of the sphere to cylinder diameter ratio. The flow Reynolds number was taken as 100 and the result shows an interesting similarity with the results obtained through boundary layer analysis. The separation angle reaches a minimum when the diameter ratio is around 0.5. Since

different flow rates are used while comparing the numerical results with the boundary layer analysis, the magnitude of the separation angle differs. In boundary layer analysis the Reynolds number was around 3000, but in the numerical case it is much less (to consider an axisymmetric flow). Figure 6-17 gives a plot of the separation angle as a function of Reynolds number with a constant sphere and cylinder size. This has also been compared with the flow over an unbounded sphere. In the case of free flow, the separation angle is given by $\theta_s = 180 - 42.5[\ln(Re/20)]^{0.483}$, but in the bounded case no explicit equation has been proposed here due to the lack of several data points. The drag force as obtained from the experiment has been calculated with the numerical program. Since the sphere surface was not properly obtained from the 'r-z' coordinates, a good result should not be anticipated. Figure 6-18 provides a comparison between the experimental and numerical results. By increasing the number of grid points on the sphere surface, the drag force results initially approach the experimental values. But further increase in the grid point number did not help the cause to a large extent. Finally some prdicted flow patterns for β(ratio of diameter between sphere and cylinder) of 0.5 and 0.1 are shown in Figures 6-19 through 6-22 for Reynolds numbers of 50 and 250.

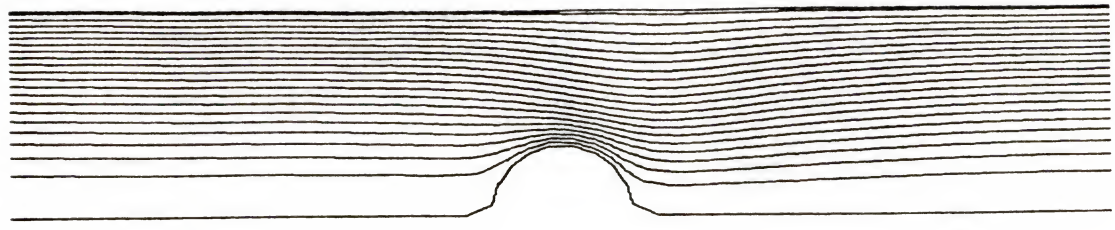

a. Streamlines (Re=30)

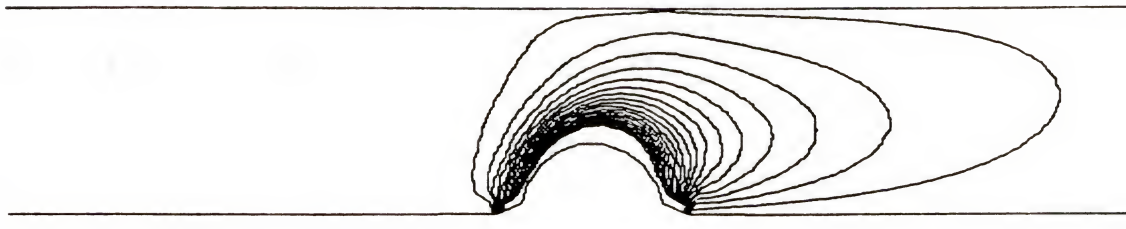

b. Vorticity (Re=30)

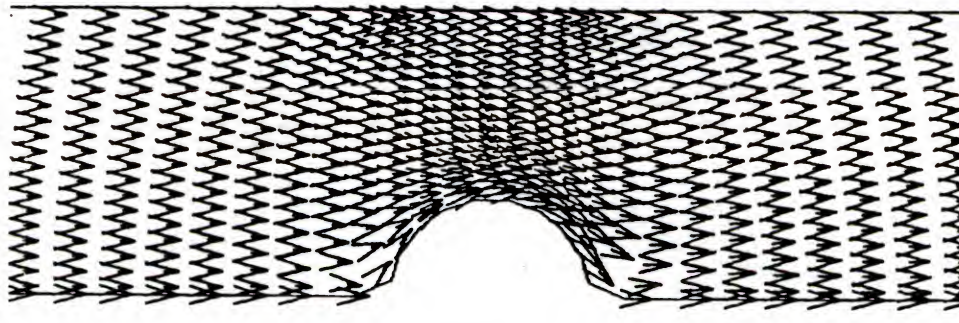

c. Velocity vector (Re=30)

Figure 6-13. Flow patters for Reynolds number of 30

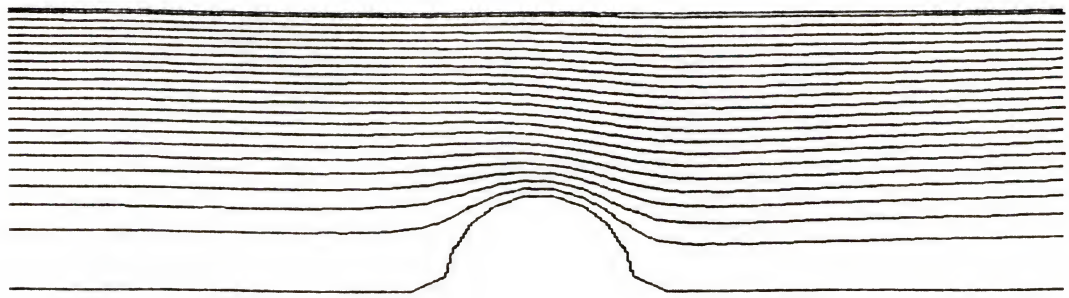

a. Streamline (Re=55)

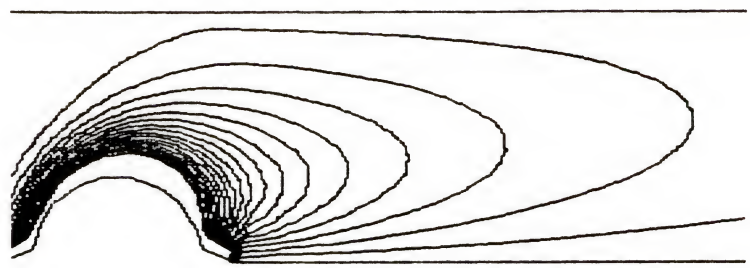

b. Vorticity (Re=55)

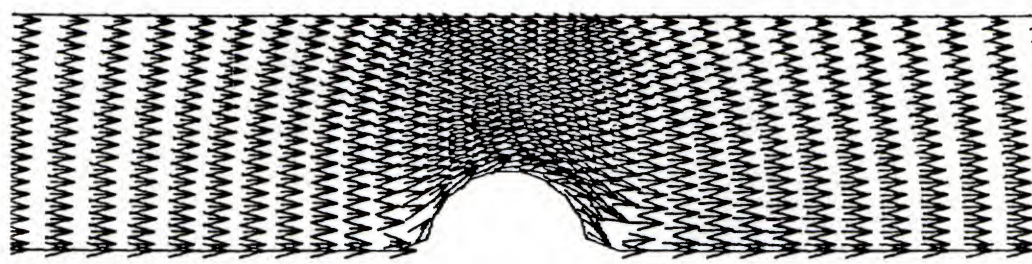

c. Velocity vector (Re=55)

Figure 6-14 Flow patters for Reynolds number of 55

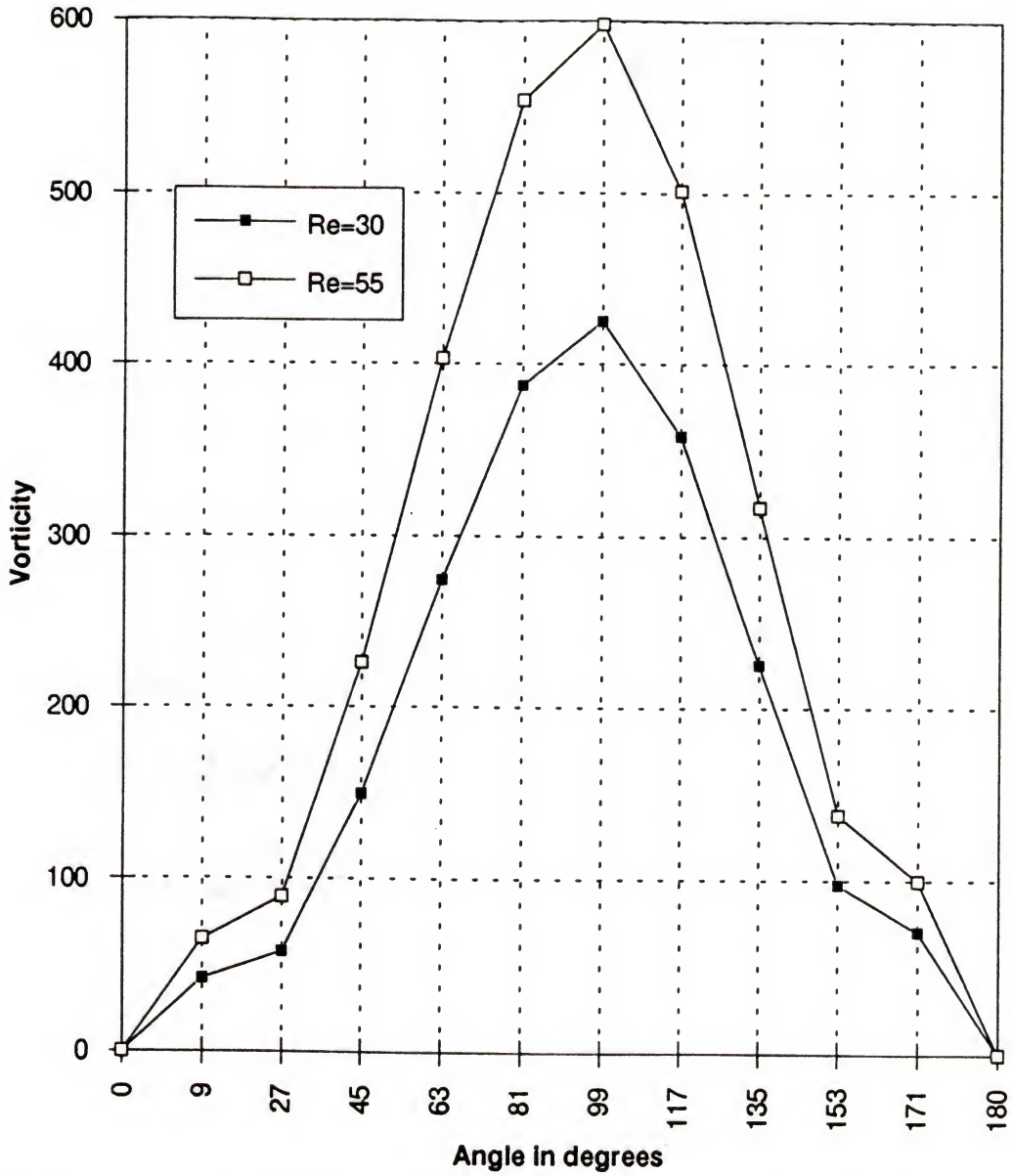

Figure 6-15 Vorticity distribution on sphere surface (ß=0.35)

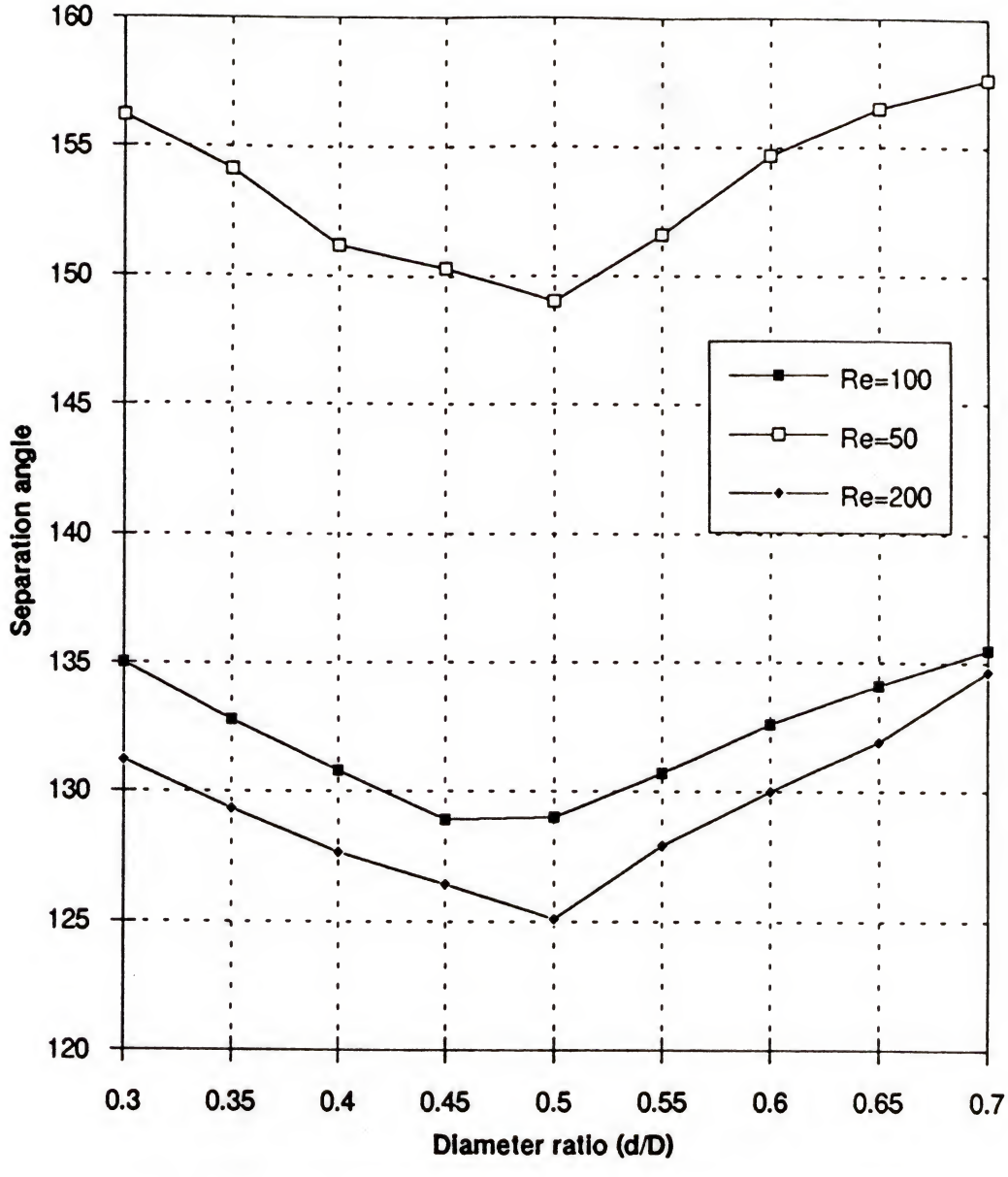

Figure 6-16 Plot of separation angle and different sphere to cylinder diameter ratio

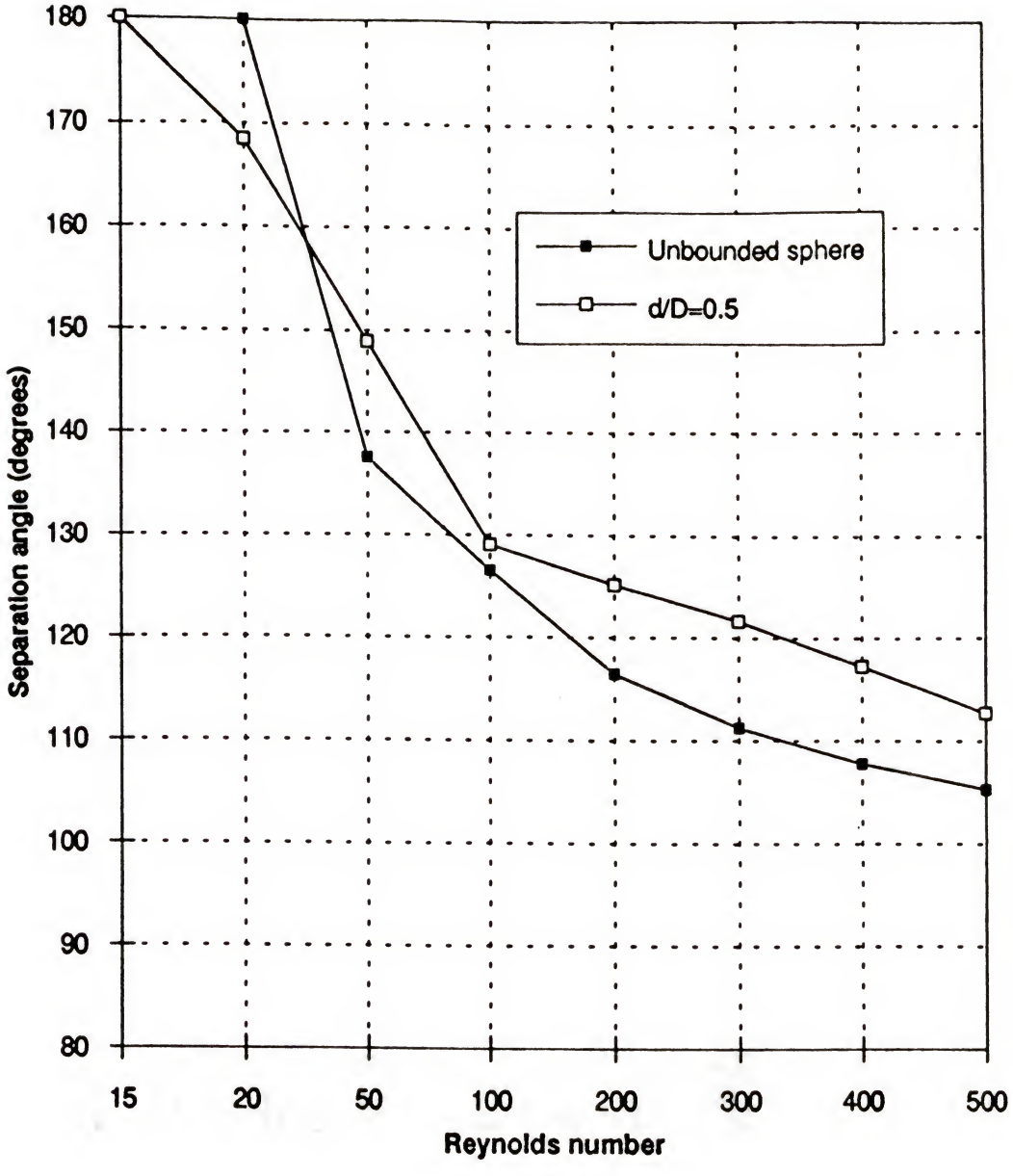

Figure 6-17 Plot of separation angle for different flow Reynolds number

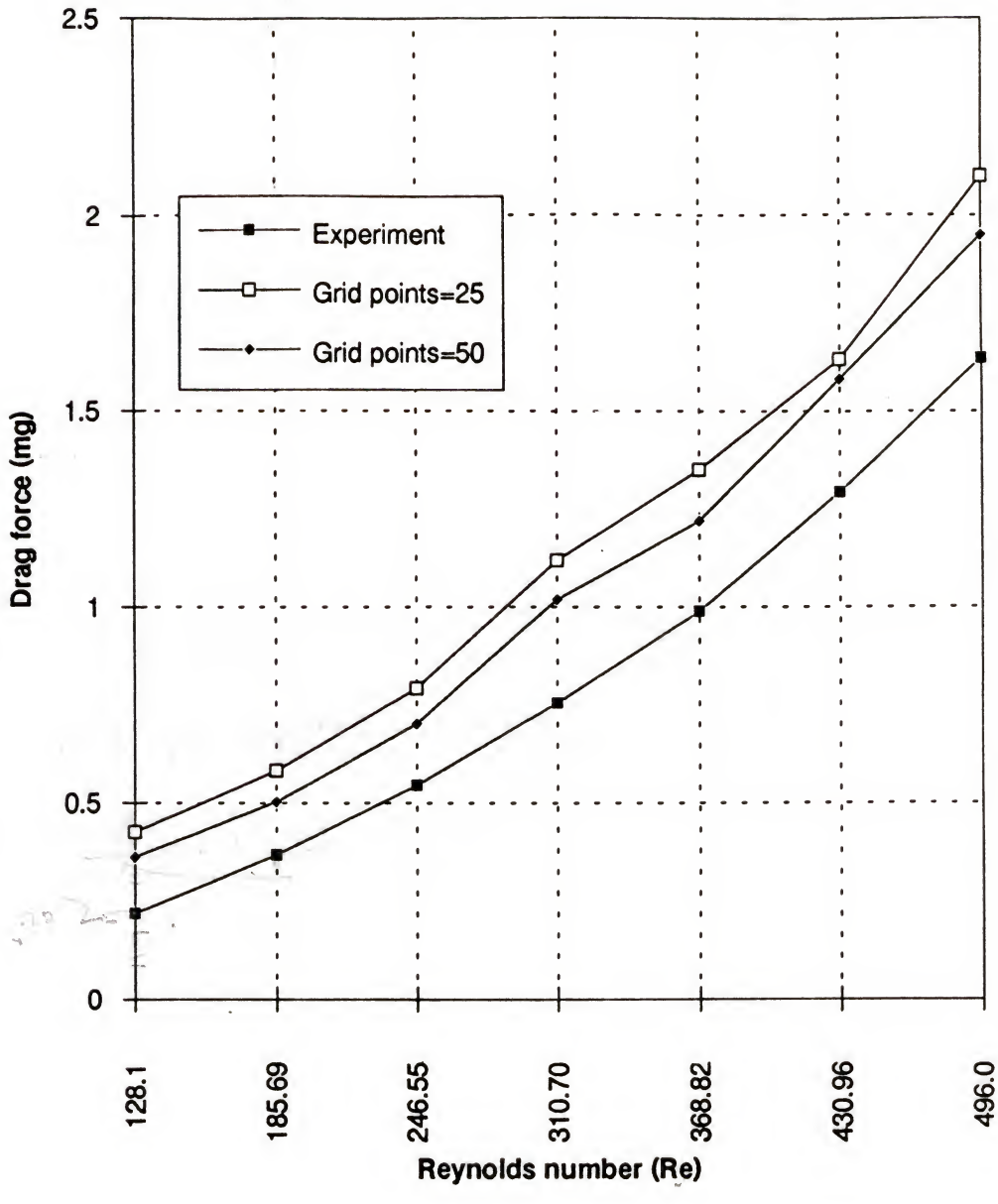

Figure 6-18 Drag force calculation on sphere (ß=0.5)

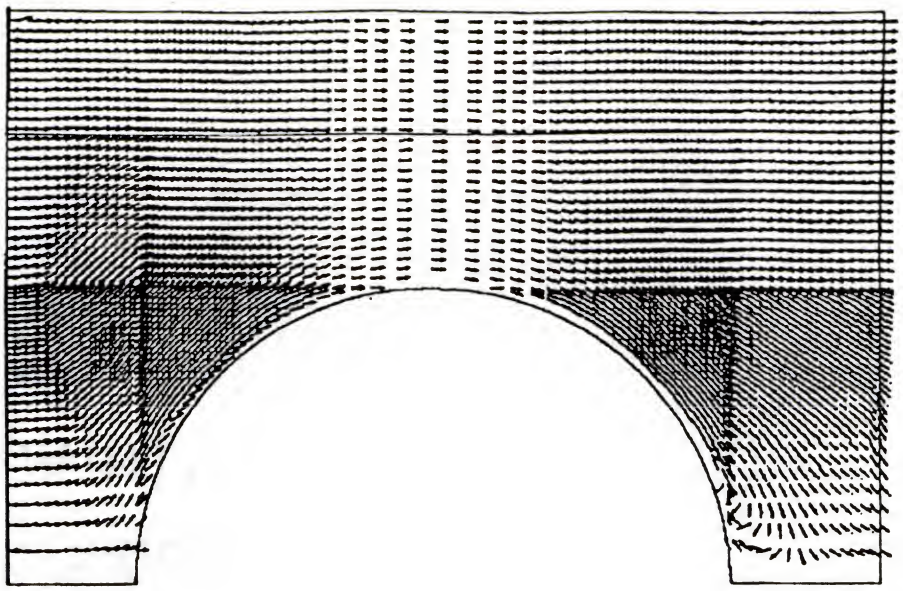

a. Reynolds number = 50, $\Phi_{separation}$= 165.08 degrees

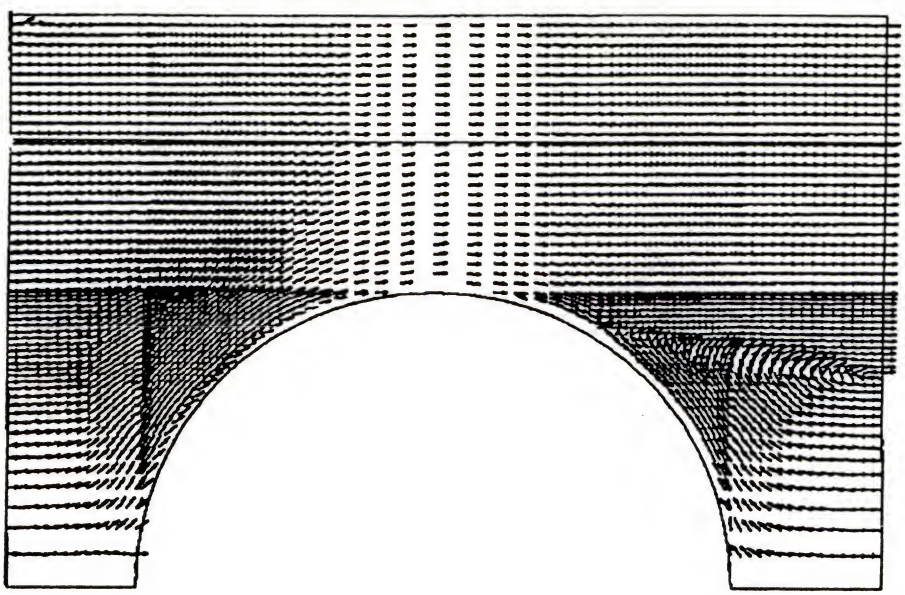

b. Reynolds number = 250, $\Phi_{separation}$= 122.86 degrees

Figure 6-19 Velocity vectors for β=0.5

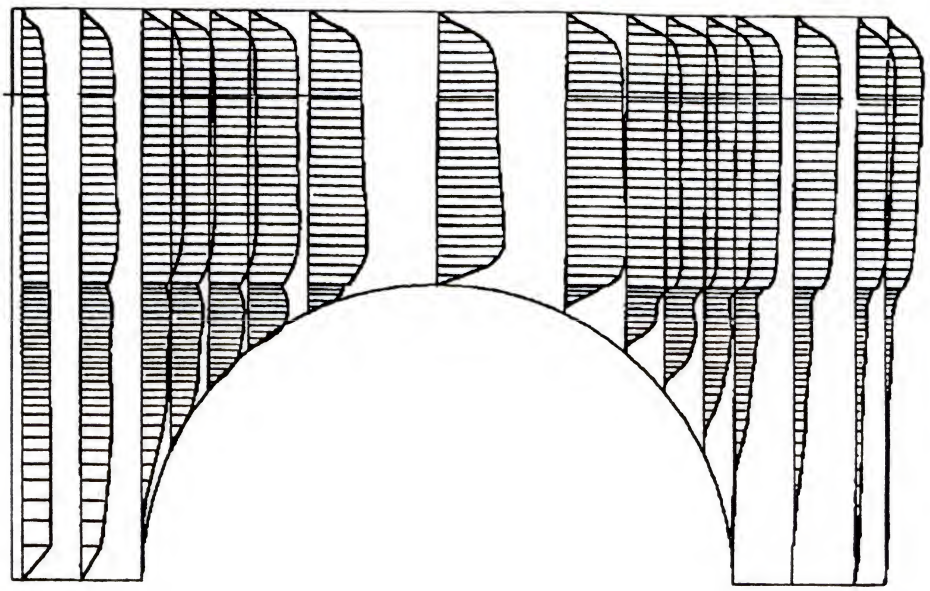

a. Reynolds number = 50, $\Phi_{separation}$= 165.08 degrees

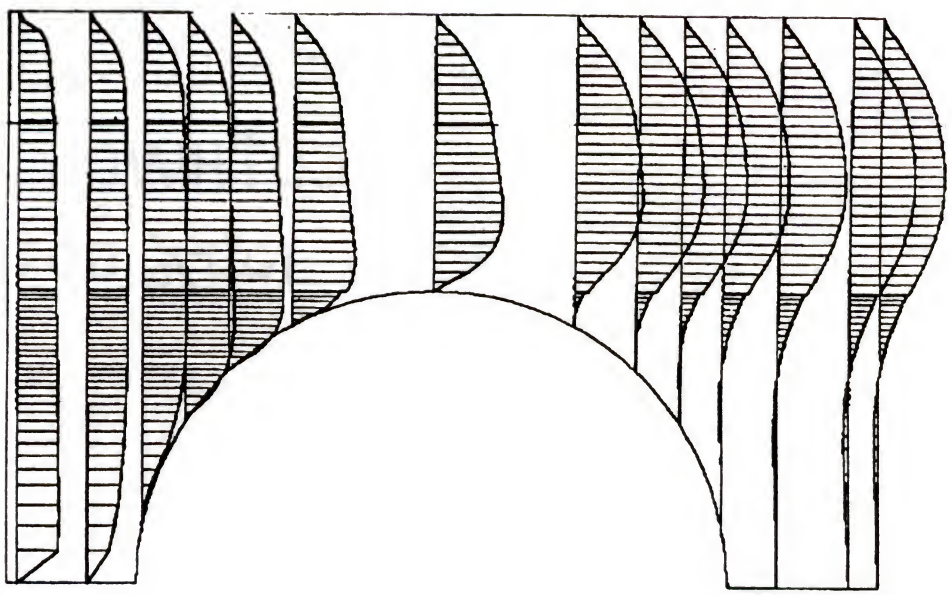

b. Reynolds number = 250, $\Phi_{separation}$= 122.86 degrees

Figure 6-20 Velocity (U) profile for β=0.5

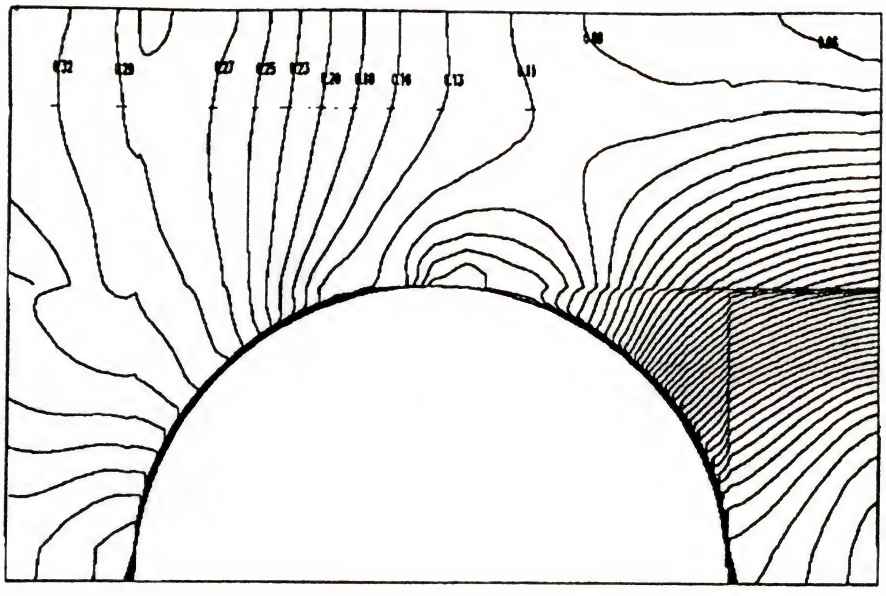

a. Reynolds number = 50, $\Phi_{separation}$= 165.08 degrees

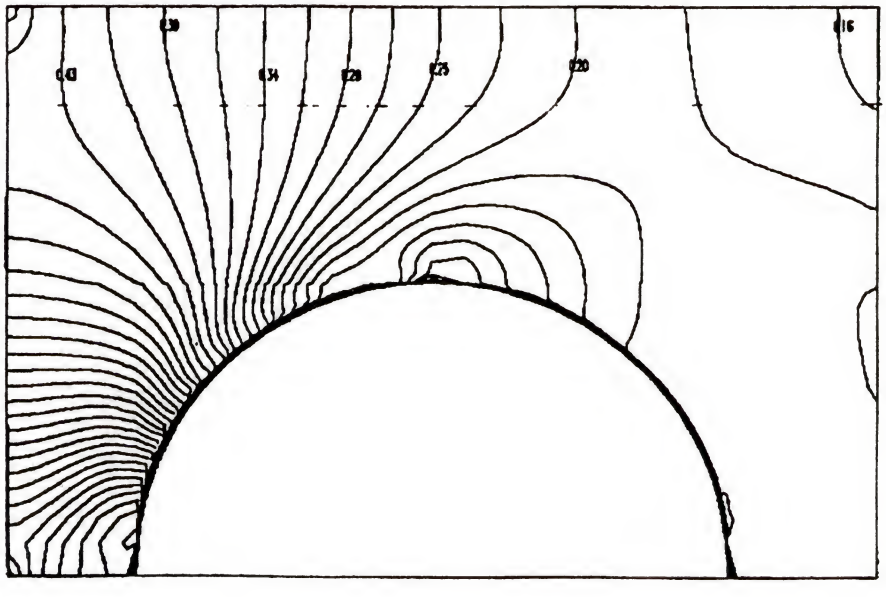

b. Reynolds number = 250, $\Phi_{separation}$= 122.86 degrees

Figure 6-21 Pressure contours for β=0.5

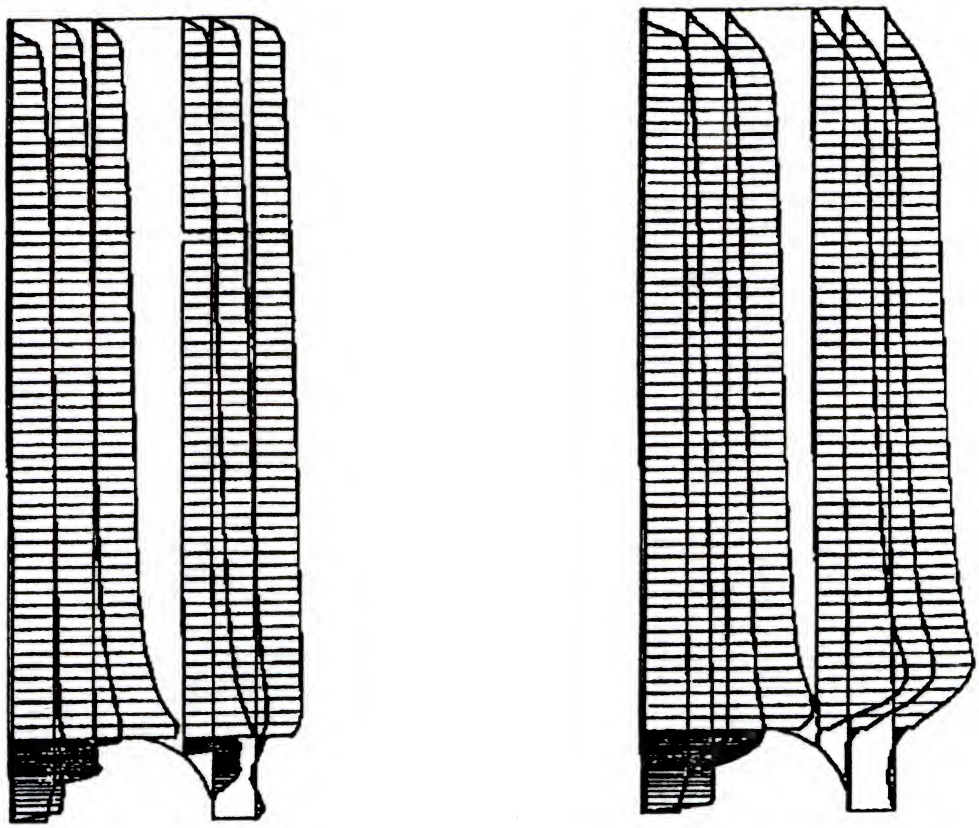

a. Reynolds number = 50

$\theta_{separation}$= 173.95 degrees

b. Reynolds number =250

$\theta_{separation}$= 142.76 degrees

Figure 6-22 Velocity profile for β=0.1

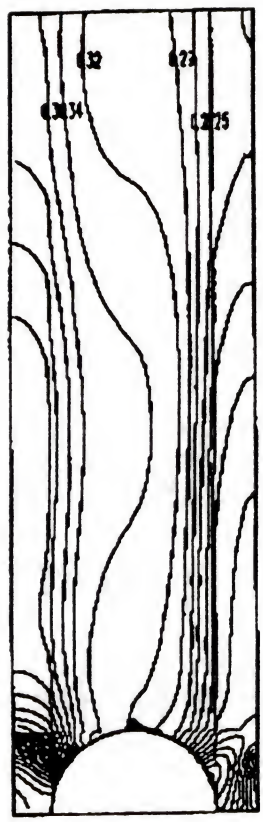

a. Reynolds number = 50

$\theta_{separation}$= 173.95 degrees

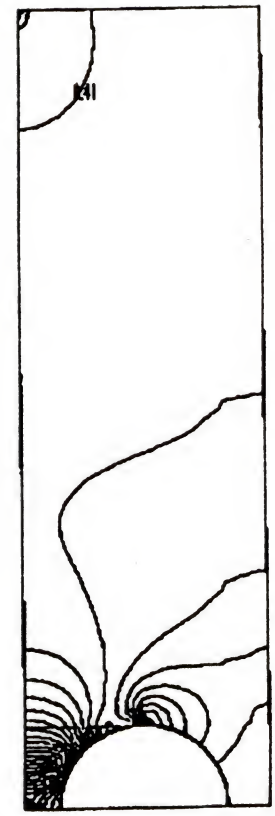

b. Reynolds number =250

$\theta_{separation}$= 142.76 degrees

Figure 6-22 Pressure contours for β=0.1

CHAPTER 7
SUMMARY AND CONCLUSION

The current study tries to further the investigation of a fundamental fluid flow problem; the drag force measurement on a cylindrically bounded sphere. This work is then extended for the viscosity measurements of gases. The methodology proposed for such viscometric measurements has very attractive features when the gas is corrosive or has a high temperature.

Previous work in the area of drag measurement for spheres in a cylinder had focussed on sedimenting spheres. For very low flow rates analytical work was performed by neglecting the convective terms. Later improvements were initiated by taking other factors into consideration- like linearizing the inertial term, taking the wall effect etc. The results of these studies provided a means of measuring the viscosity of fluids. However, since gases have a low viscosity the sedimentation study had a practical implication for liquid viscosity measurements only. Among other ideas, the capillary tube and the oscillating body were of less restrictive nature and as such are used as a primary viscometer till date. However even these primary instruments run into difficulty when the fluid is of

corrosive nature. Unresearched materials compatibility and the unknown performance of the measuring device give rise to the uncertainty in the final results. The present work involves the drag measurement on a sphere which is rigidly supported at the center of a cylinder. The viscosity is ascertained by knowing an accurate plot of the coefficient of drag and the flow Reynolds number. For an unknown gas the coefficient of drag can be had from its flow rate and then from the plot the Reynolds number is obtained. This provides the numerical value of the viscosity. An interesting feature of the setup is that the measuring devise is not exposed to the fluid. As such during the measurements, one is not concerned with the reaction between the fluid and the drag measuring device. This helps the methodology to be successfully applied for any corrosive gas. For high temperature, the sphere is only heated, and the temeperature gradient is felt near the sphere surface only. As a result the flowing gas has a much lower temperature as it exits the system and most the problems related with the high temperature is eliminated. In the actual study, only clean gases like Oxygen and Helium were used at room temperature, and the results were quite good.

Very low flow rates are however desirable in order to determine an accurate value of viscosity. At creeping zone, Haberman and Sayre (1958) give the drag force on a fixed and rigid sphere in a Poiseuille flow as

$$DRAG = 6\ \pi\mu R\ U_{max}\ K \qquad (7\text{-}1)$$

where
$$K = \frac{1 - \frac{2}{3}\beta^2 - 0.20217\beta^5}{1 - 2.105\beta + 2.0865\beta^3 - 1.7068\beta^5 + 0.72603\beta^6}$$

β is the diameter ratio between the sphere and the cylinder, μ is the viscosity of the fluid, R is the radius of the sphere and U_{max} is the centerline velocity for Poiseuille flow. In order to get the maximum sensitivity in the final results, one needs to choose a large sphere. For the present microbalance the maximum weight restriction is 3.5 grams. If one uses teflon ball then we can choose a sphere of diameter around 12.5 mm. and for nitrogen the drag forces are:

Diameter Ratio (β)	Drag Force (kg)
0.1	2.6764 E-7
0.2	3.4876 E-7
0.3	4.7572 E-7
0.4	6.8617 E-7
0.5	1.0605 E-6
0.6	1.7869 E-6
0.7	3.3484 E-6
0.8	7.0558 E-6
0.9	1.5959 E-5

Thus the drag force can be measured with a resolution of one part per thousand (since the sensitivity of instrument is 0.1 μg and the drag force is in mg). Instrument this precise

were not available earlier, and gas viscosity measurements by direct drag measurement were previously ignored.

The sphere is suspended by a nylon string and it can have its presence felt in two ways. Firstly the drag measured in the experiment is the sum of the drag on the sphere and the string. In order to eliminate the drag on the string, two different string lengths for the same geometry and flow conditions were used. This method provided very accurate results as is seen from Table 3-1. Secondly the fluid flow parameters for an isolated sphere versus a sphere supported by a string can be different. However it has been found by several authors that if the diameter of the string is small in comparison to that of the sphere then the flow remains unaffected. Seeley (1973) found the flow pattern affected when D/d was equal to 18.8 and 10.9, where D was the sphere diameter and d was the string diameter. Taneda (1956) found that if D/d ratio is 30 then the wake remained unaffected from Reynolds number of 5 to 300. Also Kalra and Uhlher (1971) investigating the flow over a supported sphere concluded that the string had negligible effect on the separation angle and the wake dimension when D/d was 36 and the Reynolds number ranged from 30 to 750. In our experiment the string was 0.07 mm in diameter and the sphere diameter ranged from 7.88mm to 12.67mm and as such its effect on the flow can be safely neglected.

One of the parameters of paramount importance for the fluid flow over a bluff body is the separation angle. It is very difficult to ascertain it correctly by experimentation or by numerical approach. In this study a boundary layer analysis is performed to observe the dependance of the separation angle on the diameter ratio between the sphere and the cylinder (ß). This study is based on the assumption that the Reynolds number is fairly high but low enough to have a laminar boundary layer. The results show that the separation angle reaches a minimum around ß = 0.5. Interestingly enough the same pattern is also provided by the numerical studies. However the Reynolds number for the numerical studies should be low so that the flow is two dimensional throughout. This is necessary since the code was written for axisymmetric case only.

The results of the drag force calculation is best modelled by obtaining a relationship between the coefficient of drag (C_D) and the flow Reynolds number. Previous authors who had performed investigation had come up with correlations linking the coefficient of drag for an unbounded sphere ($C_{D\infty}$) to the coefficient of drag for a bounded sphere (C_D) for the same Reynolds number. However different correlations were propounded due to different results obtained in the experiments. One of the disturbing features has been the nebulous definition of the Reynolds number while comparing the unbounded and the bounded sphere.

Some authors have used the mean velocity in the tube and the others have chosen the centerline velocity as the representative velocity to define the Reynolds number. There has also been a dilemma over the choice of cylinder diameter over the sphere diameter in this regard. As far as the velocity is concerned, a problem arises since there is a velocity distribution for a bounded sphere but an unbounded sphere is assumed to encounter a constant mean velocity. Thus based on the physics of the problem the current work proposes a characteristic velocity which gives the same dynamic force as exerted by the velocity distribution seen by the sphere. It is given by $U_c = U_{max} \sqrt{\{1-(2\beta^2/3)+(\beta^4/5)\}}$ where U_{max} is the centerline velocity, and β is the diameter ratio between the sphere and the cylinder. In the above relationship the mean is obtained in a linear way. If an area averaging is done then the characteristic velocity is given by $U_{C1} = U_{max}\sqrt{\{1-(\beta^2/2)+(\beta^4/3)\}}$. If the Reynolds number is based on these characteristic velocities and the diameter of the sphere, then a simple relationship is obtained, as given by Equation 5-18 or 5-19, for the coefficient of drag between a bounded and unbounded flow.

Finally an attempt was made to explain the fluid flow phenomenon by numerical studies. The two popular approaches to incompressible fluid flow are the streamfunction-vorticity method and the primitive variable method. During streamfunction-vorticity method a boundary fitted coordinate

system was applied. Although it appears to be attractive for the geometry in hand, but the results can be erroneous. The grid was generated by elliptic grid generation technique. This resulted in smooth grid lines, but relatively sparse grid density close to the sphere surface. As has been found in test cases, for boundary fitted coordinate in streamfunction-vorticity method, the convergence did not guarantee a good result. A stretching parameter of 1.2 was used in the present case. The root cause of the deviation in the answers, from exact values, had been during the iterative solution for the streamfunction. This has been discussed in chapter 6 and concluded by using analytical values for the metrices. The program also showed little signs of convergence after the Reynolds number reached 100. Attention was paid to the primitive variable method which employed r-z coordinates. Here the sphere surface was not properly described by the grid lines, but the results were satisfactory. In this latter method, a linear flux spline was used to model the fluxes in the control volume, during the process of discretization. This has been found to handle problems in an efficient way when the flow is highly non-aligned to the grid lines. The results obtained show the same trend as has been shown by the experiment. From the experience gathered in this process, the following recommendations can be made for future studies. Firstly a body fitted system for the primitive variable approach

should be used. By using different stretching factors, the results will not change as dramatically as in the streamfunction-vorticity method. As had been found in the streamfunction-vorticity method, during the iteration for the vorticity and streamfunction, the numerical results for the metrices gave a satisfactory value for the vorticity but not for the streamfunction. This situation does not exist in the primitive variable method, were conservative equations like those for the computation of vorticity is used all the time. However one will still not get good resolution for the front and aft of the sphere, by using elliptic equations. If one uses a grid that is forced to follow the sphere surface, then the value of the metrices may cause the results to diverge from the actual results. One of the remedies to overcome this is to use a multiblock composite configuration. In this procedure, the physical space is divided up into convenient number of regions (blocks) and a body fitted coordinate is used for each of them. Caution must be taken to link each of the blocks through the common layer they include amongst themselves. Figure 7-1 shows the mapping of the physical space to the computational space by this procedure.

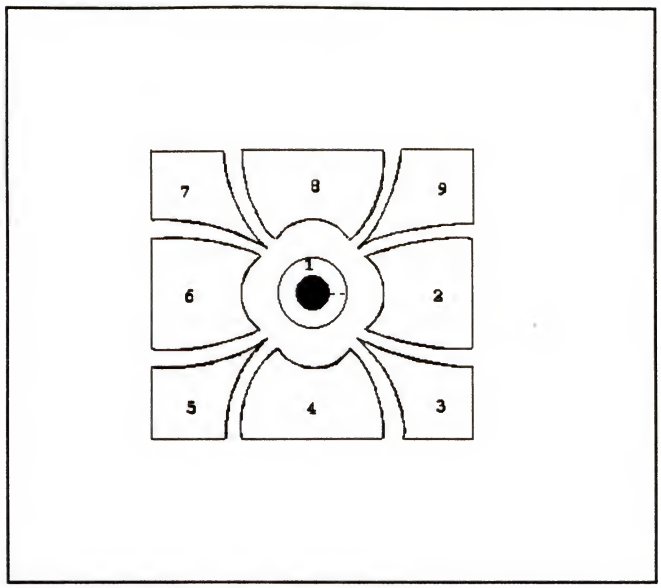

a. Physical region

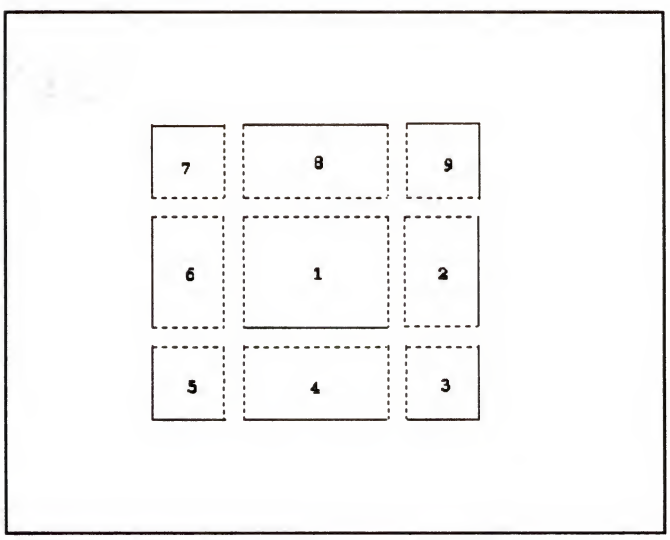

b. Computational region

Figure 7-1 Multiblock composite configuration

APPENDIX A

NUMERICAL VALUES USED FOR BOUNDARY LAYER CALCULATION

The calculations were carried out by expanding the outer velocity (U), the local radius of curvature (r) and the stream function (Ψ) respectively as a power series (Schlichting 1968):

$$U = u_1x + u_3x^3 + u_5x^5 + u_7x^7 + \ldots \quad \text{(A-1)}$$

$$r = r_1x + r_3x^3 + r_5x^5 + r_7x^7 + \ldots \quad \text{(A-2)}$$

$$\Psi = \Psi_1x + \Psi_3x^3 + \Psi_5x^5 + \Psi_7x^7 + \ldots \quad \text{(A-3)}$$

where x is measured along the body as shown in Figure 4-2. The terms f_1, f_3, f_5, etc. as needed in Section 4.4 have to be calculated. For this, two sets of coefficients need to be ascertained. The first is u_1, u_3, u_5 ... etc. whose values have already been obtained in Section 4.4 and are repeated here for convenience:

$u_1 = K\ U_0T_1/r$, $u_3 = K\ U_0T_3/r^3$, $u_5 = K\ U_0T_5/r^5$, ... and so on. Here K is a constant, U_0 is the velocity hitting the sphere at the front stagnation point, $T_1, T_3, T_5, \ldots$, etc. are the coefficients obtained by expanding the term $(\sin\Phi)/(1-\beta^2\sin^2\Phi)$ and r is the local radius of curvature of the sphere. The second set of coefficients is r_1, r_3, r_5, ... etc. For a sphere the local radius of curvature (r) is given by

$R\sin\Phi$, where Φ is the angle subtended by the length x of the sphere of radius R at the center.

Therefore, $r = R\sin\Phi$

$$= R(\Phi - \Phi^3/3! + \Phi^5/5! - \Phi^7/7! + \ldots)$$

$$= R(x/R - x^3/(R^3 3!) + x^5/(R^5 5!) - x^7/(R^7 7!) + \ldots \quad \text{(A-4)}$$

Comparing coefficients of Equations (A-2) and (A-4) we get:

$r_1 = 1$, $r_3 = 1/(6R^3)$, $r_5 = 1/(120R^5)$, $r_7 = 1/(5040R^7)$ ...

The accuracy of this power series type of solution depends on the number of terms taken. Here the expansion was carried out for seven terms and following Scholkemeier (1949) we get:

$$f_3 = g_3 + \frac{r_3 u_1}{r_1 u_3} h_3 = g_3 - \frac{h_3}{T_3} \quad \text{(A-5)}$$

$$f_5 = g_5 + \frac{r_5 u_1}{r_1 u_5} h_5 + \frac{u_3^2}{u_1 u_5} k_5 + \frac{r_3 u_3}{r_1 u_5} j_5 + \frac{r_3^2 u_1}{r_1^2 u_5} q_5$$

$$= g_5 + \frac{h_5}{T_5} + \frac{10}{3}\frac{T_3^2 k_5}{T_5} - \frac{10}{3}\frac{T_3 j_5}{T_5} + \frac{10}{3}\frac{q_5}{T_5} \quad \text{(A-6)}$$

$$f_7 = g_7 + \frac{r_7 u_1}{r_1 u_7} h_7 + \frac{r_3^2 u_3}{r_1^2 u_7} j_7 + \frac{u_3^3}{u_1^2 u_7} k_7 + \frac{r_5 u_3}{r_1 u_7} l_7 + \frac{u_3 u_5}{u_1 u_7} p_7$$

$$+ \frac{r_3^2 u_1}{r_1^3 u_7} q_7 + \frac{r_3 r_5 u_1}{r_1^2 u_7} v_7 + \frac{r_3 u_3^2}{r_1 u_1 u_7} t_7 + \frac{r_3 u_5}{r_1 u_7} z_7$$

$$i.e.\quad f_7=g_7-\frac{h_7}{T_7}+\frac{70}{3}\frac{T_3}{T_7}j_7+\frac{70}{3}\frac{T_3^3}{T_7}k_7+7\frac{T_3}{T_7}l_7+7\frac{T_3T_5}{T_7}p_7 \qquad (A\text{-}7)$$
$$-\frac{70}{3}\frac{q_7}{T_7}-\frac{70}{3}\frac{T_3^2}{T_7}t_7-7\frac{v_7}{T_7}-7\frac{T_5}{T_7}z_7$$

In order to calcualte the shear stress the values at the body surface ($\eta=0$) for $f_1''(0), f_3''(0), f_5''(0), \ldots$, etc. are needed.

$f_1''(0) = 0.9277$	$g_3''(0) = 1.0475$
$h_3''(0) = 0.0448$	$g_5''(0) = 0.9054$
$h_5''(0) = 0.0506$	$k_5''(0) = 0.1768$
$j_5''(0) = 0.0291$	$q_5''(0) = -0.024$
$g_7''(0) = 0.8210$	$h_7''(0) = 0.0500$
$j_7''(0) = -0.020$	$k_7''(0) = 0.0040$
$l_7''(0) = 0.0410$	$p_7''(0) = 0.2740$
$q_7''(0) = 0.0150$	$t_7''(0) = 0.0100$
$v_7''(0) = -0.047$	$z_7''(0) = 0.0130$

These can be sustituted in the following equations:

$$f_3''=g_3''-\frac{h_3''}{T_3} \qquad (A\text{-}8)$$

$$f_5''=g_5''+\frac{h_5''}{T_5}+\frac{10}{3}\frac{T_3^2k_5''}{T_5}-\frac{10}{3}\frac{T_3j_5''}{T_5}+\frac{10}{3}\frac{q_5''}{T_5} \qquad (A\text{-}9)$$

$$f_7'' = g_7'' - \frac{h_7''}{T_7} + \frac{70}{3}\frac{T_3}{T_7} j_7'' + \frac{70}{3}\frac{T_3^3}{T_7} k_7'' + 7\frac{T_3}{T_7} l_7'' + 7\frac{T_3 T_5}{T_7} p_7''$$

$$- \frac{70}{3}\frac{q_7''}{T_7} - \frac{70}{3}\frac{T_3^2}{T_7} t_7'' - 7\frac{v_7''}{T_7} - 7\frac{T_5}{T_7} z_7''$$

(A-10)

to get the needed results.

APPENDIX B

DISCRETIZATION USING CONTROL VOLUME

The generalized time dependant governing equation in axisymmetric cylindrical coordinate (r-z with symmetry about θ) that needs to be discretized so that it reduces to an algebraic form is

$$\frac{\partial(\rho\phi)}{\partial t}+\frac{\partial(\rho V_r\phi)}{\partial r}+\frac{\partial(\rho V_z\phi)}{\partial z}=\frac{\partial}{\partial z}(\Gamma\frac{\partial\phi}{\partial z})+\frac{\partial}{\partial r}(\Gamma\frac{\partial\phi}{\partial r})+\frac{\partial}{\partial r}(\frac{\Gamma\phi}{r}) \tag{B-1}$$

where t is the time, V_r and V_z are the velocities in the r and z direction respectively, ρ is the density of the fluid, Φ is a dependent variable and Γ is the diffusion coefficient.

Figure B-1 shows a typical control volume whose space satisfies Equation B-1. Integrating each term of the governing equation with respect to the dz,dr and dt we get for the time dependent term (first term of Equation B-1):

$$\int_t^{(t+\Delta t)ne}\iint_{sw}\frac{\partial(\rho\phi)}{\partial t}dzdrdt=(\rho_p\phi_p-\rho_p^0\phi_p^0)\Delta z\Delta r \tag{B-2}$$

where the index '0' denotes value at time t.

The second and third term on the left side of Equation B-1 are the convective terms and their integration yields:

$$\int_{t}^{(t+\Delta t)} \iint_{sw}^{ne} \frac{\partial(\rho V_r \phi)}{\partial r} dz dr dt = [(\rho V_r \phi)_n - (\rho V_r \phi)_s] \Delta z \Delta t \qquad (B\text{-}3)$$

$$= [\frac{(\rho V_r)_n}{2} \phi_N + \{\frac{(\rho V_r)_n}{2} - \frac{(\rho V_r)_s}{2}\} \phi_P - \frac{(\rho V_r)_s}{2} \phi_S] \Delta z \Delta t$$

In Equation B-3 the value of Φ at the n and s face is obtained by averaging i.e.

$$\Phi_n = (\Phi_P + \Phi_N)/2 \text{ and } \Phi_s = (\Phi_P + \Phi_S)/2$$

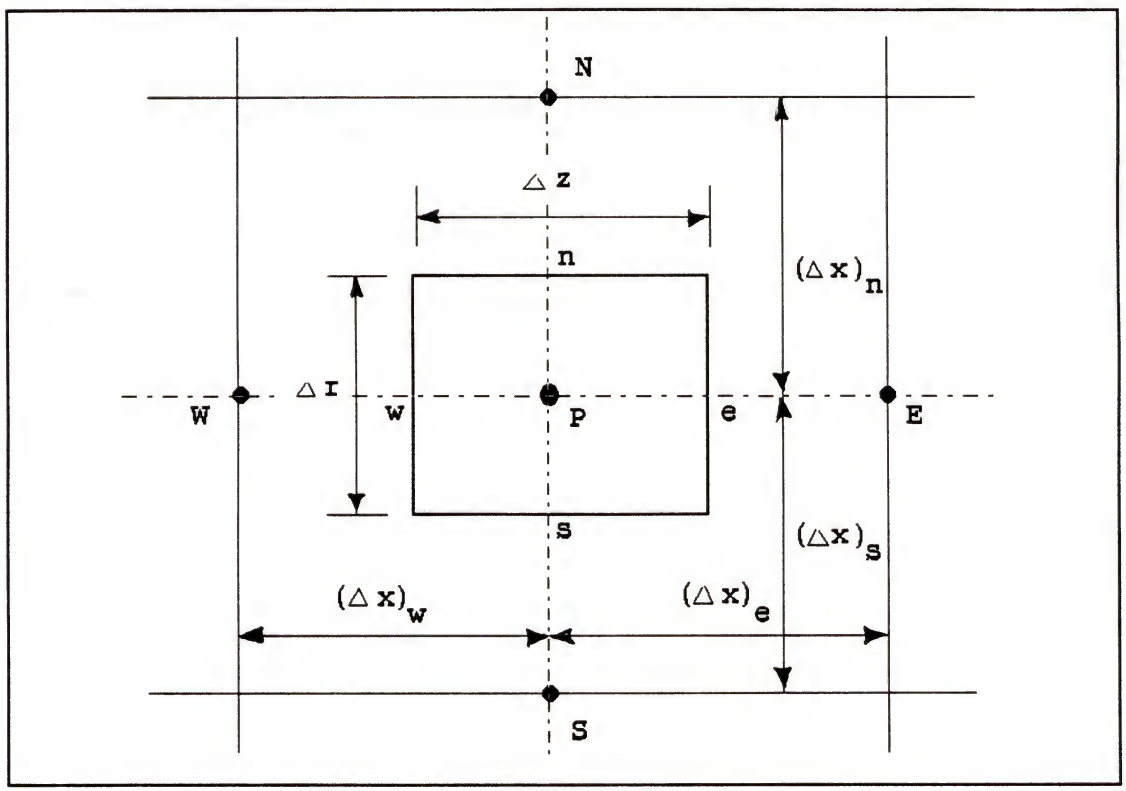

Figure B-1 A Typical Control Volume for Discretization

Similarly for the other convective term we get

$$\int_t^{(t+\Delta t)} \iint_{sw}^{ne} \frac{\partial(\rho V_z \phi)}{\partial z} dz dr dt = [(\rho V_z \phi)_e - (\rho V_z \phi)_w] \Delta r \Delta t \qquad (B\text{-}4)$$

$$= [\frac{(\rho V_z)_e}{2} \phi_E + \{\frac{(\rho V_z)_e}{2} - \frac{(\rho V_z)_w}{2}\} \phi_P - \frac{(\rho V_z)_w}{2} \phi_W] \Delta r \Delta t$$

The first two terms on the right side of Equation B-1 are the diffusive terms and we can integrate them as

$$\int_t^{(t+\Delta t)} \iint_{sw}^{ne} \frac{\partial}{\partial z}(\Gamma \frac{\partial \phi}{\partial z}) dz dr dt = \{\Gamma_e \frac{\partial \phi}{\partial z}\Big|_e - \Gamma_w \frac{\partial \phi}{\partial z}\Big|_w\} \Delta r \Delta t \qquad (B\text{-}5)$$

$$= \{\Gamma_e \frac{\phi_E - \phi_P}{(\Delta x)_e} - \Gamma_w \frac{\phi_P - \phi_W}{(\Delta x)_w}\} \Delta r \Delta t$$

$$= [\frac{\Gamma_e}{(\Delta x)_e} \phi_E + \frac{\Gamma_w}{(\Delta x)_w} \phi_W - \{\frac{\Gamma_e}{(\Delta x)_e} + \frac{\Gamma_w}{(\Delta x)_w}\} \phi_P] \Delta r \Delta t$$

$$\int_t^{(t+\Delta t)} \iint_{sw}^{ne} \frac{\partial}{\partial r}(\Gamma \frac{\partial \phi}{\partial r}) dz dr dt = \{\Gamma_n \frac{\partial \phi}{\partial r}\Big|_n - \Gamma_s \frac{\partial \phi}{\partial r}\Big|_s\} \Delta z \Delta t \qquad (B\text{-}6)$$

$$= \{\Gamma_n \frac{\phi_N - \phi_P}{(\Delta x)_n} - \Gamma_s \frac{\phi_P - \phi_S}{(\Delta x)_s}\} \Delta z \Delta t$$

$$= [\frac{\Gamma_n}{(\Delta x)_n} \phi_N + \frac{\Gamma_s}{(\Delta x)_s} \phi_S - \{\frac{\Gamma_n}{(\Delta x)_n} + \frac{\Gamma_s}{(\Delta x)_s}\} \phi_P] \Delta z \Delta t$$

Finally one can integrate the source term, which is the last term of Equation B-1, and get

$$\int_t^{(t+\Delta t)} \iint_{sw}^{ne} \frac{\partial}{\partial r}(\frac{\Gamma \phi}{r}) dz dr dt = [(\frac{\Gamma \phi}{r})_n - (\frac{\Gamma \phi}{r})_s] \Delta r \Delta t \qquad (B\text{-}7)$$

$$= [\frac{\Gamma_n}{r_n} \frac{\phi_N + \phi_P}{2} - \frac{\Gamma_s}{r_s} \frac{\phi_P + \phi_s}{2}] \Delta z \Delta t$$

$$= [\frac{\Gamma_n}{2r_n} \phi_N + (\frac{\Gamma_n}{2r_n} - \frac{\Gamma_s}{2r_s}) \phi_P - \frac{\Gamma_s}{2r_s} \phi_S] \Delta z \Delta t$$

We can observe that the integrated value of the source term can be expressed as $S = S_c + S_P \Phi_P$. Here S_c is the constant

term independent of Φ_P and S_P is the coefficient of Φ_P. As has been discussed by Patankar (1980) for convergence by iterative process S_P must have a negative value. If the diffusion coefficient has a constant value (i.e. $\Gamma=\Gamma_n=\Gamma_s$) then since r_s is always less than r_n, S_P has a negative value.

Introducing the following definitions:

$$C \equiv (\rho u)\,\Delta s \quad ; \quad D \equiv (\Gamma/\Delta x)\,\Delta s$$

$$C_e \equiv (\rho V_z)_e\,\Delta r \quad ; \quad D_e \equiv (\Gamma_e/\Delta x_e)\,\Delta r$$

$$C_w \equiv (\rho V_z)_w\,\Delta r \quad ; \quad D_w \equiv (\Gamma_w/\Delta x_w)\,\Delta r$$

$$C_n \equiv (\rho V_r)_n\,\Delta z \quad ; \quad D_n \equiv (\Gamma_n/\Delta x_n)\,\Delta z$$

$$C_s \equiv (\rho V_r)_s\,\Delta z \quad ; \quad D_s \equiv (\Gamma_s/\Delta x_s)\,\Delta z$$

we can substitute these terms and the different integral values obtained for the governing Equation B-1 to get

$$\frac{\rho_P\phi_P-\rho_P^0\phi_P^0}{\Delta t}\Delta z\Delta r+\frac{C_e}{2}\phi_E-\frac{C_w}{2}\phi_W+\frac{C_n}{2}\phi_N-\frac{C_s}{2}\phi_S+\left(\frac{C_e}{2}-\frac{C_w}{2}+\frac{C_n}{2}-\frac{C_s}{2}\right)\phi_P$$
$$=D_e\phi_E+D_w\phi_W+D_n\phi_N+D_s\phi_s-(D_e+D_w+D_n+D_s)\phi_P+(S_C+S_P\phi_P)\Delta Z$$

(B-8)

$$i.e. \quad \frac{\rho_P\phi_P-\rho_P^0\phi_P^0}{\Delta t}\Delta z\Delta r+\left(\frac{C_e}{2}-\frac{C_w}{2}+\frac{C_n}{2}-\frac{C_s}{2}+D_e+D_w+D_n+D_s\right)\phi_P$$
$$=\left(D_e-\frac{C_e}{2}\right)\phi_E+\left(D_w+\frac{C_w}{2}\right)\phi_W+\left(D_n-\frac{C_n}{2}\right)\phi_N+\left(D_s-\frac{C_s}{2}\right)\phi_S+(S_C+S_P\phi_P)\Delta Z$$

(B-9)

If we finally provide the following definition as given by Patankar (1980)

$$a_E = D_e - C_e/2$$

$$a_W = D_w + C_w/2$$

$$a_N = D_n - C_n/2$$

$$a_S = D_s + C_s/2$$

$$a_P^0 = (\rho_P^0 \, \Delta z \, \Delta r)/(\Delta t)$$

$$b = S_c \, \Delta z + a_P^0 \, \Phi_P^0$$

we get $$a = a_E + a_W + a_N + a_S + a_P^0 - S_P \, \Delta z$$

$$\therefore a_P \Phi_P = a_E \Phi_E + a_W \Phi_W + a_N \Phi_N + a_S \Phi_S + b$$

APPENDIX C

DISCRETIZATION PROCEDURE FOR BOUNDARY FITTED COORDINATE

In the boundary fitted coordinate system the physical region is mapped onto a computational space which has a regular geometry with evenly spaced grid points. Let (ξ, η) be the variables of the grid points in the computational domain with (r,z) being the corresponding variables in the physical domain as described by the axisymmetric cylindrical system. The target is to convert the generalized governing Equation like Equation 6-10 or Equation B-1 from (r,z) coordinates to (ξ, η) coordinate which can then be solved in the computational region.

$$\text{Let } \xi = \xi(r,z) \tag{C-1}$$

$$\eta = \eta(r,z) \tag{C-2}$$

Then

$$\frac{\partial}{\partial z} = \xi_z \frac{\partial}{\partial \xi} + \eta_z \frac{\partial}{\partial \eta} \tag{C-3}$$

$$\frac{\partial}{\partial r} = \xi_r \frac{\partial}{\partial \xi} + \eta_r \frac{\partial}{\partial \eta} \tag{C-4}$$

$$\frac{\partial^2}{\partial z^2} = \xi_z^2 \frac{\partial^2}{\partial \xi^2} + 2\xi_z \eta_z \frac{\partial^2}{\partial \xi \partial \eta} + \eta_z^2 \frac{\partial^2}{\partial \eta^2} \tag{C-5}$$

$$\frac{\partial^2}{\partial r^2} = \xi_r^2 \frac{\partial^2}{\partial \xi^2} + 2\xi_r \eta_r \frac{\partial^2}{\partial \xi \partial \eta} + \eta_r^2 \frac{\partial^2}{\partial \eta^2} \qquad \text{(C-6)}$$

$$\text{Also } \xi_z = J\, r_\eta \qquad \text{(C-7)}$$

$$\xi_r = -J\, z_\eta \qquad \text{(C-8)}$$

$$\eta_z = -J\, r_\xi \qquad \text{(C-9)}$$

$$\eta_r = J\, z_\xi \qquad \text{(C-10)}$$

$$\textit{where} \quad J = \frac{1}{z_\xi r_\eta - r_\xi z_\eta} \qquad \text{(C-11)}$$

The metrics (C-7) through (C-11) are obtained through a procedure found in most computational fluid dynamics text books. The Jacobian, J, is interpreted as the ratio of the areas (for two dimensional cases) in the physical space to that of the computational space.

With these values, the convective terms in the governing Equation (B-1) becomes

$$\begin{aligned}\frac{\partial}{\partial z}(\rho V_z \phi) &= \xi_z \frac{\partial}{\partial \xi}(\rho V_z \phi) + \eta_z \frac{\partial}{\partial \eta}(\rho V_z \phi) \\ &= J r_\eta \frac{\partial}{\partial \xi}(\rho V_z \phi) - J r_\xi \frac{\partial}{\partial \eta}(\rho V_z \phi) \\ &= J \frac{\partial}{\partial \xi}(\rho V_z \phi r_\eta) - J \rho V_z \phi \frac{\partial}{\partial \xi}(r_\eta) \\ &\quad - J \frac{\partial}{\partial \eta}(\rho V_z \phi r_\xi) + J \rho V_z \phi \frac{\partial}{\partial \eta}(r_\xi)\end{aligned} \qquad \text{(C-12)}$$

$$\therefore \quad \frac{\partial}{\partial z}(\rho V_z \phi) = J \frac{\partial}{\partial \xi}(r_\eta \rho V_z \phi) - J \frac{\partial}{\partial \eta}(r_\xi \rho V_z \phi) \qquad \text{(C-13)}$$

$$\textit{Similarly} \quad \frac{\partial}{\partial r}(\rho V_r \phi) = J \frac{\partial}{\partial \eta}(z_\xi \rho V_r \phi) - J \frac{\partial}{\partial \xi}(z_\eta \rho V_r \phi) \qquad \text{(C-14)}$$

Let τ represent time during calculations in the computational space. Noting that t = τ one has

$$\frac{\partial}{\partial t} = \tau_t \frac{\partial}{\partial \tau} + \xi_t \frac{\partial}{\partial \xi} + \eta_t \frac{\partial}{\partial \eta} \qquad \text{(C-15)}$$

But $\xi_t = \eta_t = 0$ and $\tau_t = 1$, which transforms the time dependant term of the governing equation to the computational space as

$$\frac{\partial}{\partial t}(\rho\phi) = \frac{\partial}{\partial \tau}(\rho\phi) \qquad \text{(C-16)}$$

Taking these calculations into account the left side of the governing Equation (B-1) as given by

$$\frac{\partial}{\partial t}(\rho\phi) + \frac{\partial}{\partial z}(\rho V_z \phi) + \frac{\partial}{\partial r}(\rho V_r \phi) \qquad \text{(C-17)}$$

is now transformed for the computational space to

$$\frac{\partial}{\partial \tau}(\rho\phi) + J\frac{\partial}{\partial \xi}\{\rho\phi(r_\eta V_z - z_\eta V_r)\} + J\frac{\partial}{\partial \eta}\{\rho\phi(z_\xi V_r - r_\xi V_z)\} \qquad \text{(C-18)}$$

If we introduce

$$U = r_\eta V_z - z_\eta V_r \qquad \text{(C-19)}$$

$$\text{and} \quad V = z_\xi V_r - r_\xi V_z \qquad \text{(C-20)}$$

Equation (C-18) becomes

$$\frac{\partial}{\partial \tau}(\rho\phi) + J\frac{\partial}{\partial \xi}(\rho U\phi) + J\frac{\partial}{\partial \eta}(\rho V\phi) \qquad \text{(C-21)}$$

We are now left with the diffusive and source terms. The diffusive terms are transformed as follows:

$$\frac{\partial}{\partial z}\left(\Gamma\frac{\partial\phi}{\partial z}\right)=\xi_z\frac{\partial}{\partial\xi}\left(\Gamma\frac{\partial\phi}{\partial z}\right)+\eta_z\frac{\partial}{\partial\eta}\left(\Gamma\frac{\partial\phi}{\partial z}\right)$$

$$=Jr_\eta\frac{\partial}{\partial\xi}\left(\Gamma\frac{\partial\phi}{\partial z}\right)-Jr_\xi\frac{\partial}{\partial\eta}\left(\Gamma\frac{\partial\phi}{\partial z}\right)$$

$$=J\frac{\partial}{\partial\xi}\left(r_\eta\Gamma\frac{\partial\phi}{\partial z}\right)-J\Gamma\frac{\partial\phi}{\partial z}\frac{\partial r_\eta}{\partial\xi}-J\frac{\partial}{\partial\eta}\left(r_\xi\Gamma\frac{\partial\phi}{\partial z}\right)+J\Gamma\frac{\partial\phi}{\partial z}\frac{\partial r_\xi}{\partial\eta} \qquad \text{(C-22)}$$

$$\therefore,\ \frac{\partial}{\partial z}\left(\Gamma\frac{\partial\phi}{\partial z}\right)=J\frac{\partial}{\partial\xi}\left(r_\eta\Gamma\frac{\partial\phi}{\partial z}\right)-J\frac{\partial}{\partial\eta}\left(r_\xi\Gamma\frac{\partial\phi}{\partial z}\right) \qquad \text{(C-23)}$$

$$\textit{But,}\quad J\frac{\partial}{\partial\xi}\left(r_\eta\Gamma\frac{\partial\phi}{\partial z}\right)=J\frac{\partial}{\partial\xi}\left\{r_\eta\Gamma\left(\xi_z\frac{\partial\phi}{\partial\xi}+\eta_z\frac{\partial\phi}{\partial\eta}\right)\right\}$$

$$=J\frac{\partial}{\partial\xi}\left\{r_\eta\Gamma\left(Jr_\eta\frac{\partial\phi}{\partial\xi}-Jr_\xi\frac{\partial\phi}{\partial\eta}\right)\right\} \qquad \text{(C-24)}$$

$$=J\frac{\partial}{\partial\xi}\left\{\Gamma J\left(r_\eta^2\phi_\xi-r_\xi r_\eta\phi_\eta\right)\right\}$$

$$\textit{Similarly,}\ J\frac{\partial}{\partial\eta}\left(r_\xi\Gamma\frac{\partial\phi}{\partial z}\right)=J\frac{\partial}{\partial\eta}\left\{\Gamma J\left(r_\xi r_\eta\phi_\xi-r_\xi^2\phi_\eta\right)\right\} \qquad \text{(C-25)}$$

$$\textit{Hence,}\ \frac{\partial}{\partial z}\left(\Gamma\frac{\partial\phi}{\partial z}\right)=J\frac{\partial}{\partial\xi}\left\{\Gamma J\left(r_\eta^2\phi_\xi-r_\xi r_\eta\phi_\eta\right)\right\}$$

$$-J\frac{\partial}{\partial\eta}\left\{\Gamma J\left(r_\xi r_\eta\phi_\xi-r_\xi^2\phi_\eta\right)\right\} \qquad \text{(C-26)}$$

Carrying out calculations on the same lines, the second diffusive terms becomes

$$\frac{\partial}{\partial r}\left(\Gamma\frac{\partial\phi}{\partial r}\right)=-J\frac{\partial}{\partial\xi}\left\{J\Gamma\left(-z_\eta z_\eta\phi_\eta-z_\eta^2\right)\right\}$$

$$+J\frac{\partial}{\partial\eta}\left\{J\Gamma\left(z_\xi^2\phi_\eta-z_\eta z_\xi\phi_\xi\right)\right\} \qquad \text{(C-27)}$$

Therefore the first two terms on the right side of Equation (B-1), that happen to carry the diffusive flux, are now transformed as

$$\frac{\partial}{\partial z}(\Gamma\frac{\partial\phi}{\partial z})+\frac{\partial}{\partial r}(\Gamma\frac{\partial\phi}{\partial r})=J\frac{\partial}{\partial\xi}[\Gamma J\{(r_\eta^2+z_\eta^2)\phi_\xi-(r_\xi r_\eta+z_\eta z_\xi)\phi_\eta\}]$$
$$+J\frac{\partial}{\partial\eta}[\Gamma J\{(r_\xi^2+z_\xi^2)\phi_\eta-(r_\eta r_\xi+z_\eta z_\xi)\phi_\xi\}]$$
$$=J\frac{\partial}{\partial\xi}[\Gamma J(A_1\phi_\xi-A_2\phi_\eta)]+J\frac{\partial}{\partial\eta}[\Gamma J(A_3\phi_\eta-A_2\phi_\xi)]$$

(C-28)

where $A_1 = z_\eta^2 + r_\eta^2$ (C-29)

$A_2 = z_\eta z_\xi + r_\eta r_\xi$ (C-30)

$A_3 = z_\xi^2 + r_\xi^2$ (C-31)

Finally the source term is transformed as follows:

$$\frac{\partial}{\partial r}(\frac{\Gamma\phi}{r})=\xi_r\frac{\partial}{\partial\xi}(\frac{\Gamma\phi}{r})+\eta_r\frac{\partial}{\partial\eta}(\frac{\Gamma\phi}{r})$$
$$=-Jz_\eta\frac{\partial}{\partial\xi}(\frac{\Gamma\phi}{r})+Jz_\xi\frac{\partial}{\partial\eta}(\frac{\Gamma\phi}{r})$$
$$=-J\frac{\partial}{\partial\xi}(\frac{z_\eta\Gamma\phi}{r})+J\frac{\Gamma\phi}{r}\frac{\partial z_\eta}{\partial\xi} \qquad \text{(C-32)}$$
$$+J\frac{\partial}{\partial\eta}(\frac{z_\xi\Gamma\phi}{r})+J\frac{\Gamma\phi}{r}\frac{\partial z_\xi}{\partial\eta}$$
$$=-J\frac{\partial}{\partial\xi}(\frac{z_\eta\Gamma\phi}{r})+J\frac{\partial}{\partial\eta}(\frac{z_\xi\Gamma\phi}{r})$$

Therefore by taking Equations C-21, C-28 and C-32 we get the governing equation in the computational plane as

$$\frac{\partial}{\partial\tau}(\rho\phi)+J\frac{\partial}{\partial\xi}(\rho U\phi)+J\frac{\partial}{\partial\eta}(\rho V\phi)=J\frac{\partial}{\partial\xi}[\Gamma J(A_1\phi_\xi-A_2\phi_\eta)]$$
$$+J\frac{\partial}{\partial\eta}[\Gamma J(A_3\phi_\eta-A_2\phi_\xi)]+J\frac{\partial}{\partial\eta}(\frac{z_\xi\Gamma\phi}{r})-J\frac{\partial}{\partial\xi}(\frac{z_\eta\Gamma\phi}{r}) \qquad \text{(C-33}$$

Since the Jacobian, J, does not vary with time τ we finally get

$$\frac{\partial}{\partial\tau}\left(\frac{\rho\phi}{\tau}\right)+\frac{\partial}{\partial\xi}(\rho U\phi)+\frac{\partial}{\partial\eta}(\rho V\phi)=\frac{\partial}{\partial\xi}[\Gamma J(A_1\phi_\xi-A_2\phi_\eta)] + \frac{\partial}{\partial\eta}[\Gamma J(A_3\phi_\eta-A_2\phi_\xi)]+\frac{\partial}{\partial\eta}\left(\frac{z_\xi\Gamma\phi}{r}\right)-\frac{\partial}{\partial\xi}\left(\frac{z_\eta\Gamma\phi}{r}\right) \tag{C-34}$$

In Equation C-34 the terms U,V,A_1,A_2,A_3 and J are respectively given by Equations C-19,C-20,C-29,C-30,C-31 and C-11, respectively.

Discretization of Equation (C-34) is performed in a similar manner as shown in Appendix A. Integrating over $d\tau d\xi d\eta$ one gets:

$$\frac{\rho_P\phi_P-\rho_P^0\phi_P^0}{J_P}\frac{\Delta\xi\Delta\eta}{\Delta\tau}+\left(\frac{C_e}{2}-\frac{C_w}{2}+\frac{C_n}{2}-\frac{C_s}{2}+D_e+D_w+D_n+D_s\right)\phi_P = \left(D_e-\frac{C_e}{2}\right)\phi_E+\left(D_w+\frac{C_w}{2}\right)\phi_W+\left(D_n-\frac{C_e}{2}\right)\phi_N+\left(D_s+\frac{C_s}{2}\right)\phi_S+S \tag{C-35}$$

In Equation (C-35) the various terms are as follows:

$$C_e = (\rho U)_e\Delta\eta \quad ; \quad D_e = (\Gamma JA_1/\Delta\xi)_e\Delta\eta$$

$$C_w = (\rho U)_w\Delta\eta \quad ; \quad D_w = (\Gamma JA_1/\Delta\xi)_w\Delta\eta$$

$$C_n = (\rho V)_n\Delta\xi \quad ; \quad D_n = (\Gamma JA_3/\Delta\eta)_e\Delta\xi$$

$$C_s = (\rho V)_s\Delta\xi \quad ; \quad D_n = (\Gamma JA_3/\Delta\eta)_s\Delta\xi$$

and the source term S is given by:

$$S=\left[\left(z_\eta\Gamma\frac{\phi}{r}+\Gamma JA_2\frac{\partial\phi}{\partial\eta}\right)_w-\left(z_\eta\Gamma\frac{\phi}{r}+\Gamma JA_2\frac{\partial\phi}{\partial\eta}\right)_e\right]\Delta\eta + \left[\left(z_\xi\Gamma\frac{\phi}{r}+\Gamma JA_2\frac{\partial\phi}{\partial\xi}\right)_n-\left(z_\xi\Gamma\frac{\phi}{r}+\Gamma JA_2\frac{\partial\phi}{\partial\xi}\right)_s\right]\Delta\xi \tag{C-36}$$

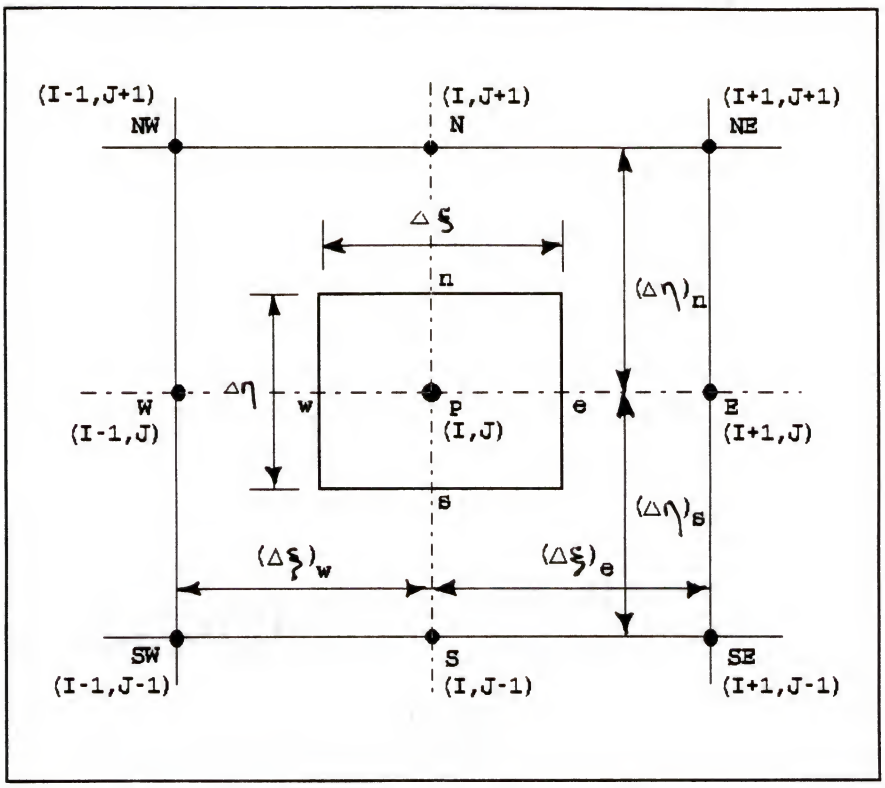

Figure C-1 A typical control volume in computational space

Equation C-35 can be finally cast in an algebraic form

$$a_P\Phi_P = a_E\Phi_E + a_W\Phi_W + a_N\Phi_N + a_S\Phi_S + b \qquad \text{(C-37)}$$

where $a_E = D_e - C_e/2$

$a_W = D_w + C_w/2$

$a_N = D_n - C_n/2$

$a_S = D_s + C_s/2$

$a_P^0 = (\rho_P \Delta\xi \Delta\eta)/(J_P \Delta t)$

$a_P = a_E + a_W + a_N + a_S + a_P^0$

$b = S + a_P\Phi_P^0$

It is interesting to note that during calculation the point P is influenced not only by points E,W,N,and S but also by points NE,NW,SE and SW. The extra four points NE,NW,SE and SW come into picture while calculating the source term S (Figure C-1).

LIST OF REFERENCES

Achenbach, E.; Experiments on the flow past spheres at very high Reynolds numbers, J. Fluid Mech., vol. 54, pp. 565-575, 1972.

Achenbach, E.; The effects of surface roughness and tunnel blockage on the flow past spheres, J. Fluid Mech., vol. 65, pp. 113-125, 1974.

Anderson, D.A., Tannehill, J.C., and Pletcher, R.H.; Computational Fluid Mechanics and Heat Transfer, Hemisphere Publishing Corporation, New York, 1984.

Boltze, E.; Grenzschichten an Rotationskörpern in Flüssigkeiten mit kleiner Reibung, Göttingen dissertation, 1908.

Bevington, P.R.; Data Reduction and Error Analysis for the Physical Sceinces, McGraw-Hill Book Company, New York, 1969.

Brenner, H. and Happel, J.; Slow viscous flow past a sphere in a cylindrical tube, J. Fluid Mech., vol. 4, pp. 195-213, 1958.

Clift, R., Grace, J.R. & Weber, M.E.; Bubbles, Drops and Particles, Academic Press, New York, 1978.

Coutanceau, M.; Mécanique des fluides, C.R. Acad. Sci., Paris, Ser. A 274, pp. 853-856, 1972.

Dennis, S.C.R. and Walker, J.D.A.; Calculation of the steady flow past a sphere at low and moderate Reynolds Number, J. Fluid Mech, vol 48, pp. 772-789, 1971.

Eichhorn, R. and Small, S.; Experiments on the lift and drag of spheres suspended in Poiseuille flow, J. Fluid Mech., vol. 20, pp 271-280, 1964.

Faxen, H.; Die Bewegung einer starren Kugel langs der Achse eines mit zaher Flussigkeit gefullten Rohres, Arkiv Mat. Astron. Fysik, vol. 17, pp. 27-42, 1923.

Fayon, A.M. and Happel, J.; Effect of a cylindrical boundary on a fixed rigid sphere in a moving viscous fluid, A.I.ChE.J., vol 6, pp. 55, 1960.

Francis, A.W.; Wall effect in falling ball method for viscosity, Physics, vol. 4, pp. 403-406, 1933.

Gluckman, M.J., Weinbaum,S. and Pfeffer, R.; Annual AIChE Meeting, 64th. San Francisco, 1971.

Haberman, W.L. and Sayre, R.M.; Motion of rigid and fluid spheres in a stationary and moving liquids inside cylindrical vessels, David Taylor Model Basin., Report No. 1143, US Navy Dept., Washington DC, 1958.

Hagen, G.; Über die Bewegung des Wassers in engen zylindrischen Röhren, Pogg. Ann., vol. 46, pp. 423-442, 1839.

Happel, J. and Brenner, H.; Low Reynolds Number Hydrodynamics, 2nd. edition, Noordham Leyden, Amsterdam, Netherlands, 1973.

Hoffman, K.A.; Computational Fluid Dynamics for Engineers, Publication of Engineering Education System, Austin, Texas, 1989.

Idelchik, I.E.; Handbook of Hydraulic Resistance, Hemisphere Publishing Corporation, New York, 1986.

Jenson,V.G.; Viscous flow around a sphere at low Reynolds Number (<40), Proc. Roy. Soc. (London), vol. A 249, pp. 346, 1959.

Johansson, H.; A numerical solution of the flow around a sphere in a circular tube, Chem. Engg. Commun., vol 1, pp 271-280, 1974.

Karki, K.C., Patankar, S.V., Runchal, A.K., and Mongia, H.C.; Improved Numerical Methods for Turbulent Viscous flows, NASA-24350, National Aeronautics and Space Administration, Cleveland, Ohio, 1988.

Kestin, J. and Wakeham, W.A.; Transport Properties of Fluids: Thermal Conductivity, Viscosityand Diffusion Coefficient, Hemisphere Publishing Corporation, New York, 1988.

Klyachko, K.V.; Equations of motion of dust particles in dust collectors, Otoplenie Vent., vol. 4 pp.27-32, 1934.

Lamb, H.; Hydrodynamics, 6th ed., Dover, New York, 1932.

Ladenburg, R.; Ann. Phys., Paris, vol. 22, pp. 287, 1907.

Le Clair, B.P., Hamielec, A.E., and Pruppacher, H.R.; A numerical study of the drag on a sphere at low and

intermediate Reynolds Number, J. Atmos. Sci., vol. 27, pp. 308-315, 1970.

Lee, H.M.; A Modification of Stokes' Law to Account for Boundary Influence, M.S. Thesis, State Univ. of Iowa, Ames, 1947.

Lunnon, R.G.; Fluid Resistance To Moving Sphere, Proceedings of the Royal Society (London), Series A, vol. 118, pp. 680-694, 1928.

McNown, J.S., Lee, H.M. and McPherson, M.B.; Influence of Boundary Proximity on the Drag of Spheres, Proceedings of the VII International Congress for Applied Mechanics, pp 17-29, 1948.

McNown, J.S. and Newlin, J.T.; Drag of Spheres within Cylindrical Boundaries, Proceedings of the US National Congress in Applied Mechanics, 1st., pp 801-806, 1951.

Monroe, H.S.; Trans. Amer. Inst. Min. Engrs., vol. 17, pp. 637, 1888.

Mott, R.A.; Some Aspects of Fluid Flow, E. Arnold and Co., London, pp.242, 1951.

Newton, I.; Principia, Lib. II, Prop, vii, Cor. 2, Quoted by Barr(1931), 1687.

Oseen, C.W.; Über die Stokessche Formel und über eine verwandte Aufgabe in der Hydrodynamik; Arkiv Math. Astronom. Fys. , vol. 6, pp. 75, 1910.

Patankar S.V.; Numerical Heat Transfer and Fluid Flow, Hemisphere Publishing Corporation, New York, 1980.

Poiseuille, J.; Récherches expérimentelles sur le mouvement des liquides dans les tubes de très petits diametres, Comptes Rendus, vol. 11, pp. 961-967, 1840; and in more detail; Mémoires des Savants Etrangers, vol. 9 , 1846.

Poisson, S.D.; Mémoire sur les équations générales de l'équilibre et du mouvement des corps solides élastiques et des fluides, J. de l'Ecole polytechn., vol. 13, pp.139-186, 1831.

Prandtl, L.; Über Flüssigkeitsbewegung bei sehr kleiner Reibung, Proceedings of III International Mathemetical Congress, Heidelberg, pp. 484-491, 1904.

Proudman, I. and Pearson J.R.A.; Expansions at small Reynolds number for the flow past a sphere and circular cylinder, J. Fluid Mech., vol. 2, pp. 237, 1957.

Rimon, Y. and Cheng, S.I.; Numerical solution of a uniform flow over a sphere at intermediate Reynolds Number, Phys. Fluids, vol. 12, pp. 949, 1969.

Roache, P.J.; Computational Fluid Dynamics, Hermosa Publisheres, Albuquerque, 1982.

Round, G.F., Latto, B., and Anzenavs, R.; Drag coefficients of freely-suspended spheres and sphere trains in a vertical tube, Second International Conference on the Hydraulic Transport of Solids in Pipes, Hydrotransport 2, Paper F1, 1972.

Schlichting, H.; Boundary Layer Theory, 6th edition, McGraw - Hill, Inc., New York, 1968.

Stokes, G.G.; On the theories of internal friction of fluids in motion, Transactions Cambridge Philosophical Society, vol. 8, pp. 287-305, 1845.

Thompson, J.F., Warsi, Z.U.A. and Mastin C.W.; Numerical Grid Generation, North Holland, 1985.

Wakiya, S.; A spherical Obstacle in the flow of a viscous fluid through a tube, J. Phys. Soc. Japan, vol. 8, pp. 254-257, 1953.

Young, D.F.; Drag and lift on spheres within cylindrical tubes, Journal of the Hydraulics Division, Proceedings of the ASCE, vol. HY6, pp 47-57, 1960.

BIOGRAPHICAL SKETCH

Ratan Kumar was born on December 28, 1961, in Arrah (India). He is the son of Kameshwar Prasad Sreewastav and Kumudini Bala and has a sister Sadhana Saxena. He got married to Kiran Sreewastav on June 20, 1987.

The author graduated from South Point High School (Calcutta, India) and joined Jadavpur University (Calcutta, India) where he earned his bachelors degree in mechanical engineering. After spending three years in a multinational firm (TIL Ltd.) as a sales engineer the author joined the University of Florida, Gainesville, to pursue a graduate degree. There he received his Master of Engineering degree in 1989 from the Department of Nuclear Engineering Sciences.

The author is a member of Alpha Nu Sigma honorary society and a student member of the American Nuclear Society and the Order of Engineer.

I certify that I have read this study and that in my opinion it conforms to acceptable standards of scholarly presentation and is fully adequate, in scope and quality, as a dissertation for the degree of Doctor of Philosophy.

Samim Anghaie

Samim Anghaie, Chairman
Professor of Nuclear
Engineering Sciences

I certify that I have read this study and that in my opinion it conforms to acceptable standards of scholarly presentation and is fully adequate, in scope and quality, as a dissertation for the degree of Doctor of Philosophy.

Edward T. Dugan

Edward T. Dugan
Associate Professor of Nuclear
Engineering Sciences

I certify that I have read this study and that in my opinion it conforms to acceptable standards of scholarly presentation and is fully adequate, in scope and quality, as a dissertation for the degree of Doctor of Philosophy.

David E. Hintenlang

David E. Hintenlang
Assistant Professor of Nuclear
Engineering Sciences

I certify that I have read this study and that in my opinion it conforms to acceptable standards of scholarly presentation and is fully adequate, in scope and quality, as a dissertation for the degree of Doctor of Philosophy.

James F. Klausner

James F. Klausner
Assistant Professor of
Mechanical Engineering

I certify that I have read this study and that in my opinion it conforms to acceptable standards of scholarly presentation and is fully adequate, in scope and quality, as a dissertation for the degree of Doctor of Philosophy.

M L Muga

Marvin L. Muga
Professor of Chemistry

This dissertation was submitted to the Graduate Faculty of the College of Engineering and to the Graduate School and was accepted as partial fulfillment of the requirements for the degree of Doctor of Philosophy.

December 1992

Winfred M. Phillips
Dean, College of Engineering

Madelyn M. Lockhart
Dean, Graduate School